

② LEVEL II  
9

AD A060627



FRANK J. SEILER RESEARCH LABORATORY

⑭ FJSRL-TR-77-0015

⑪ DEC 1977

⑫ 150 P.

⑥ HIGHER ORDER GASDYNAMIC THEORY  
OF SHOCK STRUCTURE.

⑨ Technical rept.  
Jan '73 - Aug '73

DDC  
RECEIVED  
NOV 1 1978  
B

LT COL CHARLES E. SIMON  
⑩

DDC FILE COPY



⑬ PROJECT 2307  
⑮ F1

APPROVED FOR PUBLIC RELEASE;  
DISTRIBUTION UNLIMITED.

AIR FORCE SYSTEMS COMMAND  
UNITED STATES AIR FORCE

20 10 319 920

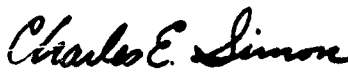
This document was prepared by the Mechanics Division, Directorate of Aerospace Mechanics Sciences, Frank J. Seiler Research Laboratory, United States Air Force Academy, CO. The research was conducted under Project Work Unit Number 2307-F1-30, Theoretical and Experimental Investigation of Shock Structure. Lt Col Charles E. Simon was the Project Engineer in charge of the work.


When US Government drawings, specifications or other data are used for any purpose other than a definitely related government procurement operation, the government thereby incurs no responsibility nor any obligation whatsoever, and the fact that the government may have formulated, furnished or in anyway supplied the said drawings, specifications or other data is not to be regarded by implication or otherwise, as in any manner licensing the holder or any other person or corporation or convey any rights or permission to manufacture, use or sell any patented invention that may in anyway be related thereto.

Inquiries concerning the technical content of this document should be addressed to the Frank J. Seiler Research Laboratory (AFSC), USAF Academy, CO 80840. Phone AC 303 472-3122.

This report has been reviewed by the Chief Scientist and is releasable to the National Technical Information Service (NTIS). At NTIS it will be available to the general public, including foreign nations.

This technical report has been reviewed and is approved for publication.

  
CHARLES E. SIMON, Lt Col, USAF  
Project Engineer

  
JOSEPH S. FORD, II, Lt Col, USAF  
Dir, Directorate of Aerospace-  
Mechanics Sciences

  
M. D. BACON, Colonel, USAF  
Commander

Copies of this report should not be returned unless return is required by security considerations, contractual obligations, or notice on a specific document.

Printed in the United States of America. Qualified requestors may obtain additional copies from the Defense Documentation Center. All others should apply to:

National Technical Information Service  
6235 Port Royal Road  
Springfield, Virginia 22161

REPORT DOCUMENTATION PAGE		READ INSTRUCTIONS BEFORE COMPLETING FORM
1. REPORT NUMBER FJSRL-TR-77-0015	2. GOVT ACCESSION NO. ADA	3. RECIPIENT'S CATALOG NUMBER
4. TITLE (and Subtitle) Higher Order Gasdynamic Theory of Shock Structure		5. TYPE OF REPORT & PERIOD COVERED Technical Report January 1973 - August 1977
		6. PERFORMING ORG. REPORT NUMBER
7. AUTHOR(s) Charles E. Simon		8. CONTRACT OR GRANT NUMBER(s)
9. PERFORMING ORGANIZATION NAME AND ADDRESS F. J. Seiler Research Laboratory (FJSRL/NA) Air Force Systems Command U.S. Air Force Academy, Colorado 80840		10. PROGRAM ELEMENT, PROJECT, TASK AREA & WORK UNIT NUMBERS 61102F/2307/F1/30
11. CONTROLLING OFFICE NAME AND ADDRESS F. J. Seiler Research Laboratory (FJSRL/NH) Air Force Systems Command U.S. Air Force Academy, Colorado 80840		12. REPORT DATE December 1977
		13. NUMBER OF PAGES
14. MONITORING AGENCY NAME & ADDRESS (if different from Controlling Office)		15. SECURITY CLASS. (of this report) Unclassified
		15a. DECLASSIFICATION/DOWNGRADING SCHEDULE N/A
16. DISTRIBUTION STATEMENT (of this Report) Approved for Public Release; Distribution Unlimited.		
17. DISTRIBUTION STATEMENT (of the abstract entered in Block 20, if different from Report)		
18. SUPPLEMENTARY NOTES		
19. KEY WORDS (Continue on reverse side if necessary and identify by block number) Shock Structure                      Normal Shock Wave Maxwell Gas                          Perturbation Methods Boltzmann Equation                Asymmetry Quotient Chapman-Enskog Development    Density Profile Temperature Profile		
20. ABSTRACT (Continue on reverse side if necessary and identify by block number) This document is the final report concerning the theoretical investigation of the structure of a normal shock wave in a gas composed of Maxwell molecules. The higher order gasdynamic differential equations for the shock structure are derived from this Boltzmann equation through fourth order in spatial derivatives (Super-Super-Burnett Order). The derivation employs a simplified version of the well known Chapman-Enskog development. Perturbation methods are used to find approximate solutions for the Super Burnett (third order) and Super-Super-Burnett (fourth order) equations which are not amenable to numerical integration by		

D D C  
RECEIVED  
NOV 1 1978  
B

conventional techniques.

The perturbation methods are shown to produce satisfactory approximate solutions for the Navier-Stokes and Burnett equations which are amenable to numerical integration. The higher order gasdynamic corrections to the Navier-Stokes shock structure for a Maxwell gas are shown to be qualitatively similar to the discrepancies between experimental results and the Navier-Stokes shock structure for a realistic intermolecular potential.

## PREFACE

This research was initiated in 1972 during the author's final year of residence at the University of Colorado, Boulder, Colorado. The work was undertaken as partial fulfillment of the requirement for a Doctor of Philosophy degree in Aerospace Engineering Sciences at the University of Colorado.

The major portion of the research was completed while the author was assigned to the Frank J. Seiler Research Laboratory (AFSC). The computational effort was accomplished primarily at the Education and Research Computer Center facilities of the United States Air Force Academy.

The perturbation technique used in this research was pursued sufficiently to reveal a more simplified procedure for rapid recovery of the coefficients which must be calculated in the derivation of the perturbation equations. The original procedure for these calculations required an extensive period of tedious effort to produce the perturbation expressions through fourth order in successive approximation. The revelation of the simplified procedure made it possible to reproduce the first four orders of results in significantly reduced time as well as calculate an additional five orders for the perturbation equations.

This report documents those results obtained from the initial effort to derive the first four orders in the expansion employing the original perturbation computational methods.

ACCESSION for	
NTIS	White Section <input checked="" type="checkbox"/>
DDC	P. L. Section <input type="checkbox"/>
UNANNOUNCED	<input type="checkbox"/>
JUSTIFICATION	
BY	
DISTRIBUTION/AVAILABILITY CODES	
Dist.	AVAIL. and/or SPECIAL
A	

10 24

## TABLE OF CONTENTS

CHAPTER	PAGE
I. INTRODUCTION . . . . .	1
II. HIGHER ORDERS OF THE CHAPMAN-ENSKOG	
DEVELOPMENT FOR MAXWELL MOLECULES . . . . .	13
Conservation Equations for the Steady State	
One Dimensional Normal Shock Wave . . . . .	13
Alternate Forms of the Viscous Stress and	
Heat Flux for the Higher Order Developments . . .	17
Spatially Ordered Equations Derived from the	
Expanded Velocity Distribution Function	
Applied to the Boltzmann Equation . . . . .	19
Determination of $P^{(1)}$ and $q^{(1)}$ . . . . .	23
Determination of $P^{(2)}$ and $q^{(2)}$ . . . . .	28
Determination of $P^{(3)}$ and $q^{(3)}$ . . . . .	32
Determination of $P^{(4)}$ and $q^{(4)}$ . . . . .	36
III. METHODS TO SOLVE THE NAVIER-STOKES EQUATIONS . . . .	39
Numerical Integration . . . . .	39
Perturbation Expansion . . . . .	43
IV. METHODS TO SOLVE THE HIGHER ORDER	
GASDYNAMIC EQUATIONS . . . . .	54
Numerical Integration of the Higher	
Order Equations . . . . .	54
Perturbation Expansion Applied to the	
Burnett Equations . . . . .	57

CHAPTER	PAGE
Perturbation Expansion Applied to the Super-Burnett Equations and the Super- Super-Burnett Equations . . . . .	61
V. SHOCK WAVE PROFILES BASED ON THE METHODS OF NUMERICAL INTEGRATION AND PERTURBATION EXPANSION . . . . .	64
Results for the Navier-Stokes Equation and the Burnett Equations Based on the Method of Numerical Integration . . . . .	64
Results for the Navier-Stokes Density Profile Based on the Methods of Numerical Integration and Perturbation Expansion . . . . .	73
Results for the Burnett Density Profile Based on the Methods of Numerical Integration and Perturbation Expansion . . . . .	85
Intuitively Trustworthy Parts of the Results for the Density Profile through Super-Super-Burnett Order Based on the Method of Perturbation Expansion . . . . .	97
VI. COMMENTS AND OUTLOOK . . . . .	107
BIBLIOGRAPHY . . . . .	112
APPENDIX	
A. THE MAXWELL EIGENFUNCTIONS . . . . .	115

APPENDIX	PAGE
B. ROOTS OF THE CHARACTERISTIC POLYNOMIALS . . . . .	119
C. GENERAL FORM OF THE EQUATIONS FROM THE PERTURBATION DEVELOPMENT AND GENERAL FORM OF THE SOLUTIONS TO THE DIFFERENTIAL EQUATIONS FOR THE NORMALIZED DENSITY . . . . .	128



## LIST OF TABLES

TABLE	PAGE
I. COEFFICIENTS $\alpha_i$ FOR $\kappa_2$ . . . . .	109
II. MAXWELL EIGENFUNCTIONS AND ASSOCIATED EIGENVALUES . . . . .	117
III. PHYSICALLY SIGNIFICANT $\kappa_2$ . . . . .	126
IV. COEFFICIENTS $A_n$ FOR THE PERTURBATION EQUATIONS . . . . .	131
V. COEFFICIENTS $B_n$ FOR $R_\rho^{(2)}$ . . . . .	136
VI. COEFFICIENTS $C_n$ FOR $R_\rho^{(3)}$ . . . . .	137

# LIST OF FIGURES

FIGURE	PAGE
1. Characteristic variation of the normalized density across a normal shock wave . . . . .	5
2. Density asymmetry quotient ( $Q_\rho$ ) in a normal shock wave as a function of upstream Mach number ( $M_1$ ) . . . . .	7
3. Gas density profiles in a normal shock wave ( $M_1=1.5$ ) based on the numerical integration of the Navier-Stokes and Burnett gasdynamic differential equations . . . . .	65
4. Gas density profiles in a normal shock wave ( $M_1=2.0$ ) based on the numerical integration of the Navier-Stokes and Burnett gasdynamic differential equations . . . . .	67
5. Gas temperature profiles in a normal shock wave ( $M_1=1.5$ ) based on the numerical integration of the Navier-Stokes and Burnett gasdynamic differential equations . . . . .	69
6. Gas temperature profiles in a normal shock wave ( $M_1=2.0$ ) based on the numerical integration of the Navier-Stokes and Burnett gasdynamic differential equations . . . . .	71

7. Mach number ( $M_1$ ) dependence of the temperature-density separation in a normal shock wave based on the numerical integration of the Navier-Stokes and Burnett gasdynamic differential equations . . . . .	74
8. Density asymmetry quotient ( $Q_\rho$ ) versus $M_1$ based on the numerical integration of the Navier-Stokes and Burnett gasdynamic differential equations . . . . .	75
9. Temperature asymmetry quotient ( $Q_T$ ) versus $M_1$ based on the numerical integration of the Navier-Stokes and Burnett gasdynamic differential equations . . . . .	76
10. Navier-Stokes density profiles in a normal shock wave ( $M_1=1.5$ ). A comparison of density profiles based on the methods of numerical integration and perturbation expansion . . . . .	77
11. Navier-Stokes density profiles in a normal shock wave ( $M_1=2.0$ ). A comparison of density profiles based on the methods of numerical integration and perturbation expansion . . . . .	79

12. Navier-Stokes density profiles in a normal shock wave ( $M_1=3.0$ ). A comparison of density profiles based on the methods of numerical integration and perturbation expansion . . . . . 81
13. Navier-Stokes density profiles in a normal shock wave ( $M_1=4.0$ ). A comparison of density profiles based on the methods of numerical integration and perturbation expansion . . . . . 83
14. Density asymmetry quotient ( $Q_\rho$ ) versus  $M_1$  from the Navier-Stokes perturbation expansion. A comparison of the results for  $Q_\rho$  based on the methods of perturbation expansion and numerical integration . . . . . 86
15. Burnett density profiles in a normal shock wave ( $M_1=1.5$ ). A comparison of density profiles based on the methods of numerical integration and perturbation expansion . . . . . 87
16. Burnett density profiles in a normal shock wave ( $M_1=2.0$ ). A comparison of density profiles based on the methods of numerical integration and perturbation expansion . . . . . 89

17.	Burnett density profiles in a normal shock wave ( $M_1=3.0$ ). A comparison of density profiles determined from the perturbation expansion . . . . .	91
18.	Burnett density profiles in a normal shock wave ( $M_1=1.0$ ). A comparison of density profiles determined from the perturbation expansion . . . . .	93
19.	Density asymmetry quotient ( $Q_\rho$ ) versus $M_1$ from the Burnett perturbation expansion. A comparison of the results for $Q_\rho$ based on the methods of perturbation expansion and numerical integration . . . . .	95
20.	Super-Burnett and Super-Super-Burnett density profiles in a normal shock wave ( $M_1=1.5$ ) . . . . .	98
21.	Super-Burnett and Super-Super-Burnett density profiles in a normal shock wave ( $M_1=2.0$ ) . . . . .	100
22.	Super-Burnett and Super-Super-Burnett density profiles in a normal shock wave ( $M_1=3.0$ ) . . . . .	102
23.	Super-Burnett and Super-Super Burnett density profiles in a normal shock wave ( $M_1=4.0$ ) . . . . .	104

24. Density asymmetry quotient ( $Q_\rho$ ) versus $M_1$ from the Super-Burnett and Super-Super-Burnett perturbation expansions . . . . .	106
25. Density asymmetry quotient ( $Q_\rho$ ) in a normal shock wave as a function of upstream Mach number ( $M_1$ ). A comparison of Navier-Stokes numerical integration (realistic potential) and third order perturbation (Maxwell molecules) results with experiment . . . .	111
26. Roots of the Navier-Stokes characteristic polynomial . . . . .	122
27. Roots of the Burnett characteristic polynomial . . . . .	123
28. Roots of the Super-Burnett characteristic polynomial . . . . .	124
29. Roots of the Super-Super-Burnett characteristic polynomial . . . . .	125

## CHAPTER I

### INTRODUCTION

The structure of a normal shock wave in a monatomic gas has been investigated extensively by theoreticians and experimentalists for many years. The shock wave may be represented as a one dimensional gasdynamic phenomenon in which large departures from thermodynamic equilibrium occur over a few mean free paths within the shock wave. The one dimensional shock wave should be completely described by the Boltzmann equation, if the Boltzmann equation is correct. But, because of the nonlinearity and complex nature of the collision integral, trustworthy solutions of the Boltzmann equation have been obtained only in cases close to equilibrium, and certainly not for strong shock waves.<sup>1</sup>

This effort is a theoretical investigation of the higher order gasdynamic equations for shock wave structure obtained by applying the well known Chapman-Enskog development to the Boltzmann equation through fourth order in spatial derivatives. The motivation

---

<sup>1</sup>The relative change in macroscopic variables over a local mean free path becomes appreciable even for modest upstream Mach numbers ( $M_1$ ). For example, for  $M_1 = 1.5$  the relative change in macroscopic variables over a local mean free path is less than 0.1, but for  $M_1 = 2.5$  the relative change in macroscopic variables over a local mean free path exceeds 0.4 in the interior of the shock wave. These estimates are based on numerical integration of the Navier-Stokes differential equations.

of this work is to strive toward a test of the nonlinear features of the Boltzmann equation, which has not been done before. The Chapman-Enskog development has been used because it has been shown to have quantitative physical significance beyond the Navier-Stokes level in studies of high frequency sound propagation.<sup>2</sup>

An additional motivation for using the Chapman-Enskog development has been the desire to reconcile conflicting opinions in the literature about its utility drawn from studies of high frequency sound waves<sup>3</sup> and weak shock waves.<sup>4</sup>

The gasdynamic equations derived and investigated in this report are for a gas of Maxwell molecules (inverse fifth power repulsion). The restriction to Maxwell molecules affords considerable mathematical simplification in the Boltzmann collision operator. Although such an idealized molecular model has analytical advantage, it cannot be expected to lead to decisive comparison with experiment. Nevertheless, it seems reasonable to hope that results for shock waves in a gas of Maxwell molecules may provide qualitative insights and guides to future work with a realistic potential, for such correspondence has been found for other phenomena.

---

<sup>2</sup>J. D. Foch Jr and G. W. Ford, in Studies in Statistical Mechanics, edited by J. de Boer and G. E. Uhlenbeck (North Holland, Amsterdam, 1970), Vol. V.

<sup>3</sup>C. S. Wang Chang and G. E. Uhlenbeck, in Studies in Statistical Mechanics, edited by J. de Boer and G. E. Uhlenbeck (North Holland, Amsterdam, 1970), Vol. V.

<sup>4</sup>L. Talbot and F. S. Sherman, NASA Memorandum 12-14-58W (1959); F. S. Sherman and L. Talbot, in Proceedings of the First International Symposium on Rarefied Gas Dynamics, edited by F. M. Devienne (New York: Pergamon, 1960), 161.



The Chapman-Enskog expansion applied to the Boltzmann equation yields successively the Euler (zeroth order), Navier-Stokes (first order), Burnett (second order), Super-Burnett (third order), Super-Super-Burnett (fourth order), ..... gasdynamic differential equations.

The derivation and solution of the Navier-Stokes equations are well documented in the literature.<sup>5</sup> Gilbarg and Paolucci<sup>6</sup> successfully integrated the first order equations, thus providing a practical method for constructing shock profiles from the differential equations. Standard Runge-Kutta numerical integration methods yield results for the variation of gas properties through the shock for any incident Mach number ( $M_1$ ).

The results of similar efforts applied to the Burnett differential equations were reported by Sherman and Talbot,<sup>7</sup> who found that numerical integration was successful only for Mach numbers less than about 2.1.<sup>8</sup> One of the early findings in the present work was that

---

<sup>5</sup>S. Chapman and T. G. Cowling, The Mathematical Theory of Non-Uniform Gases (Third edition, Cambridge University Press, 1970); W. G. Vincenti and C. H. Kruger Jr., Introduction to Physical Gas Dynamics (John Wiley & Sons, 1965); L. M. Schwartz and D. F. Hornig, Physics of Fluids 12, 1669 (1963); D. Gilbarg and D. Paolucci, Journal of Rational Mechanics and Analysis 2, 617 (1953).

<sup>6</sup>Gilbarg and Paolucci, Journal of Rational Mechanics, op. cit.

<sup>7</sup>Talbot and Sherman, NASA Memorandum, op. cit.; Sherman and Talbot, Proceedings of the First International Symposium, op. cit.

<sup>8</sup>The equations used by Sherman and Talbot contain an error, but the error has negligible effect on their results. In the expression for  $p_{xx}$  on page 28 of reference 2, and again on page 164 of reference 3, the coefficient of  $(\mu^2/p) \cdot (du/dx)^2$  is 40/27; it should be 8/9.

the Super-Burnett and Super-Super-Burnett equations are not amenable to conventional methods of numerical integration for any Mach number. Nevertheless, Montgomery<sup>9</sup> has reported a proof of the existence of shock wave solutions for the higher order gasdynamic equations for Mach numbers close to unity, although the uniqueness of these solutions is not yet established.

Recent experimental findings of Alsmeyer<sup>10</sup> and earlier findings of Schmidt<sup>11</sup> provide evidence of the inadequacy of the Navier-Stokes equations for describing shock wave structure. The discrepancy between the first order Navier-Stokes theory and experiment becomes conspicuous when the asymmetry  $Q_\rho$  of the normalized density profile  $R_\rho(z)$  is examined as a function of Mach number  $M_1$ . Following the conventions of Schmidt and Alsmeyer,  $R_\rho(z)$  and  $Q_\rho$  are defined according to the following relationships:

$$R_\rho(z) = \frac{\rho(z) - \rho_1}{\rho_2 - \rho_1} \quad (\text{I-1})$$

$$Q_\rho = \frac{\int_{-\infty}^0 R_\rho(z) dz}{\int_0^\infty [1 - R_\rho(z)] dz} \quad (\text{I-2})$$

In equation (I-1) the subscript 1 corresponds to conditions far upstream of the shock wave, and the subscript 2 corresponds to conditions far downstream of the shock wave. This notation and the

---

<sup>9</sup>J. T. Montgomery, Physics of Fluids 18, 148 (1975).

<sup>10</sup>H. Alsmeyer, to be published in Journal of Fluid Mechanics.

<sup>11</sup>B. Schmidt, Journal of Fluid Mechanics 39, 361 (1969).

choice of the origin of the coordinate system at the center of the density profile ( $R_\rho = 0.5$ ) are illustrated in Figure 1.

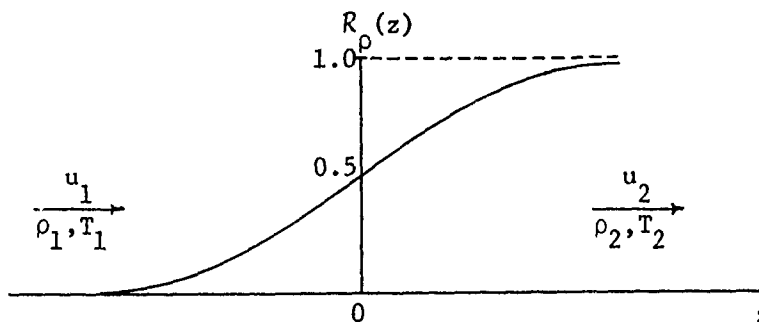


Figure 1 - Characteristic variation of the normalized density across a normal shock wave.

The Navier-Stokes theoretical result for  $Q_\rho$  based on a realistic potential (viscosity  $\mu \propto T^{0.68}$ ) and the data from electron beam measurements of  $R_\rho(z)$  (Schmidt 1969, Alsmeyer 1975) are plotted versus the upstream Mach number  $M_1$  in Figure 2. It is quite evident from Figure 2 that the Navier-Stokes theory gives unsatisfactory results even at low Mach numbers.

The failure of numerical integration methods to provide solutions to the higher order gasdynamic differential equations necessitated the development in this effort of an analytic (perturbation) method to obtain the solutions. The gas properties were sought as perturbation expansions, with the expansion parameter a suitable function of the shock Mach number. These perturbation methods were applied to yield successive approximations for gas property variations across the shock.

The numerical integration solutions for the Navier-Stokes and Burnett equations served as test cases for the perturbation

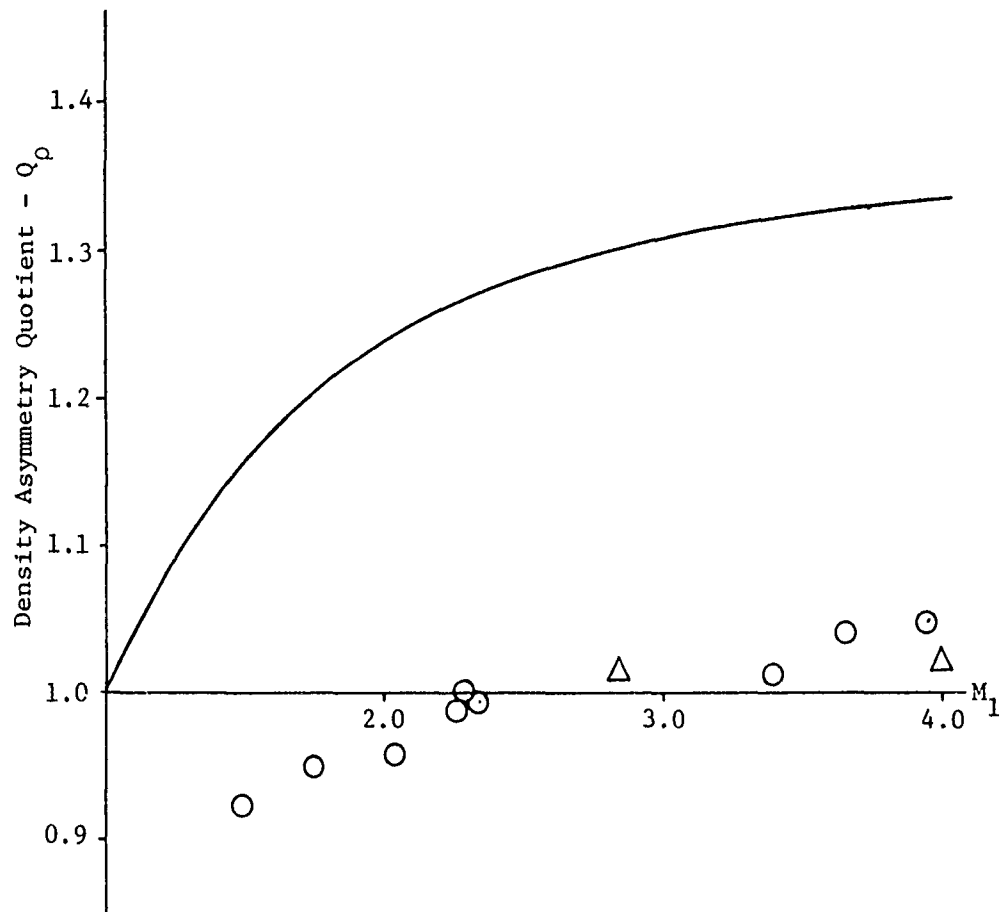


Figure 2 - Density asymmetry quotient ( $Q_\rho$ ) in a normal shock wave as a function of upstream Mach number ( $M_1$ ). A comparison of the Navier-Stokes numerical integration results for a realistic potential with experiment.

— Navier-Stokes numerical integration

⊙ Experiment - Alsmeyer (1975)

△ Experiment - Schmidt (1969)

expansions. Reasonable agreement between the results of the two approaches was obtained for the Navier-Stokes and Burnett equations and this agreement served as the rationale for carrying out the perturbation calculations for the higher order gasdynamic equations.

In addition to the authors already mentioned, some additional references are appropriate here to cite other theoretical and experimental efforts of relevance to this report. No attempt will be made to give an historical account of the extensive efforts of the many investigators of shock wave structure. For such an account, the reader is referred to a stimulating and thorough publication by Fiszdon<sup>12</sup> containing an extensive bibliography of some 150 theoretical and experimental references on the subject. In his paper, Fiszdon classifies the theoretical attempts to obtain solutions for shock structure as a) Continuum Gas Theories, b) Kinetic Models of the Boltzmann Collision Integral, c) Kinetic Models of the Distribution Functions, d) Monte Carlo Methods.

In the first theoretical class, the principal method is the application of the Chapman-Enskog development to the Boltzmann equation to obtain the constitutive gasdynamic relations for shock structure. In the second class, the BGK method<sup>13</sup> is one of the best known efforts to develop a simplified model of the Boltzmann

---

<sup>12</sup>W. Fiszdon, in Proceedings of the Ninth International Symposium on Rarefied Gas Dynamics, edited by E. Becker (Academic Press, 1974) 2, B.23.

<sup>13</sup>P. L. Bhatnagar, E. P. Gross, and M. Krook, Physical Review 94, 511 (1954).

collision integral. However, as Alsmeyer<sup>14</sup> reports, experimental results show clearly the failure of the BGK solutions even for low Mach numbers.

The bimodal velocity distribution function introduced by Mott-Smith<sup>15</sup> and the subsequent shock thickness calculations of Muckenfuss<sup>16</sup> are characteristic of the kinetic model investigations in the third theoretical class. The Mott-Smith method yields symmetric density profiles at all Mach numbers, whereas the experimental density profiles are asymmetric for all Mach numbers.

In recent years, some of the most interesting studies of shock structure have centered on the development of Monte Carlo techniques in an effort to find a solution of the complete Boltzmann equation. Hicks and Yen and their associates<sup>17</sup> have used Nordsieck's Monte Carlo method<sup>18</sup> to "solve" the Boltzmann equation for the plane steady

---

<sup>14</sup>Alsmeyer, op. cit.

<sup>15</sup>H. M. Mott-Smith, *Physical Review* 82, 885 (1951).

<sup>16</sup>C. Muckenfuss, *Physics of Fluids* 5, 1325 (1962).

<sup>17</sup>A. Nordsieck and B. L. Hicks, in Proceedings of the Fifth International Symposium on Rarefied Gas Dynamics, edited by C. L. Brundin (Academic Press, 1967) 1, 695; S. M. Yen, *Physics of Fluids* 9, 1417 (1966); B. L. Hicks and S. M. Yen, *Physics of Fluids* 10, 458 (1967); T. Holtz, E. P. Muntz, and S. M. Yen, *Physics of Fluids* 14, 545 (1971); S. M. Yen, *International Journal of Heat and Mass Transfer* 14, 1865 (1971); B. L. Hicks, S. M. Yen, and J. Reilly, *Journal of Fluid Mechanics* 53, 85 (1972); S. M. Yen, W. P. Walters, W. Ng, and J. R. Flood, in Proceedings of the Eighth International Symposium on Rarefield Gas Dynamics, edited by K. Karamcheti (Academic Press, 1974) 1, 137; S. M. Yen, W. Ng, R. M. Osten, and W. P. Walters, *Coordinated Science Laboratory Progress Report*, July 1971 through June 1972, August 1972; S. M. Yen and W. Ng, *Journal of Fluid Mechanics* 65, 127 (1974).

<sup>18</sup>Nordsieck and Hicks, op. cit.

shock wave. In an independent effort, Bird<sup>19</sup> has developed a Monte Carlo direct simulation method or numerical experiment in which he tracks, in physical space, the motions and interactions of the molecules across the shock. Bird<sup>20</sup> has claimed that his direct simulation method is entirely consistent with solving the Boltzmann equation.

The manifestly different stochastic techniques called Monte Carlo methods by Hicks, Yen and associates and by Bird yield substantially different quantitative results for the density profiles for both elastic spheres and Maxwell molecules. This conspicuous difference in the results for each of the molecular models is clearly illustrated in the references<sup>21</sup> and is attributed to the differences in the Monte Carlo method used.

The Monte Carlo methods have been reported to give the best agreement with experiment. In addition to the elastic sphere and Maxwell molecule data calculated by Hicks, Yen (et al.) and by Bird, Bird's method has been used to calculate shock profiles for a number of other repulsive intermolecular potentials. Schmidt<sup>22</sup> reported excellent agreement between his experimental results in argon and

---

<sup>19</sup>G. A. Bird, *Physics of Fluids* 6, 1518 (1963); G. A. Bird, in *Proceedings of the Fourth International Symposium on Rarefied Gas Dynamics*, edited by J. H. de Leeuw (Academic Press, 1965) 1, 216; G. A. Bird, *Journal of Fluid Mechanics* 30, 479 (1967); G. A. Bird, in *Proceedings of the Sixth International Symposium on Rarefied Gas Dynamics*, edited by L. Trilling and H. Y. Wachman (Academic Press, 1969) 1, 301; G. A. Bird, *Physics of Fluids* 13, 1172 and 2676 (1970).

<sup>20</sup>Bird, *Physics of Fluids* 13, op. cit.

<sup>21</sup>W. Fiszdon, op. cit.; Yen and Ng, op. cit.

<sup>22</sup>Schmidt, op. cit.

Bird's inverse twelfth-power force data at one Mach number ( $M_1 = 8.0$ ). In later experiments, Alsmeyer<sup>23</sup> indicates excellent agreement between his experimental data and the Bird Monte Carlo calculations for the inverse tenth-power force data for the complete range of Mach numbers up to  $M_1 = 9.0$ . Alsmeyer also suggests that it is reasonable to expect improved results from the Hicks and Yen method for more realistic intermolecular potentials.

In a recent effort to infer the intermolecular potential from shock structure, Sturtevant and Steinhilper<sup>24</sup> determined intermolecular potential parameters for four monatomic gases from accurate shock tube experiments using Bird's Monte Carlo results. The results indicate that the profiles are generally insensitive to different potentials at high Mach numbers. Reliable results at low Mach numbers are not yet available.

The present efforts to derive and solve higher order gas-dynamic equations of shock structure will be discussed briefly to summarize the developments given in the succeeding chapters of this report.

Chapter II includes the derivation of the higher order differential equations for the density (or velocity) and temperature as functions of distance through the shock wave. The conservation equations

---

<sup>23</sup>Alsmeyer, op. cit.

<sup>24</sup>B. Sturtevant and E. A. Steinhilper, in Proceedings of the Eighth International Symposium on Rarefied Gas Dynamics, edited by K. Karamcheti (Academic Press, 1974) 1, 159.



are given for conditions inside the shock and the higher order constitutive relationships are obtained from the Chapman-Enskog expansion applied to the Boltzmann equation. The derivation of the differential equations in each spatial order involves the determination of the corresponding heat flux and viscous stress contributions. The highest order of the spatial derivatives determined in these contributions specify the order of the corresponding differential equations.

Chapter III includes methods to solve the Navier-Stokes equations of shock structure. The standard numerical integration methods are presented, followed by the introduction of the perturbation technique which was developed to obtain solutions of the higher order differential equations. The perturbation method, though not specifically required to provide solutions of the Navier-Stokes equations, is introduced in Chapter III because the rationale for its applicability to the higher order developments is the same as that applied to the Navier-Stokes equations.

Chapter IV provides a discussion of the limitations of standard numerical integration methods in the Burnett and higher order developments. The results of the higher order perturbation calculations are presented, and a pattern is discerned among the resulting equations which reveals a formal similarity among the Navier-Stokes and higher order results.

In Chapter V, shock profiles obtained from the numerical integration and perturbation methods are presented and compared.

The utility of the perturbation method is evident from the relative agreement between the results of the two methods in the Navier-Stokes and Burnett ( $M_1 < 2.1$ ) developments.

Chapter VI provides a qualitative look at the present theoretical results for Maxwell molecules in light of recent experimental findings. The potential need and means for extending the perturbation method to higher orders are discussed as an outlook for future work.

## CHAPTER II

### HIGHER ORDERS OF THE CHAPMAN-ENSKOG

#### DEVELOPMENT FOR MAXWELL MOLECULES

##### Conservation Equations for the Steady State One Dimensional Normal Shock Wave

The higher order gasdynamic equations for a Maxwell gas will be derived from the Boltzmann equation in this chapter as a first step in the calculation of the structure of a normal shock wave. The derivation is patterned after the well known Chapman-Enskog development for solving the Boltzmann equation in successive approximation.

The starting point for the Chapman-Enskog development is the Boltzmann equation for the velocity distribution function  $f(\vec{r}, \vec{v}, t)$ ,

$$\frac{\partial f}{\partial t} = -v_1 \frac{\partial f}{\partial r_1} + \int_{v_1} d\vec{v}_1 \int d\Omega g \sigma(g, \chi) [f' f'_1 - f f_1]. \quad (\text{II-1})$$

The first term on the right gives the rate of change of molecules of velocity class  $v$  which are contained in a specific volume element of physical space with velocity in a specific volume element of velocity space due to free flight. The integral on the right-hand side provides the rate of change of molecules of velocity class  $v$  due to collisions with other molecules. The integral sum of all encounters with molecules (specified as class  $v_1$ ) includes the collisional processes which either replenish or deplete the molecular

count in the volume elements of the physical and velocity space. The velocity distribution functions  $f$  and  $f_1$  in the collision integral are representative of conditions both prior to (unprimed) and after (primed) collision.

In the collision integral  $g$  is  $|\vec{v} - \vec{v}_1|$ , and  $\sigma(g, \chi)$  is the differential cross section for an encounter in which the relative velocity vector is turned or scattered through an angle  $\chi$  into the element of solid angle  $d\Omega$ . For a gas consisting of atoms of mass  $m$  interacting with an intermolecular potential  $\phi(r) = \frac{\kappa}{r^4}$ , the expression for the cross section is written as

$$g\sigma(g, \chi) = \left(\frac{2\kappa}{m}\right)^{\frac{1}{2}} F(\chi). \quad (\text{II-2})$$

Such a (fictitious) gas was considered by Maxwell, and is referred to as the Maxwell model.

To develop the Chapman-Enskog expansion for departures from the equilibrium condition, the velocity distribution function is sought in the form

$$f = f^{(0)} + f^{(1)} + f^{(2)} + \dots \quad (\text{II-3})$$

where  $f^{(0)}$  is the local Maxwell distribution,  $f^{(1)}$  is proportional to spatial derivatives,  $f^{(2)}$  is proportional to squares of spatial derivatives and second derivatives, etc. The local equilibrium distribution  $f^{(0)}$  is given by

$$f^{(0)} = n \left(\frac{m}{2\pi kT}\right)^{\frac{3}{2}} \exp\left\{-\frac{m}{2kT} (\vec{v} - \vec{u})^2\right\} \quad (\text{II-4})$$

where  $m$  is the molecular mass,  $n$  is the local molecular number density,  $T$  is the local gas temperature, and  $k$  is Boltzmann's constant.

The expression  $(\vec{v} - \vec{u})$  is called the peculiar or thermal velocity of the gas, is denoted by  $\vec{V}$ , and is equal to the difference between the molecular velocity ( $\vec{v}$ ) and the mean flow velocity of the molecules ( $\vec{u}$ ). The combination  $(\frac{m}{2kT})^{\frac{1}{2}}$  has dimensions of (1/velocity) and will be employed frequently in nondimensionalizing velocity terms throughout this work.

Using the Boltzmann equation, as presented above, and taking moments with respect to  $v$  of 1,  $v$ , and  $\frac{1}{2} v^2$  yields the one-dimensional conservation equations for the normal shock wave. The mean gas flow direction is taken along the  $Z$ -coordinate. Detailed treatments of the moment calculations are plentiful in the literature<sup>1</sup> and will not be repeated in this report. The results are given below.

MASS:

$$\frac{\partial n}{\partial t} + u \frac{\partial n}{\partial z} + n \frac{\partial u}{\partial z} = 0 \quad (\text{II-5})$$

MOMENTUM:

$$\frac{\partial u}{\partial t} + u \frac{\partial u}{\partial z} + \frac{1}{nm} \frac{\partial p}{\partial z} = 0 \quad (\text{II-6})$$

ENERGY:

$$\frac{3}{2} nk \left( \frac{\partial T}{\partial t} + u \frac{\partial T}{\partial z} \right) + \frac{\partial q}{\partial z} + p \frac{\partial u}{\partial z} = 0 \quad (\text{II-7})$$

---

<sup>1</sup>J. D. Foch Jr. and G. W. Ford, in Studies in Statistical Mechanics, edited by J. de Boer and G. E. Uhlenbeck (North Holland, Amsterdam, 1970), Vol. V; S. Chapman and T. G. Cowling, The Mathematical Theory of Non-Uniform Gases (Third edition, Cambridge University Press, 1970); W. G. Vincenti and C. H. Kruger Jr., Introduction to Physical Gas Dynamics (John Wiley & Sons, 1965).

In these equations

$$P = P(z, t) \equiv \int d\vec{V} f m v_z^2 \quad (\text{II-8})$$

and

$$q = q(z, t) \equiv \int d\vec{V} f \frac{m}{2} v^2 v_z \quad (\text{II-9})$$

where  $P$  is the pressure minus the viscous stress and  $q$  is the heat flux.

The steady state equations for a normal shock wave are easily found from the above by neglecting the time derivatives and noting that the momentum equation can be used in the energy equation to form an exact energy differential equation. Since, in steady state, all three differential equations are exact, each equation can be integrated once to give the results below.

MASS:

$$\rho u = \rho_1 u_1 \quad (\text{II-5a})$$

MOMENTUM:

$$\rho u^2 + P = \rho_1 u_1^2 + n_1 k T_1 \quad (\text{II-6a})$$

ENERGY:

$$\left( \frac{3}{2} \frac{k}{m} T + \frac{u^2}{2} \right) \rho u + uP + q = \left( \frac{5}{2} \frac{k}{m} T_1 + \frac{u_1^2}{2} \right) \rho_1 u_1 \quad (\text{II-7a})$$

In these equations  $\rho$  is the mass density. The quantities on the right-hand sides of the equations are integration constants, evaluated either upstream ( $i = 1$ ) or downstream ( $i = 2$ ), which represent the constant fluxes of mass, momentum, and energy. Equations (II-5a), (II-6a), and (II-7a) describe the shock wave illustrated in Figure 1.

# Alternate Forms of the Viscous Stress and Heat Flux for the Higher Order Developments

The uniformity expansion for the velocity distribution function induces uniformity expansions for the heat flux  $q_i$  and stress  $P_{ij}$ , which reduce in the one-dimensional case to  $q_z$  and  $P_{zz}$ , or simply  $q$  and  $P$ . Following methods employed in the Chapman-Enskog solution of the Boltzmann equation, the velocity distribution function is further defined in the following expanded series form:

$$f = f^{(0)} \left( 1 + \phi^{(1)} + \phi^{(2)} + \phi^{(3)} + \dots \right)^{\dagger} \quad (\text{II-10})$$

In zeroth order,  $f = f^{(0)}$ , which implies  $q = 0$  and  $P = nkT$ , and the conservation equations reduce to the equations of equilibrium flow. The inclusion of the higher order contributions to  $f$  leads to the Navier-Stokes, Burnett, and higher order macroscopic equations of gas dynamics.

Again following Chapman and Enskog, the following requirements will be imposed in the development:

$$\int d\vec{v} f^{(n)} = 0, \quad n \geq 1 \quad (\text{II-11})$$

$$\int d\vec{v} f^{(n)} v_z = 0, \quad n \geq 1 \quad (\text{II-12})$$

$$\int d\vec{v} f^{(n)} v^2 = 0, \quad n \geq 1. \quad (\text{II-13})$$

These requirements are consistent with the equilibrium solution but are not necessitated by it. The requirements will introduce some

---

<sup>†</sup>Note: For clarity in expressing the results of the moment calculations throughout the remainder of this chapter, the arguments  $(v)$  and  $(v_1)$  for the velocity distribution functions have been omitted in the equations.

very effective simplifications in the host of moment calculations which are required to determine the gasdynamic forms of  $P$  and  $q$ .

It is convenient to express the integral requirements (II-11), (II-12), and (II-13) in terms of the peculiar velocity  $\vec{V}$ :

$$\int d\vec{V} f^{(n)} = 0, \quad n \geq 1 \quad (\text{II-11a})$$

$$\int d\vec{V} f^{(n)} \vec{V} = 0, \quad n \geq 1 \quad (\text{II-12a})$$

$$\int d\vec{V} f^{(n)} V = 0, \quad n \geq 1. \quad (\text{II-13a})$$

Introducing the expanded form for the velocity distribution function in (II-8) and (II-9), the latter expressions give

$$P = nkT + P^{(1)} + P^{(2)} + P^{(3)} + \dots, \quad (\text{II-14})$$

$$q = q^{(1)} + q^{(2)} + q^{(3)} + \dots, \quad (\text{II-15})$$

where

$$P^{(n)} = \int d\vec{V} f^{(n)} m V_z^2, \quad n \geq 1, \quad (\text{II-16})$$

$$q^{(n)} = \int d\vec{V} f^{(n)} \frac{m}{2} V^2 V_z, \quad n \geq 1. \quad (\text{II-17})$$

With the aid of (II-12a) and (II-13a) the expressions for (II-16) and (II-17) may also be written in the form

$$P^{(n)} = \frac{2}{3} \int d\vec{V} f^{(n)} m \left( \frac{3}{2} V_z^2 - \frac{V^2}{2} \right), \quad (\text{II-18})$$

$$q^{(n)} = - \int d\vec{V} f^{(n)} \frac{m}{2} \left( \frac{5}{2} V_z - V^2 V_z \right), \quad (\text{II-19})$$

where the equality of  $d\vec{v}$  and  $d\vec{V}$  in velocity space has been employed. The velocity forms in (II-18) and (II-19), nondimensionalized by factors of  $\left( \frac{m}{2kT} \right)^{\frac{1}{2}}$ , are eigenfunctions associated with the linearized collision operator for Maxwell molecules. These and other



eigenfunctions (and their eigenvalues) are tabulated in Appendix A.

Using  $\vec{c} = \left(\frac{m}{2kT}\right)^{1/2} \vec{v}$  and the notation of Appendix A leads to

$$P^{(n)} = \frac{4}{3} nkT \frac{1}{\pi^{3/2}} \int d\vec{c} e^{-c^2} \phi^{(n)} \psi_{02}(\vec{c}), \quad (\text{II-20})$$

$$q^{(n)} = -nkT \left(\frac{2kT}{m}\right)^{1/2} \frac{1}{\pi^{3/2}} \int d\vec{c} e^{-c^2} \phi^{(n)} \psi_{11}(\vec{c}). \quad (\text{II-21})$$

### Spatially Ordered Equations Derived from the Expanded Velocity Distribution Function Applied to the Boltzmann Equation

The developments which follow in the remaining sections of this chapter involve solution of the Boltzmann equation using the expanded form of the velocity distribution function through  $f^{(4)} = f^{(0)} \phi^{(4)}$ , but only to the extent necessary to determine  $P$  and  $q$  through  $P^{(4)}$  and  $q^{(4)}$ .

In applying the full Chapman-Enskog method to the solution of the Boltzmann equation, the usual procedure is to substitute expanded forms of the velocity distribution (i.e.,  $f = f^{(0)}$ ,  $f = f^{(0)} + f^{(1)}$ , ... etc.) into both sides of the equation and, in successive approximation, solve for the  $\phi^{(n)}$ . Subsequently, the  $\phi^{(n)}$  are used in the integrals which define  $P^{(n)}$  and  $q^{(n)}$ .

The present effort has been designed to circumvent complete determination of the  $\phi^{(n)}$ , since the required expressions for the viscous stress and heat flux contributions may be obtained by less cumbersome means.

In the present effort, as in the Chapman-Enskog method, an essential point is the elimination of substantial derivatives of

density, flow velocity, and temperature in favor of spatial derivatives using conservation equations (II-5), (II-6), and (II-7). It is this point, as will become apparent subsequently, that leads to dependence of the  $f^{(n)}$  on spatial derivatives.

By suitably expanding the expressions involving  $f$  and  $f_1$  in the collision integral, contributions involving the  $\phi^{(n)}$  may be separated according to the order of their spatial derivatives.

Once the ordering exercise is complete for each term in the Boltzmann equation, the ordered contributions on the left and right-hand sides are equated, giving a series of equations based on the order of the spatial derivatives. After some preliminary rearrangements, the resulting equations are in suitable format for calculating moments involving specific  $\phi(v)$ , such as those occurring in the definitions of  $P$  and  $q$ . The "selected"  $\phi(v)$  consist of only those velocity functions which are indispensable for calculating the  $P^{(n)}$  and  $q^{(n)}$ .

As will be seen, the working equations employed in this method have considerable utility in that they allow the calculation of  $P^{(n)}$  and  $q^{(n)}$  from lower order moments involving only a few eigenfunctions such as  $\psi_{02}(\vec{c})$  and  $\psi_{11}(\vec{c})$ . In most cases, the lower order moments needed in a given order are already known from the previous orders. However, each new order does introduce a few new moments which must be evaluated. Even so, the explicit forms of the  $\phi^{(n)}$  need not be known for any of the higher order work in determining the heat flux and viscous stress contributions. In fact,

once the lower order moments have been calculated, the remaining effort requires only a very careful algebraic exercise.

To carry out the specific calculations as outlined above, the one-dimensional form of the Boltzmann equation is written as

$$\frac{\partial f}{\partial t} + v_z \frac{\partial f}{\partial z} = \int_{v_1} d\vec{v}_1 \int d\Omega \left( \frac{2\kappa}{m} \right)^{\frac{1}{2}} F(\chi) [f'f'_1 - ff_1] , \quad (\text{II-22})$$

where, to repeat the differential scattering cross section for Maxwell molecules

$$\sigma(g, \chi) = \left( \frac{2\kappa}{m} \right)^{\frac{1}{2}} \frac{F(\chi)}{g} . \quad (\text{II-23})$$

The time derivative of the velocity distribution becomes

$$\begin{aligned} \frac{\partial f}{\partial t} = & f^{(0)} \frac{\partial}{\partial t} \left[ 1 + \phi^{(1)} + \phi^{(2)} + \phi^{(3)} + \dots \right] \\ & + \left[ 1 + \phi^{(1)} + \phi^{(2)} + \phi^{(3)} + \dots \right] \frac{\partial f^{(0)}}{\partial t} \end{aligned} \quad (\text{II-24})$$

and the streaming term can be expressed as

$$\begin{aligned} v_z \frac{\partial f}{\partial z} = & (u + v_z) f^{(0)} \frac{\partial}{\partial z} \left[ 1 + \phi^{(1)} + \phi^{(2)} + \phi^{(3)} + \dots \right] \\ & + (u + v_z) \left[ 1 + \phi^{(1)} + \phi^{(2)} + \phi^{(3)} + \dots \right] \frac{\partial f^{(0)}}{\partial z} . \end{aligned} \quad (\text{II-25})$$

With  $\phi^{(n)}$  of order  $n$  in spatial derivatives, the left-hand side of the Boltzmann equation, (II-22), may be rearranged according to the order of the spatial derivatives as

$$\begin{aligned}
\frac{\partial f}{\partial t} + v_z \frac{\partial f}{\partial z} = & \left\{ \frac{D_1 f^{(0)}}{dt} + v_z \frac{\partial f^{(0)}}{\partial z} \right\}_1 \\
& + \left\{ \frac{D_2}{Dt} \left[ f^{(0)} + f^{(0)} \phi^{(1)} \right] + v_z \frac{\partial}{\partial z} \left[ f^{(0)} \phi^{(1)} \right] \right\}_2 \\
& + \left\{ \frac{D_3}{Dt} \left[ f^{(0)} + f^{(0)} \phi^{(1)} + f^{(0)} \phi^{(2)} \right] + v_z \frac{\partial}{\partial z} \left[ f^{(0)} \phi^{(2)} \right] \right\}_3 \\
& + \left\{ \frac{D_4}{Dt} \left[ f^{(0)} + f^{(0)} \phi^{(1)} + f^{(0)} \phi^{(2)} + f^{(0)} \phi^{(3)} \right] + v_z \frac{\partial}{\partial z} \left[ f^{(0)} \phi^{(3)} \right] \right\}_4 \\
& + \dots,
\end{aligned} \tag{II-26}$$

where  $\frac{Dk}{Dt}$  represents the  $k$ th order part (in the sense of spatial derivatives) of the substantial derivative of the quantity differentiated. Similarly,  $\{ \}_k$  means all terms within the enclosure that are of order  $k$ .

Substitution of  $f$  and  $f_1$  in the collision term results in a similar ordering according to the order of the spatial derivatives of the  $\phi^{(n)}$ . Since, in local equilibrium, the products of the distribution functions before and after collision are equal as a consequence of conservation of energy and momentum (i.e.,  $f^{(0)} f_1^{(0)'} = f^{(0)} f_1^{(0)}$ ), the spatially ordered form of the collision integral may be arranged as

$$\begin{aligned}
& \int_{V_1} d\vec{v}_1 \int d\Omega \left( \frac{2\kappa}{m} \right)^{\frac{1}{2}} F(\chi) \left[ f' f_1' - f f_1 \right] = \\
& \int_{V_1} d\vec{v}_1 \int d\Omega \left( \frac{2\kappa}{m} \right)^{\frac{1}{2}} F(\chi) f^{(0)} f_1^{(0)} \left[ \left\{ \phi^{(1)'} + \phi_1^{(1)'} - \phi^{(1)} - \phi_1^{(1)} \right\}_1 \right. \\
& \left. + \left\{ \phi^{(2)'} + \phi_1^{(2)'} + \phi^{(1)'} \phi_1^{(1)'} - \phi^{(2)} - \phi_1^{(2)} - \phi^{(1)} \phi_1^{(1)} \right\}_2 \right]
\end{aligned}$$

$$\begin{aligned}
& + \left\{ \phi^{(3)'} + \phi_1^{(3)'} + \phi^{(2)'} \phi_1^{(1)'} + \phi_1^{(2)'} \phi^{(1)'} - \phi^{(3)} - \phi_1^{(3)} - \phi^{(2)} \phi_1^{(1)} - \phi_1^{(2)} \phi^{(1)} \right\}_3 \\
& + \left\{ \phi^{(4)'} + \phi_1^{(4)'} + \phi^{(3)'} \phi_1^{(1)'} + \phi^{(1)'} \phi_1^{(3)'} + \phi_1^{(2)'} \phi^{(2)'} \right. \\
& \quad \left. - \phi^{(4)} - \phi_1^{(4)} - \phi^{(3)} \phi_1^{(1)} - \phi^{(1)} \phi_1^{(3)} - \phi_1^{(2)} \phi^{(2)} \right\}_4 + \dots \quad (II-27)
\end{aligned}$$

Equating the spatially ordered expressions in (II-26) and (II-27) leads to the basic equations for determining  $P^{(n)}$  and  $q^{(n)}$ .

#### Determination of $P^{(1)}$ and $q^{(1)}$

The first-order calculations required to obtain  $P^{(1)}$  and  $q^{(1)}$  require the evaluation of the derivatives and the associated integrals which arise from the first-order terms in (II-26) and (II-27).

In preparation for the evaluation of the substantial and spatial derivative expressions which will be used throughout the remainder of this chapter, the following preliminary relationships will be helpful.

Starting with the equation for the equilibrium distribution

$$f^{(0)} = n \left( \frac{m}{2\pi kT} \right)^{3/2} \exp \left\{ - \frac{m}{2kT} \left[ v_x^2 + v_y^2 + (v_z - u)^2 \right] \right\}, \quad (II-28)$$

the substantial derivative  $\frac{Df^{(0)}}{Dt}$  may be conveniently obtained from

$$\left( \frac{\partial}{\partial t} + u \frac{\partial}{\partial z} \right) n f^{(0)} = \frac{1}{f^{(0)}} \left( \frac{\partial}{\partial t} + u \frac{\partial}{\partial z} \right) f^{(0)}, \quad (II-29)$$

with

$$\begin{aligned} \ln f^{(0)} = \ln n + \frac{3}{2} \ln \left( \frac{m}{2\pi k} \right) - \frac{3}{2} \ln T \\ - \frac{m}{2kT} \left[ v_x^2 + v_y^2 + (v_z - u)^2 \right]. \end{aligned} \quad (\text{II-30})$$

The resulting substantial derivative may be expressed in the form

$$\frac{Df}{Dt}^{(0)} = f^{(0)} \left[ \frac{1}{n} \frac{Dn}{Dt} - \frac{1}{T} \left( \frac{3}{2} - \frac{mV^2}{2kT} \right) \frac{DT}{Dt} + 2 \left( \frac{mV_z}{2kT} \right) \frac{Du}{Dt} \right]. \quad (\text{II-31})$$

Converting to dimensionless velocity forms and recognizing from the tables for the  $\Psi_{r\ell}(\vec{c})$  in Appendix A that

$$\Psi_{00}(\vec{c}) = 1, \quad (\text{II-32a})$$

$$\Psi_{10}(\vec{c}) = \left( \frac{3}{2} - c^2 \right), \quad (\text{II-32b})$$

$$\Psi_{01}(\vec{c}) = c_z, \quad (\text{II-32c})$$

the substantial derivative may be further expressed as

$$\begin{aligned} \frac{Df}{Dt}^{(0)} = f^{(0)} \left[ \Psi_{00}(\vec{c}) \frac{1}{n} \frac{Dn}{Dt} - \Psi_{10}(\vec{c}) \frac{1}{T} \frac{DT}{Dt} \right. \\ \left. + 2 \left( \frac{m}{2kT} \right)^{1/2} \Psi_{01}(\vec{c}) \frac{Du}{Dt} \right]. \end{aligned} \quad (\text{II-33})$$

Similar operations on the remaining spatial derivative term of equation (II-26) yields

$$\begin{aligned} v_z \frac{\partial f^{(0)}}{\partial z} = f^{(0)} \left\{ \Psi_{01}(\vec{c}) \left( \frac{2kT}{m} \right)^{1/2} \frac{1}{n} \frac{\partial n}{\partial z} + \left[ \Psi_{01}(\vec{c}) - \Psi_{11}(\vec{c}) \right] \left( \frac{2kT}{m} \right)^{1/2} \frac{1}{T} \frac{\partial T}{\partial z} \right. \\ \left. + 2 \left[ \frac{1}{2} \Psi_{00}(\vec{c}) - \frac{1}{3} \Psi_{10}(\vec{c}) + \frac{2}{3} \Psi_{02}(\vec{c}) \right] \frac{\partial u}{\partial z} \right\}. \end{aligned} \quad (\text{II-34})$$

The above result requires some "construction" of the terms  $\Psi_{r\ell}(\vec{c})$  from the dimensionless velocity forms.

To assist in examining the order of the contributions in the conservation equations as applied to the substantial derivatives in (II-33), the conservation equations are written below so as to isolate the substantial derivatives on one side of the equation. For later reference, the spatial order of each term is entered above the term, taking into account the final order of the term after carrying out the differentiations and multiplications indicated.

$$\frac{Dn}{Dt} = -n \frac{\partial u}{\partial z} \quad (II-35)$$

$$\begin{aligned} \frac{Du}{Dt} = & -\frac{kT}{m} \left( \frac{1}{T} \frac{\partial T}{\partial z} \right) - \frac{kT}{m} \frac{1}{n} \left( \frac{\partial n}{\partial z} \right) \\ & - \frac{1}{nm} \frac{\partial}{\partial z} \left[ P^{(1)} + P^{(2)} + P^{(3)} + P^{(4)} + \dots \right] \end{aligned} \quad (II-36)$$

$$\begin{aligned} \frac{DT}{Dt} = & -\frac{2}{3} T \frac{\partial u}{\partial z} - \frac{2}{3nk} \left[ P^{(1)} + P^{(2)} + P^{(3)} + P^{(4)} + \dots \right] \frac{\partial u}{\partial z} \\ & - \frac{2}{3nk} \frac{\partial}{\partial z} \left[ q^{(1)} + q^{(2)} + q^{(3)} + q^{(4)} + \dots \right] \end{aligned} \quad (II-37)$$

The first-order part of (II-26) is constructed from the first-order part of (II-33) and this involves contributions from all three of the above equations. Summing the contributions from (II-33) and (II-34) yields

$$\frac{D_1 f^{(0)}}{Dt} + v_z \frac{\partial f^{(0)}}{\partial z} = f^{(0)} \left\{ \frac{4}{3} \left[ \Psi_{02}(\vec{c}) \right] \frac{\partial u}{\partial z} - \left( \frac{2kT}{m} \right)^{1/2} \left[ \Psi_{11}(\vec{c}) \right] \frac{1}{T} \frac{\partial T}{\partial z} \right\}. \quad (II-38)$$

The remaining work to determine the explicit forms of  $p^{(1)}$  and  $q^{(1)}$  involves the evaluation of the first-order part of the collision integral given in (II-27), which is written below as

$$\int_{v_1} d\vec{v}_1 \int d\Omega \left( \frac{2\kappa}{m} \right)^{1/2} F(\chi) f^{(0)}(v) f_1^{(0)}(v_1) \Delta \left[ \phi^{(1)} \right], \quad (\text{II-39})$$

where

$$\Delta \phi^{(1)} \equiv \phi^{(1)'} + \phi_1^{(1)'} - \phi^{(1)} - \phi_1^{(1)},$$

$$d\vec{v}_1 = d\vec{v}_1,$$

and  $f^{(0)}(v)$  is independent of the integration over  $v_1$ .

Expression (II-39) is  $f^{(0)}(v)$  times the linearized collision operator  $J$  which, when operating on the various  $\psi_{r\ell}(\vec{c})$  introduced earlier, yields

$$J \left[ \psi_{r\ell}(\vec{c}) \right] = \varepsilon_{r\ell} \left[ \psi_{r\ell}(\vec{c}) \right].$$

Here,  $J$  has been defined by

$$J \left[ \psi_{r\ell}(\vec{c}) \right] \equiv \int_{v_1} d\vec{v}_1 \int d\Omega \left( \frac{2\kappa}{m} \right)^{1/2} F(\chi) f_1^{(0)} \Delta \left[ \psi_{r\ell}(\vec{c}) \right]. \quad (\text{II-40})$$

Appendix A provides the following results:

$$\frac{1}{\pi^{3/2}} \int d\vec{c}_1 e^{-c_1^2} \int d\Omega F(\chi) \Delta \left[ \psi_{11}(\vec{c}) \right] = -\pi \tilde{A}_2 \left[ \psi_{11}(\vec{c}) \right] \left( \frac{m}{2\kappa} \right)^{1/2} \quad (\text{II-41})$$

$$\frac{1}{\pi^{3/2}} \int d\vec{c}_1 e^{-c_1^2} \int d\Omega F(\chi) \Delta \left[ \psi_{02}(\vec{c}) \right] = -\frac{3}{2} \pi \tilde{A}_2 \left[ \psi_{02}(\vec{c}) \right] \left( \frac{m}{2\kappa} \right)^{1/2} \quad (\text{II-42})$$

In the above  $\tilde{A}_2$  is a pure number determined from

$$\tilde{A}_2 = \int_0^\pi d\chi \sin\chi (1 - \cos^2\chi) F(\chi)$$

and  $\chi$  is the deflection angle associated with binary collisions.



A comparison of (II-41) and (II-42) with (II-38) shows that

$$\phi^{(1)} = \frac{\left(\frac{m}{2\kappa}\right)^{1/2}}{n} \left\{ -\frac{1}{\epsilon_{11}} [\psi_{11}(\vec{c})] \frac{\left(\frac{2kT}{m}\right)^{1/2}}{T} \frac{\partial T}{\partial z} + \frac{4}{3\epsilon_{02}} [\psi_{02}(\vec{c})] \frac{\partial u}{\partial z} \right\} \quad (\text{II-43})$$

where  $\epsilon_{11} = -\pi\tilde{A}_2$  and  $\epsilon_{02} = -\frac{3}{2}\pi\tilde{A}_2$  are the eigenvalues corresponding to  $\psi_{11}(\vec{c})$  and  $\psi_{02}(\vec{c})$ .

Knowing  $\phi^{(1)}$ , the first-order contributions to the viscous stress and heat flux may also be determined from the definitions (II-20) and (II-21). From the orthogonality of the  $\psi_{r\ell}(\vec{c})$  it follows that

$$\begin{aligned} P^{(1)} &= -\frac{4}{3} nkT \frac{\left(\frac{m}{2\kappa}\right)^{1/2}}{n\epsilon_{02}} \left[ \frac{4}{3} \frac{\partial u}{\partial z} \right] - \frac{1}{\pi^{3/2}} \int d\vec{c} \, \vec{c}^2 [\psi_{02}(\vec{c})]^2, \\ &= -\frac{8}{9} kT \frac{\left(\frac{m}{2\kappa}\right)^{1/2}}{\pi\tilde{A}_2} \frac{\partial u}{\partial z}, \end{aligned} \quad (\text{II-44})$$

where the integral is of a type tabulated in Appendix A.

Introducing the abbreviation

$$\mu = \frac{2}{3} kT \frac{\left(\frac{m}{2\kappa}\right)^{1/2}}{\pi\tilde{A}_2}, \quad (\text{II-45})$$

the first-order viscous stress term may be written as

$$P^{(1)} = -\frac{4}{3} \mu \frac{\partial u}{\partial z}, \quad (\text{II-46})$$

with  $\mu$  recognizable as the gas viscosity.

A similar calculation gives the first-order heat flux term

$$q^{(1)} = -\frac{5}{2} \frac{k^2 T}{m} \frac{\left(\frac{m}{2\kappa}\right)^{1/2}}{\pi\tilde{A}_2} \frac{\partial T}{\partial z}, \quad (\text{II-47})$$

or

$$q^{(1)} = -K \frac{\partial T}{\partial z}, \quad (\text{II-48})$$

with the thermal conductivity  $K$  defined by

$$K = \frac{15}{4} \frac{k}{m} \mu. \quad (\text{II-49})$$

Determination of  $P^{(2)}$  and  $q^{(2)}$

The integral equation for  $\phi^{(2)}$  is composed of the second-order parts of (II-26) and (II-27). Separating the collision integrals which involve  $\phi^{(2)}$  from those which involve  $\phi^{(1)}$  the expressions for  $P^{(2)}$  and  $q^{(2)}$  can be determined from

$$\begin{aligned} & \int_{v_1} d\vec{v}_1 \int d\Omega \left( \frac{2K}{m} \right)^{1/2} F(\chi) f^{(0)}(v) f_1^{(0)}(v_1) \left[ \phi^{(2)'} + \phi_1^{(2)'} - \phi^{(2)} - \phi_1^{(2)} \right] = \\ & - \int_{v_1} d\vec{v}_1 \int d\Omega \left( \frac{2K}{m} \right)^{1/2} F(\chi) f^{(0)}(v) f_1^{(0)}(v_1) \left[ \phi^{(1)'} \phi_1^{(1)'} - \phi^{(1)} \phi_1^{(1)} \right] \\ & + \frac{D_2}{Dt} \left[ f^{(0)} \phi^{(1)} \right] + \frac{D_2 f^{(0)}}{Dt} + v_z \frac{\partial}{\partial z} \left[ f^{(0)} \phi^{(1)} \right]. \end{aligned} \quad (\text{II-50})$$

In order to determine  $P^{(2)}$  without solving explicitly for  $\phi^{(2)}$ , multiply (II-50) by  $mV_z^2$ , integrate over all  $\vec{v}$ , and use the H-Theorem transformations on the collision integrals. These operations yield

$$\begin{aligned}
& \int_{\mathbf{v}} d\vec{v} f^{(0)} \phi^{(2)} \int_{\mathbf{v}_1} d\vec{v}_1 f_1^{(0)} \int d\Omega \left( \frac{2\kappa}{m} \right)^{\frac{1}{2}} F(\chi) m \Delta \left[ v_z^2 \right] = \\
& - \frac{1}{2} \int_{\mathbf{v}} d\vec{v} f^{(0)} \phi^{(1)} \int_{\mathbf{v}_1} d\vec{v}_1 f_1^{(0)} \phi_1^{(1)} \int d\Omega \left( \frac{2\kappa}{m} \right)^{\frac{1}{2}} F(\chi) m \Delta \left[ v_z^2 \right] \\
& + \int_{\mathbf{v}} d\vec{v} m v_z^2 \frac{D_2}{Dt} (f^{(0)} \phi^{(1)}) + \int_{\mathbf{v}} d\vec{v} m v_z^3 \frac{\partial}{\partial z} (f^{(0)} \phi^{(1)}) \\
& + \int_{\mathbf{v}} d\vec{v} m v_z^2 \frac{D_2 f^{(0)}}{dt} , \tag{II-51}
\end{aligned}$$

where, for any  $\Psi(\vec{v})$ ,

$$\Delta[\Psi] = [\Psi' + \Psi_1' - \Psi - \Psi_1] .$$

Using the explicit results for the relationship between  $\mathbf{v}'$ ,  $\mathbf{v}_1'$  and  $\mathbf{v}$ ,  $\mathbf{v}_1$  (from the dynamics of binary collisions), integration over the solid angle in the collision integrals of (II-51) may be effected with the result that

$$\begin{aligned}
& \int d\Omega F(\chi) m \Delta \left[ v_z^2 \right] = m \int_0^\pi d\chi \sin\chi (1 - \cos^2\chi) F(\chi) \cdot \\
& \left\{ - \frac{3\pi}{2} \left[ \left( v_z^2 - \frac{1}{3} v^2 \right) + \left( v_{1z}^2 - \frac{1}{3} v_1^2 \right) - 2v_z v_{1z} + \frac{2}{3} \vec{v} \cdot \vec{v}_1 \right] \right\} . \tag{II-52}
\end{aligned}$$

Several of the terms of the right-hand side of (II-52) do not survive the subsequent integration over  $\vec{v}$  and  $\vec{v}_1$ , either because they occur as odd functions of velocity times the even function  $f^{(0)}$ , or because of the requirements (II-11), (II-12), or II-13). Thus, the collision integral on the left-hand side of (II-51) reduces to

$$\int_{\mathbf{v}} d\mathbf{v} f^{(0)} \phi^{(2)} \int_{\mathbf{v}_1} d\mathbf{v}_1 f_1^{(0)} \int d\Omega \left( \frac{2\kappa}{m} \right)^{\frac{1}{2}} F(\chi)_{m\Delta} \left[ \frac{v_z^2}{z} \right] =$$

$$- \frac{3}{2} \pi \tilde{A}_2 n \left( \frac{2\kappa}{m} \right)^{\frac{1}{2}} P^{(2)}. \quad (\text{II-53})$$

The collision integral on the right-hand side of (II-51) vanishes.

The remaining integrals in (II-51) containing the substantial and spatial derivatives can be rewritten by noting that the integration over velocity space and the differentiation with respect to time and physical space are independent, and hence commute. Thus,

$$\int_{\mathbf{v}} d\mathbf{v} m V_z^2 \frac{D_2}{Dt} (f^{(0)} \phi^{(1)}) =$$

$$\frac{D_2}{Dt} \int_{\mathbf{v}} d\mathbf{v} m V_z^2 (f^{(0)} \phi^{(1)}) - \int_{\mathbf{v}} d\mathbf{v} f^{(0)} \phi^{(1)} \frac{D_1}{Dt} (m V_z^2), \quad (\text{II-54})$$

and

$$\int_{\mathbf{v}} d\mathbf{v} m V_z^3 \frac{\partial}{\partial z} (f^{(0)} \phi^{(1)}) =$$

$$\frac{\partial}{\partial z} \int_{\mathbf{v}} d\mathbf{v} m V_z^3 f^{(0)} \phi^{(1)} - \int_{\mathbf{v}} d\mathbf{v} f^{(0)} \phi^{(1)} \frac{\partial}{\partial z} (m V_z^3). \quad (\text{II-55})$$

Recalling that  $V_z = v_z - u(z, t)$ , which implies  $\frac{\partial V_z}{\partial z} = -\frac{\partial u}{\partial z}$ , the preceding results may be combined to give

$$- \frac{3}{2} \pi \tilde{A}_2 \left( \frac{2\kappa}{m} \right)^{\frac{1}{2}} n P^{(2)} =$$

$$\frac{D_2}{Dt} \int_{\mathbf{v}} d\mathbf{v} m V_z^2 f^{(0)} \phi^{(1)} + \frac{\partial}{\partial z} \int_{\mathbf{v}} d\mathbf{v} m V_z^3 f^{(0)} \phi^{(1)}$$

$$+ \int_{\mathbf{v}} d\mathbf{v} f^{(0)} \phi^{(1)} (3m V_z^2) \frac{\partial u}{\partial z} + \int_{\mathbf{v}} d\mathbf{v} m V_z^2 \frac{D_2 f^{(0)}}{Dt}. \quad (\text{II-56})$$

Since  $f^{(0)}$  and  $\phi^{(1)}$  are known explicitly, the remaining integrals in (II-56) may now be evaluated explicitly. Doing so (and then performing the differentiations) gives

$$\begin{aligned}
P^{(2)} = \frac{\mu^2}{p} & \left\{ \frac{8}{9} \left( \frac{\partial u}{\partial z} \right)^2 - \frac{4}{3} \frac{k}{mn} \frac{\partial n}{\partial z} \frac{\partial T}{\partial z} \right. \\
& + \frac{4}{3} \frac{kT}{mn^2} \left( \frac{\partial n}{\partial z} \right)^2 - \frac{4}{3} \frac{kT}{mn} \frac{\partial^2 n}{\partial z^2} \\
& \left. + \frac{2}{3} \frac{k}{m} \frac{\partial^2 T}{\partial z^2} + \frac{2kT}{m} \left( \frac{1}{T} \frac{\partial T}{\partial z} \right)^2 \right\}, \quad (II-57)
\end{aligned}$$

with  $p$  the pressure,  $p = nkT$ .

The  $q^{(2)}$  calculations proceed in exactly the same manner except (II-50) is multiplied throughout by  $\frac{1}{2} m V_z^2$  and integrated over all  $\vec{v}$ . The intermediate result from this operation is

$$\begin{aligned}
- \frac{\pi \tilde{A}_2}{\left( \frac{m}{2\kappa} \right)^{\frac{1}{2}}} n q^{(2)} &= \frac{D_2}{Dt} \int \vec{v} d\vec{v} \frac{m}{2} V_z^2 (f^{(0)} \phi^{(1)}) \\
&+ \int \vec{v} d\vec{v} f^{(0)} \phi^{(1)} \frac{m}{2} \left( 2V_z^2 + v^2 \right) \frac{D_1 u}{Dt} + \frac{\partial}{\partial z} \int \vec{v} d\vec{v} \frac{m}{2} V_z^2 (f^{(0)} \phi^{(1)}) \\
&+ \int \vec{v} d\vec{v} f^{(0)} \phi^{(1)} \frac{m}{2} \left( 2V_z^3 + 2V_z^2 V_z \right) \frac{\partial u}{\partial z} + \int \vec{v} d\vec{v} \frac{m}{2} V_z^2 \frac{D_2 f^{(0)}}{Dt}. \quad (II-58)
\end{aligned}$$

Performing the integrations and extracting the second-order contributions, the final result for  $q^{(2)}$  is found to be

$$q^{(2)} = \frac{\mu^2}{\rho} \left\{ \frac{95}{8} \frac{\partial u}{\partial z} \frac{1}{T} \frac{\partial T}{\partial z} - \frac{7}{4} \frac{\partial^2 u}{\partial z^2} - \frac{2}{n} \frac{\partial n}{\partial z} \frac{\partial u}{\partial z} \right\}. \quad (II-59)$$

The derivatives of the number density  $n$  in  $P^{(2)}$  and  $q^{(2)}$  may be eliminated in favor of derivatives of the flow velocity  $u$  by using the integrated continuity equation ( $nu = \text{constant}$ ).

The results for  $P^{(2)}$  and  $q^{(2)}$ , when substituted into the general conservation equations (II-6) and (II-7) yield a pair of

coupled, nonlinear second-order differential equations for the velocity and temperature within a normal shock wave in a Maxwell gas.

### Determination of $P^{(3)}$ and $q^{(3)}$

The third order calculation to determine  $P^{(3)}$  and  $q^{(3)}$  follows the same pattern as employed in the previous order. For third-order, (II-26) and (II-27) give

$$\begin{aligned} & \int_{v_1} d\vec{v}_1 \int d\Omega \left( \frac{2\kappa}{m} \right)^{\frac{1}{2}} F(\chi) f^{(0)}(v) f_1^{(0)}(v_1) \Delta [\phi^{(3)}] = \\ & - \int_{v_1} d\vec{v}_1 \int d\Omega \left( \frac{2\kappa}{m} \right)^{\frac{1}{2}} F(\chi) f^{(0)} f_1^{(0)} \left[ \phi^{(1)'} \phi_1^{(2)'} + \phi^{(2)'} \phi_1^{(1)'} \right. \\ & \left. - \phi^{(1)} \phi_1^{(2)} - \phi^{(2)} \phi_1^{(1)} \right] + \frac{D_3}{Dt} (f^{(0)} \phi^{(2)}) + \frac{D_3}{Dt} (f^{(0)} \phi^{(1)}) \\ & + \frac{D_3 f^{(0)}}{Dt} + v_z \frac{\partial}{\partial z} (f^{(0)} \phi^{(2)}) . \end{aligned} \quad (\text{II-60})$$

Multiplying (II-60) throughout by  $mV_z^2$  and integrating over all  $\vec{v}$ , the intermediate result for  $P^{(3)}$  is obtained as

$$\begin{aligned} - \frac{3}{2} \frac{\pi \tilde{A}_2}{\left( \frac{m}{2\kappa} \right)^{1/2}} n P^{(3)} &= \frac{D_3}{Dt} [P^{(2)} + P^{(1)}] \\ &+ \frac{7}{3} \frac{\partial u}{\partial z} P^{(2)} + \frac{8}{15} \frac{\partial \epsilon}{\partial z} P^{(2)} \\ &+ \frac{2}{5} \frac{\partial}{\partial z} \left[ nm \frac{2kT}{\pi^{3/2}} \int d\vec{c} e^{-c^2} \phi^{(2)} \psi_{03}(\vec{c}) \right] . \end{aligned} \quad (\text{II-61})$$

The moment of  $\Psi_{03}(\vec{c})$  with respect to  $\phi^{(2)}$  may be determined from the integral equation (II-50) for  $\phi^{(2)}$ , without solving explicitly for  $\phi^{(2)}$ , in much the same way as the moment of  $\Psi_{02}(\vec{c})$  with respect to  $\phi^{(2)}$  ( $\propto P^{(2)}$ ) was determined.

Starting from the identity (see Appendix A)

$$\frac{1}{\pi} \int d\vec{c}_1 e^{-c_1^2} \int d\Omega F(\chi) \Delta \left[ \Psi_{03}(\vec{c}) \right] = \epsilon_{03} \left[ \Psi_{03}(\vec{c}) \right], \quad (\text{II-62})$$

$$\text{with } \epsilon_{03} = -\frac{9}{4} \pi \tilde{A}_2,$$

this implies

$$\begin{aligned} & \frac{\left(\frac{2kT}{m}\right)^{3/2}}{\pi} \int d\vec{c} e^{-c^2} \phi^{(2)} \Psi_{03}(\vec{c}) = \\ & \frac{\left(\frac{m}{2\kappa}\right)^{1/2}}{\epsilon_{03} n} \int_{\mathbf{v}} d\vec{v} f^{(0)} \phi^{(2)} \int_{\mathbf{v}_1} d\vec{v}_1 f_1^{(0)} \int d\Omega \left(\frac{2\kappa}{m}\right)^{1/2} F(\chi) \left(\frac{2kT}{m}\right)^{3/2} \Delta \left[ \Psi_{03}(\vec{c}) \right]. \end{aligned} \quad (\text{II-63})$$

Now multiply (II-50) by  $\Psi_{03}(\vec{c})$ , integrate over all  $\vec{v}$ , and use the H-Theorem transformations on the collision integrals. Proceeding as in the preceding section leads to an alternative form for the right-hand side of (II-63) or, expressed otherwise, a trap for the moment of  $\Psi_{03}(\vec{c})$  with respect to  $\phi^{(2)}$ :

$$\begin{aligned} & \frac{\left(\frac{2kT}{m}\right)^{3/2}}{\pi} \int d\vec{c} e^{-c^2} \phi^{(2)} \Psi_{03}(\vec{c}) = \\ & -\frac{5}{2mn} \frac{\left(\frac{m}{2\kappa}\right)^{1/2}}{\pi \tilde{A}_2} \left[ \frac{4}{5} \frac{P^{(1)}}{n} \frac{D_1 u}{Dt} + \frac{4}{5} \frac{k}{mn} \frac{\partial}{\partial z} (TP^{(1)}) + \frac{32}{75} \frac{q^{(1)}}{n} \frac{\partial u}{\partial z} \right]. \end{aligned} \quad (\text{II-64})$$

Using (II-64) in (II-61) and performing the necessary differentiations,  $P^{(3)}$  is found to be

$$\begin{aligned}
P^{(3)} = \frac{\mu^3}{p^2} \left\{ \frac{kT}{m} \left[ -\frac{31}{9} \left( \frac{1}{T} \frac{\partial^2 T}{\partial z^2} \right) \frac{\partial u}{\partial z} + \frac{40}{9} \left( \frac{1}{n} \frac{\partial^2 n}{\partial z^2} \right) \frac{\partial u}{\partial z} \right. \right. \\
- \frac{64}{9} \left( \frac{1}{n} \frac{\partial n}{\partial z} \right)^2 \frac{\partial u}{\partial z} - 7 \left( \frac{1}{T} \frac{\partial T}{\partial z} \right)^2 \frac{\partial u}{\partial z} \\
+ \frac{47}{3} \left( \frac{1}{n} \frac{\partial n}{\partial z} \right) \left( \frac{1}{T} \frac{\partial T}{\partial z} \right) \frac{\partial u}{\partial z} - \frac{2}{3} \left( \frac{1}{n} \frac{\partial n}{\partial z} \right) \frac{\partial^2 u}{\partial z^2} \\
\left. \left. - \frac{47}{9} \left( \frac{1}{T} \frac{\partial T}{\partial z} \right) \frac{\partial^2 u}{\partial z^2} + \frac{2}{9} \frac{\partial^3 n}{\partial z^3} \right] + \frac{16}{27} \left( \frac{\partial u}{\partial z} \right)^3 \right\} . \quad (II-65)
\end{aligned}$$

In obtaining the above result for  $P^{(3)}$ , substantial derivatives of the lower order  $P^{(n)}$  and  $q^{(n)}$  in (II-61) were determined using the identities

$$\frac{D}{Dt} \left( \frac{\partial F}{\partial z} \right) = \frac{\partial}{\partial z} \left( \frac{DF}{Dt} \right) - \frac{\partial u}{\partial z} \frac{\partial F}{\partial z} \quad (II-66a)$$

and

$$\frac{D}{Dt} \left( \frac{\partial^2 F}{\partial z^2} \right) = \frac{\partial^2}{\partial z^2} \left[ \frac{DF}{Dt} \right] - \frac{\partial^2 u}{\partial z^2} \frac{\partial F}{\partial z} - 2 \frac{\partial u}{\partial z} \frac{\partial^2 F}{\partial z^2} . \quad (II-66b)$$

The third-order contribution to the heat flux,  $q^{(3)}$ , is obtained by multiplying (II-60) throughout by  $\frac{1}{2} m v_z^2$  and integrating that result over all  $\vec{v}$ . The intermediate form for  $q^{(3)}$  turns out to be

$$\begin{aligned}
- \frac{\pi \tilde{A}_2}{\left( \frac{m}{2K} \right)^{1/2}} n q^{(3)} = \frac{D_3}{Dt} \left[ q^{(2)} + q^{(1)} \right] + P^{(2)} \left[ \frac{D_1 u}{Dt} \right] \\
+ \frac{5}{2} n k T \frac{D_3 u}{Dt} + P^{(1)} \left[ \frac{D_2 u}{Dt} \right] \\
+ \frac{\partial}{\partial z} \left[ \frac{7}{2} \frac{kT}{m} P^{(2)} \right] + \frac{16}{5} q^{(2)} \frac{\partial u}{\partial z}
\end{aligned}$$



$$\begin{aligned}
& + \frac{\partial u}{\partial z} \left\{ \frac{4}{5} nkT \left( \frac{2kT}{m} \right)^{1/2} \int d\vec{c} e^{-c^2} \phi^{(2)} \left[ \psi_{03}(\vec{c}) \right] \right\} \\
& + \frac{\partial}{\partial z} \left\{ \frac{4}{3} \frac{n^2 k^2 T^2}{nm} \frac{1}{\pi^{3/2}} \int d\vec{c} e^{-c^2} \phi^{(2)} \left[ \psi_{20}(\vec{c}) - \psi_{12}(\vec{c}) \right] \right\} \quad . \quad (\text{II-67})
\end{aligned}$$

Although the  $P^{(3)}$  calculations have already provided the result for the second-order moment of  $\psi_{03}(\vec{c})$ , the additional second-order moments of the eigenfunctions  $\psi_{20}(\vec{c})$  and  $\psi_{12}(\vec{c})$  must still be evaluated. However, methods used to evaluate the  $\psi_{03}(\vec{c})$  result may be used to evaluate the additional moments occurring in (II-67). The calculations of the second moments of  $\psi_{20}(\vec{c})$  and  $\psi_{12}(\vec{c})$  give

$$\begin{aligned}
& \frac{\partial}{\partial z} \left\{ \frac{1}{3nm} \left( \frac{2kT}{m} \right)^2 \frac{1}{\pi^{3/2}} \int d\vec{c} e^{-c^2} \phi^{(2)} \left[ \psi_{20}(\vec{c}) - \psi_{12}(\vec{c}) \right] \right. \\
& \quad \frac{m}{3} \frac{\partial}{\partial z} \left\{ - \frac{33}{28} \frac{[P^{(1)}]^2}{m^2 n} - \frac{\left( \frac{m}{2\kappa} \right)^{1/2}}{\pi A_2} \left[ \frac{36}{5mn} \frac{D_1 u}{Dt} q^{(1)} \right. \right. \\
& \quad \left. \left. + \frac{36}{5} \frac{kT}{m^2 n} \frac{\partial q^{(1)}}{\partial z} + \frac{102}{5} \frac{k}{m^2 n} \frac{\partial r}{\partial z} q^{(1)} \right. \right. \\
& \quad \left. \left. + \frac{72}{7} \frac{kT}{m^2 n} \frac{\partial u}{\partial z} P^{(1)} + 6 \frac{k}{m^2 n} \frac{D_1 T}{Dt} P^{(1)} \right] \right\} \quad . \quad (\text{II-68})
\end{aligned}$$

Performing the derivatives and eliminating derivatives of  $n$  in favor of derivatives of  $u$  yields

$$\begin{aligned}
q^{(3)} &= \frac{\mu^3}{\rho^2} \left\{ - \frac{157}{16} \left( \frac{1}{T} \frac{\partial^3 T}{\partial z^3} \right) + \frac{5}{8} \left( \frac{1}{u} \frac{\partial^3 u}{\partial z^3} \right) \right. \\
&\quad - \frac{71}{8} \left( \frac{1}{u} \frac{\partial u}{\partial z} \right) \left( \frac{1}{u} \frac{\partial^2 u}{\partial z^2} \right) + \frac{33}{4} \left( \frac{1}{u} \frac{\partial u}{\partial z} \right)^3 - \frac{813}{16} \left( \frac{1}{T} \frac{\partial T}{\partial z} \right)^3 \\
&\quad \left. - \frac{1451}{16} \left( \frac{1}{T} \frac{\partial T}{\partial z} \right) \left( \frac{1}{T} \frac{\partial^2 T}{\partial z^2} \right) - \frac{917}{8} \left( \frac{1}{u} \frac{\partial u}{\partial z} \right) \left( \frac{1}{T} \frac{\partial T}{\partial z} \right)^2 \right\}
\end{aligned}$$

$$\begin{aligned}
& + \frac{265}{16} \left( \frac{1}{T} \frac{\partial T}{\partial z} \right) \left( \frac{1}{u} \frac{\partial u}{\partial z} \right)^2 - \frac{701}{16} \left( \frac{1}{T} \frac{\partial T}{\partial z} \right) \left( \frac{1}{u} \frac{\partial^2 u}{\partial z^2} \right) \\
& - \frac{397}{16} \left( \frac{1}{u} \frac{\partial u}{\partial z} \right) \left( \frac{1}{T} \frac{\partial^2 T}{\partial z^2} \right) + \frac{m}{kT} \left[ - \frac{166}{21} \left( \frac{1}{u} \frac{\partial u}{\partial z} \right) \left( \frac{\partial u}{\partial z} \right)^2 \right. \\
& \left. + \frac{949}{168} \left( \frac{\partial u}{\partial z} \right) \left( \frac{\partial^2 u}{\partial z^2} \right) - \frac{8035}{336} \left( \frac{1}{T} \frac{\partial T}{\partial z} \right) \left( \frac{\partial u}{\partial z} \right)^2 \right] \Bigg\} . \quad (\text{II-69})
\end{aligned}$$

The substitution of the viscous stress and heat flux contributions through third-order into the general conservation equations (II-6) and (II-7) yields a pair of coupled, nonlinear third-order differential equations which govern the spatial dependence of the velocity and temperature in a normal shock wave. The third-order results are known as the Super-Burnett differential equations for the structure of a normal shock wave in a Maxwell gas.

#### Determination of $P^{(4)}$ and $q^{(4)}$

The fourth-order contributions of the viscous stress and heat flux are found by applying the same moment methods to the integral equation for  $\phi^{(4)}$  obtained from (II-26) and II-27)

$$\begin{aligned}
& \int_{v_1} d\vec{v}_1 \int d\Omega \left( \frac{2K}{m} \right)^{1/2} F(\chi) f^{(0)} f_1^{(0)} \Delta \left[ \phi^{(4)} \right] = \\
& - \int_{v_1} d\vec{v}_1 \int d\Omega \left( \frac{2K}{m} \right)^{1/2} F(\chi) f^{(0)} f_1^{(0)} \left[ \phi^{(3)'} \phi_1^{(1)'} + \phi_1^{(3)'} \phi^{(1)'} - \phi^{(3)} \phi_1^{(1)} \right. \\
& \left. - \phi^{(1)} \phi_1^{(3)} \right] - \int_{v_1} d\vec{v}_1 \int d\Omega \left( \frac{2K}{m} \right)^{1/2} F(\chi) f^{(0)} f_1^{(0)} \left[ \phi^{(2)'} \phi_1^{(2)'} - \phi^{(2)} \phi_1^{(2)} \right] \\
& + \frac{D_4}{Dt} \left[ f^{(0)} \phi^{(3)} + f^{(0)} \phi^{(2)} + f^{(0)} \phi^{(1)} + f^{(0)} \right] + v_z \frac{\partial}{\partial z} \left[ f^{(0)} \phi^{(3)} \right] . \quad (\text{II-70})
\end{aligned}$$

The moments with respect to  $m\mathbf{v}_z^2$  and  $\frac{1}{2}m\mathbf{v}_z^2$  yield the following intermediate results for  $P^{(4)}$  and  $q^{(4)}$  respectively:

$$\begin{aligned}
 -\frac{3}{2}\pi\tilde{A}_2\left(\frac{2\kappa}{m}\right)^{1/2} n P^{(4)} &= \frac{8}{15} \frac{\partial q^{(3)}}{\partial z} \\
 &+ \frac{D_4}{Dt} \left[ P^{(3)} + P^{(2)} + P^{(1)} \right] + \frac{7}{3} P^{(3)} \frac{\partial u}{\partial z} \\
 &+ \frac{\partial}{\partial z} \left[ \frac{nm}{\pi^{3/2}} \left(\frac{2kT}{m}\right)^{3/2} \frac{2}{5} \int d\vec{c} \vec{c}^2 \phi^{(3)} \Psi_{03}(\vec{c}) \right] ; \quad (II-71)
 \end{aligned}$$

$$\begin{aligned}
 -\frac{\pi\tilde{A}_2}{\left(\frac{m}{2\kappa}\right)^{1/2}} n q^{(4)} &= \frac{D_4}{Dt} \left[ q^{(3)} + q^{(2)} + q^{(1)} \right] \\
 &+ \frac{D_1 u}{Dt} P^{(3)} + \frac{D_2 u}{Dt} P^{(2)} + \frac{D_3 u}{Dt} P^{(1)} + \frac{D_4 u}{Dt} \left[ \frac{5}{2} nkT \right] \\
 &+ \frac{16}{5} \frac{\partial u}{\partial z} q^{(3)} + \frac{7}{2} \frac{\partial}{\partial z} \left[ \left(\frac{kT}{m}\right) P^{(3)} \right] \\
 &+ \frac{\partial u}{\partial z} \left\{ \frac{4}{5} nkT \frac{\left(\frac{2kT}{m}\right)^{1/2}}{\pi^{3/2}} \int d\vec{c} \vec{c}^2 \phi^{(3)} \left[ \Psi_{03}(\vec{c}) \right] \right\} \\
 &+ \frac{\partial}{\partial z} \left\{ \frac{4}{3} n \frac{k^2 T^2}{m} \frac{1}{\pi^{3/2}} \int d\vec{c} \vec{c}^2 \phi^{(3)} \left[ \Psi_{20}(\vec{c}) - \Psi_{12}(\vec{c}) \right] \right\} . \quad (II-72)
 \end{aligned}$$

The evaluation of the third-order moments of  $\Psi_{03}(\vec{c})$ ,  $\Psi_{20}(\vec{c})$ , and  $\Psi_{12}(\vec{c})$  proceeds as in the previous sections. The calculations of the nonlinear expressions for  $P^{(4)}$  and  $q^{(4)}$  were carried out to the point where the results were known in terms of substantial derivatives, spatial derivatives and the lower order viscous stress and heat flux contributions. For reasons which will become apparent in the next chapter, it was not necessary to perform all the

differentiations and substitutions to reduce these very involved expressions to the spatial derivative formats as was done in the previous developments. In fact, only the terms in  $P^{(4)}$  and  $q^{(4)}$

which are proportional to the fourth-order spatial derivatives

$\frac{\partial^4 n}{\partial z^4}$ ,  $\frac{\partial^4 u}{\partial z^4}$ , or  $\frac{\partial^4 T}{\partial z^4}$  will be needed later in this report. Neglecting

all other terms leads to the linearized results

$$P^{(4)} = \frac{\mu^4}{p^3} \left\{ -\frac{1}{3} \frac{k^2 T^2}{nm^2} \frac{\partial^4 n}{\partial z^4} + \frac{197}{42} \frac{k^2 T}{m^2} \frac{\partial^4 T}{\partial z^4} \right\} \quad (\text{II-73})$$

and

$$q^{(4)} = -\frac{8335}{336} \frac{\mu^4}{p\rho^2} \frac{\partial^4 u}{\partial z^4} \quad (\text{II-74})$$

If the complete nonlinear results for  $P^{(4)}$  and  $q^{(4)}$  were included with the lower order viscous stress and heat flux contributions, the general conservation equations (II-6) and (II-7) would yield two coupled, nonlinear fourth-order differential equations for the temperature and velocity in a normal shock wave. These fourth-order results are known as the Super-Super-Burnett equations.

## CHAPTER III

### METHODS TO SOLVE THE NAVIER-STOKES EQUATIONS

#### Numerical Integration

It is convenient to rearrange the general conservation equations (II-5a), (II-6a), and (II-7a) in two ways. First, use the continuity equation (II-5a) to eliminate  $\rho$  in favor of  $u$  in the momentum and energy equations; then, use the momentum equation to eliminate  $P$  from the energy equation. These rearrangements give

$$\frac{5}{3\rho_1 u_1 a_1} [q] + \frac{3}{2} (\tau-1) - \frac{5}{6} M_1^2 (u-1)^2 + (u-1) = 0, \quad (\text{III-1})$$

and

$$\frac{5M_1^2 u}{3\rho_1 u_1^2} [P] + \frac{5}{3} M_1^2 u(u-1) + (\tau-u) = 0, \quad (\text{III-2})$$

where the dimensionless velocity ( $u$ ) and the dimensionless temperature ( $\tau$ ) are defined by

$$u = \frac{u}{u_1}, \quad (\text{III-3})$$

and

$$\tau = \frac{T}{T_1}, \quad (\text{III-4})$$

with  $i = 1$  corresponding to conditions far upstream and  $i = 2$  corresponding to conditions far downstream. The quantity  $M_i$  is the Mach number,

$$M_i = \frac{u_i}{a_i}, \quad (\text{III-5})$$

in which  $a_i$  is the speed of sound determined from

$$a_i^2 = \frac{5}{3} \frac{k}{m} T_i. \quad (\text{III-6})$$

In the Navier-Stokes order of fluid mechanics, the expressions for  $P$  and  $q$  are

$$P = P^{(1)} = -\frac{4}{3} \mu \frac{du}{dz} \quad (\text{III-7})$$

and

$$q = q^{(1)} = -K \frac{dT}{dz}. \quad (\text{III-8})$$

For Maxwell molecules,  $\mu$  and  $K$  are given by

$$\mu(T) = \mu_i \left( \frac{T}{T_i} \right) = \mu_i \tau \quad (\text{III-9})$$

and

$$K(T) = \frac{15}{4} \frac{k\mu_i}{m} \tau. \quad (\text{III-10})$$

In due course, following the convention of other authors, distance in the direction of the mean flow will be measured in multiples of the upstream Maxwellian mean free path  $\lambda_1$ , defined by

$$\lambda_1 = \frac{16}{[30\pi]^{1/2}} \frac{\mu_1}{\rho_1 a_1} \quad (\text{III-11})$$

Anticipating the eventual introduction of  $\lambda_1$ , the Navier-Stokes equations for a Maxwell gas may be written in the form

$$\frac{20}{9} \left[ \frac{\mu_i M_i}{\rho_i a_i} \right] u \tau \frac{d u}{d z} = \frac{5}{3} M_i^2 u(u-1) + (\tau-u), \quad (\text{III-12})$$

$$\frac{15}{4} \left[ \frac{\mu_i M_i}{\rho_i a_i} \right] \frac{\tau}{M_i} \frac{d \tau}{d z} = \frac{3}{2} (\tau-1) - \frac{5}{6} M_i^2 (u-1)^2 + (u-1). \quad (\text{III-13})$$

Gilbarg and Paolucci provided an extensive analysis of the solution of (III-12) and (III-13). Everything depends on the mathematical nature of the singular points of (III-12) and (III-13) in the auxiliary  $u$ - $\tau$  phase plane. The physically significant solution of (III-12) and (III-13) may be represented by a trajectory which connects these two points. Such a solution exists and may be obtained by numerical integration, but the numerical integration must be initiated near the downstream singularity and proceed upstream. Numerical integration from upstream toward downstream will necessarily fail.

This requirement for successful numerical integration may be understood by examining all the mathematical solutions including the nonphysical ones very near the singular points. To accomplish this, linearize the Navier-Stokes equations, and put

$$T \equiv T_i + \tilde{T} e^{K_i z}, \quad (\text{III-14})$$

$$u \equiv u_i + \tilde{u} e^{K_i z}, \quad (\text{III-15})$$

or

$$\tau = 1 + \tilde{\tau} e^{K_i z}, \quad (\text{III-16})$$

$$u = 1 + \tilde{u} e^{\kappa_1 z} . \quad (\text{III-17})$$

The characteristic or secular equation for  $\kappa_1$  may be written in the form

$$20 L_1^2 + (9 - 23M_1^2) L_1 + 6 M_1^2 (M_1^2 - 1) = 0, \quad (\text{III-18})$$

where

$$L_1 = \left[ \frac{\mu_1 M_1}{\rho_1 a_1} \right] \kappa_1 . \quad (\text{III-19})$$

The roots of this characteristic polynomial are given graphically in Appendix B along with a table of the physically significant roots used in the subsequent calculations of the gas property profiles. An examination of the characteristic roots shows for all Mach numbers that upstream, both roots are real and both are positive, whereas downstream the roots are real but of opposite sign. Therefore, near the upstream singularity, the most general solution of the linearized Navier-Stokes equations involves a linear combination of exponentials with the two positive values of  $\kappa_1$ . These exponentials tend to zero as  $z \rightarrow -\infty$ , giving  $u \rightarrow u_1$  and  $T \rightarrow T_1$ . However, near the downstream singularity, the two values of  $\kappa_2$  have opposite sign and the most general solution diverges as  $z \rightarrow +\infty$ . There is only one trajectory for which  $u \rightarrow u_2$  and  $T \rightarrow T_2$  as  $z \rightarrow +\infty$ .

Thus, it is the signs of the roots of the characteristic equation (III-18) that determine whether the Navier-Stokes equations are amenable to numerical integration, and, if so, in which direction through the shock wave. The means used to attain this insight



are extremely important, for they illuminate difficulties encountered later in attempting numerically to integrate the higher order gasdynamic equations.

The results of numerical integration of the Navier-Stokes equations will be discussed later in this report in Chapter V.

### Perturbation Expansion

It will be seen shortly, that some difficulties arise when numerical integration is attempted in the higher order gasdynamic equations. Thus, at this point in the thesis, it is convenient to introduce the development of a perturbation expansion method which can be used to integrate the higher order equations where the numerical integration fails. It is appropriate to discuss the development of the perturbation expansion now, in conjunction with the Navier-Stokes equations for it will be assumed that such a method will be trustworthy if it gives good agreement with the results of numerical integration of the Navier-Stokes equations.

A successful perturbation expansion presumably must be based on a dimensionless parameter that is always less than of order unity (even for  $M_1 \gg 1$ ). In addition, the perturbation expansion should not lead to approximate results that violate the Rankine-Hugoniot relations (which connect upstream and downstream values). Finally, the perturbation expansion must somehow do justice to the enormous variation in shock wave thickness between the extremes of  $M_1 \approx 1$  and  $M_1 \gg 1$ .

In consideration of the above, the choice of the expansion parameter is  $\epsilon \equiv M_2^2 - 1$ , and, from this definition, it is noted that  $\epsilon$  varies monotonically from 0 to -0.8 as  $M_1$  increases from 1 to  $\infty$ .

In order to avoid violations of the Rankine-Hugoniot relations induced by the perturbation expansion, a normalized density  $R_\rho$  and normalized temperature  $R_T$  are regarded as basic dependent variables, where

$$R_\rho(z) = \frac{\rho(z) - \rho_1}{\rho_2 - \rho_1} , \quad (\text{III-21})$$

$$R_T(z) = \frac{T(z) - T_1}{T_2 - T_1} . \quad (\text{III-22})$$

These normalized quantities may be expected to vary from 0 to 1, independent of  $M_1$ . Since the boundary conditions which these variables must satisfy are independent of  $M_1$ , it is unlikely that approximations to  $R_\rho$  and  $R_T$  will fail to have the correct asymptotic values. From (III-21) and (III-22) and the Rankine-Hugoniot relations it follows that

$$\frac{\rho}{\rho_1} = \frac{u_1}{u} = 1 + \frac{3(M_1^2 + 1)}{(M_1^2 + 3)} R_\rho(z) , \quad (\text{III-23})$$

$$\frac{T}{T_1} = 1 + \frac{(M_1^2 - 1)(5M_1^2 + 3)}{16 M_1^2} R_T(z) . \quad (\text{III-24})$$

Note for future reference that one could have introduced a normalized density  $R_\rho$  and normalized temperature  $R_T$  defined by

$$R_\rho(z) = \frac{\rho_2 - \rho(z)}{\rho_2 - \rho_1} = 1 - R_\rho(z) , \quad (\text{III-25})$$

$$R_T(z) = \frac{T_2 - T(z)}{T_2 - T_1} = 1 - R_T(z) , \quad (\text{III-26})$$

in terms of which

$$\frac{\rho}{\rho_2} = \frac{u_2}{u} = 1 + \frac{3(M_2^2 - 1)}{(M_2^2 + 3)} R_\rho(z) , \quad (\text{III-27})$$

$$\frac{T}{T_2} = 1 + \frac{(M_2^2 - 1)(5M_2^2 + 3)}{16 M_2^2} R_T(z) . \quad (\text{III-28})$$

The pronounced dependence of shock wave thickness on Mach number suggests the introduction of a Mach number dependent length scale to "tame" the differential equations. The idea is to regard  $R_\rho$  and  $R_T$  as functions of

$$\zeta \equiv \kappa(M) \cdot z \quad (\text{III-29})$$

with  $\kappa(M)$  chosen so that the thickness of the shock wave (in units of  $\zeta$ ) does not show a pronounced dependence on Mach number.

How does this lead to a choice for  $\kappa(M)$ ? It is known that far upstream  $R_\rho$  and  $R_T$  are proportional to  $e^{\kappa_1 z}$ , with the physically significant choice for  $\kappa$  (positive, tending to zero as  $M_1 \rightarrow 1$ ),

$$\kappa_1 = \frac{\rho_1 a_1}{\mu_1 M_1} \frac{1}{40} \left\{ (23 M_1^2 - 9) - \left[ (23 M_1^2 - 9)^2 - 480 M_1^2 (M_1^2 - 1) \right]^{1/2} \right\} . \quad (\text{III-30})$$

Far downstream, however,  $R_\rho$  and  $R_T$  are proportional to  $e^{\kappa_2 z}$ , with the physically significant choice for  $\kappa_2$  (negative, tending to zero as  $M_1 \rightarrow 1$ ),

$$\kappa_2 = \frac{\rho_2 a_2}{\mu_2 M_2} \frac{1}{40} \left\{ (23 M_2^2 - 9) - \left[ (23 M_2^2 - 9)^2 - 480 M_2^2 (M_2^2 - 1) \right]^{1/2} \right\}. \quad (\text{III-31})$$

For  $M \sim 1$ , the two reciprocal length scales (III-30) and (III-31) are both proportional to  $(M_1^2 - 1)$ , but for  $M_1 \gg 1$ ,  $\kappa_1 \sim M_1$  and  $\kappa_2 \sim \frac{1}{M_1}$ .

Now, it will be shown that in the interior of the shock wave, for  $M_1 \gg 1$ ,  $\kappa \sim \frac{1}{M_1}$ . To do this, start from the full nonlinear Navier-Stokes equations,

$$\frac{20}{9} \left[ \frac{\mu_i M_i}{\rho_i a_i} \right] u \tau \frac{du}{dz} = \frac{5}{3} M_i^2 u(u-1) + (\tau-u), \quad (\text{III-32})$$

$$\frac{15}{4} \left[ \frac{\mu_i M_i}{\rho_i a_i} \right] \frac{\tau}{M_i^2} \frac{d\tau}{dz} = \frac{3}{2} (\tau-1) - \frac{5}{6} M_i^2 (u-1)^2 + (u-1), \quad (\text{III-33})$$

set  $i = 1$  and think of  $u$  and  $\tau$  expressed in terms of  $R_\rho$  and  $R_T$ .

Next, assume the existence of an "interior" of the shock wave where  $R_\rho$  and  $R_T$  are both of order 0.5. It then follows from (III-32) and (III-33) that within such a region, for  $M_1 \gg 1$ ,

$$\frac{dR_\rho}{dz} \sim \frac{1}{M_1}$$

$$\frac{dR_T}{dz} \sim \frac{1}{M_1}.$$

In other words,  $\kappa \sim \frac{1}{M_1}$  in the interior of the shock wave for  $M_1 \gg 1$ .

Hence, relying on the foregoing analysis, the Mach number dependent length scale for the perturbation expansion will be based on (III-31). This choice may be expected to be appropriate throughout the shock wave for  $M_1 \sim 1$ , and everywhere except far upstream for  $M_1 \gg 1$ . Its actual utility can only be judged a posteriori.

Based on the above developments, the perturbation expansion can now proceed by rewriting (III-32) and (III-33) for  $i = 2$  in terms of  $R_\rho$ ,  $R_T$ , and  $\zeta$ , defined by  $\zeta = \kappa_2(M_1) \cdot z$  and then seek  $R_\rho$  and  $R_T$  in successive approximation by writing

$$R_\rho(\zeta) = R_\rho^{(0)}(\zeta) + \epsilon R_\rho^{(1)}(\zeta) + \epsilon^2 R_\rho^{(2)}(\zeta) + \dots \quad (\text{III-34})$$

$$R_T(\zeta) = R_T^{(0)}(\zeta) + \epsilon R_T^{(1)}(\zeta) + \epsilon^2 R_T^{(2)}(\zeta) + \dots \quad (\text{III-35})$$

Since  $\kappa_2$  is brought into the differential equations (III-32) and (III-33) when they are written in terms of  $\zeta$ , the  $\epsilon$  expansion for

$\frac{\mu_2 M_2}{\rho_2 a_2} \kappa_2$  will be needed and is given by

$$\frac{\mu_2 M_2}{\rho_2 a_2} \kappa_2 = \left\{ \frac{3}{7} \epsilon - \frac{9}{2(7)^3} \epsilon^2 + \frac{369}{4(7)^5} \epsilon^3 - \frac{13509}{8(7)^7} \epsilon^4 + \dots \right\} \quad (\text{III-36})$$

In zeroth-order (III-32) and (III-33) are satisfied identically. In first-order, both (III-32) and (III-33) yield the same relationship

$$R_\rho^{(0)}(\zeta) = R_T^{(0)}(\zeta).$$

In second-order (III-32) and (III-33) yield, respectively,<sup>†</sup>

$$\begin{aligned} \frac{1}{2} R_T^{(1)} - \frac{1}{2} R_\rho^{(1)} - \frac{9}{8} R_\rho^{(0)} - \frac{3}{16} R_T^{(0)} \\ + \frac{9}{8} R_\rho^{(0)} R_T^{(0)} + \frac{3}{16} \left[ R_\rho^{(0)} \right]^2 + \frac{5}{7} \frac{dR_\rho^{(0)}}{d\zeta} = 0 \quad (\text{III-38}) \end{aligned}$$

and

$$\begin{aligned} \frac{1}{2} R_T^{(1)} - \frac{1}{2} R_\rho^{(1)} + \frac{1}{8} R_\rho^{(0)} - \frac{3}{16} R_T^{(0)} \\ + \frac{3}{4} R_\rho^{(0)} R_T^{(0)} - \frac{11}{16} \left[ R_\rho^{(0)} \right]^2 - \frac{15}{28} \frac{dR_\rho^{(0)}}{d\zeta} = 0. \quad (\text{III-39}) \end{aligned}$$

<sup>†</sup>For clarity, the argument  $\zeta$  will be dropped throughout the remainder of this report.

Using (III-37) to express  $R_T^{(0)}$  in terms of  $R_\rho^{(0)}$ , the last two equations may be looked upon as involving  $R_T^{(1)}$ ,  $R_\rho^{(1)}$ , and  $R_\rho^{(0)}$ . The difference between (III-38) and (III-39) is a first-order differential equation for  $R_\rho^{(0)}$  in the form

$$\frac{dR_\rho^{(0)}}{d\zeta} = R_\rho^{(0)} - \left[ R_\rho^{(0)} \right]^2. \quad (\text{III-40})$$

Forming the sum of (III-38) and (III-39), the derivative of  $R_\rho^{(0)}$  may be eliminated using (III-40) to give an algebraic equation for  $R_T^{(1)}$  as

$$R_T^{(1)} = R_\rho^{(1)} + \frac{67}{8(7)} R_\rho^{(0)} - \frac{67}{8(7)} \left[ R_\rho^{(0)} \right]^2. \quad (\text{III-41})$$

For convenience in calculating the asymmetry of the normalized density profiles, the origin of the coordinate system is taken where  $R_\rho^{(0)}(\zeta) = 0.5$ . With this specification, the integration of the second-order result gives

$$R_\rho^{(0)}(\zeta) = \frac{1}{2} \left[ 1 + \tanh \left( \frac{\zeta}{2} \right) \right] \quad (\text{III-42})$$

and from (III-37)

$$R_T^{(0)}(\zeta) = \frac{1}{2} \left[ 1 + \tanh \left( \frac{\zeta}{2} \right) \right]. \quad (\text{III-43})$$

Equation (III-41) will yield immediate results for  $R_T^{(1)}$  once  $R_\rho^{(1)}$  has been determined from the succeeding perturbation calculations.

The third-order expressions obtained from (III-32) and (III-33) introduce the next higher order of the perturbation quantities. The results are

$$\begin{aligned}
& \frac{1}{2} R_T^{(2)} - \frac{1}{2} R_\rho^{(2)} - \frac{9}{8} R_\rho^{(1)} + \frac{9}{32} R_\rho^{(0)} - \frac{3}{16} R_T^{(1)} \\
& + \frac{9}{8} R_\rho^{(0)} R_T^{(1)} - \frac{45}{64} R_\rho^{(0)} R_T^{(0)} + \frac{9}{8} R_\rho^{(1)} R_T^{(0)} + \frac{27}{32} \left[ R_\rho^{(0)} \right]^2 R_T^{(0)} \\
& + \frac{3}{8} R_\rho^{(0)} R_\rho^{(1)} - \frac{33}{32} \left[ R_\rho^{(0)} \right]^2 + \frac{27}{64} \left[ R_\rho^{(0)} \right]^3 + \frac{3}{16} R_T^{(0)} \\
& + \frac{5}{14} R_T^{(0)} \frac{dR_\rho^{(0)}}{d\zeta} - \frac{275}{4(7)^3} \frac{dR_\rho^{(0)}}{d\zeta} + \frac{5}{7} \frac{dR_\rho^{(1)}}{d\zeta} = 0 \quad (\text{III-44})
\end{aligned}$$

and

$$\begin{aligned}
& \frac{1}{2} R_T^{(2)} - \frac{1}{2} R_\rho^{(2)} - \frac{3}{8} R_\rho^{(1)} + \frac{3}{32} R_\rho^{(0)} + \frac{5}{16} R_T^{(1)} \\
& + \frac{3}{4} R_\rho^{(0)} R_T^{(1)} + \frac{9}{32} R_\rho^{(0)} R_T^{(0)} + \frac{3}{4} R_\rho^{(1)} R_T^{(0)} + \frac{9}{32} \left[ R_\rho^{(0)} \right]^2 R_T^{(0)} \\
& - \frac{11}{8} R_\rho^{(0)} R_\rho^{(1)} - \frac{21}{32} \left[ R_\rho^{(0)} \right]^2 - \frac{15}{8(7)} R_T^{(0)} \frac{dR_T^{(0)}}{d\zeta} \\
& - \frac{45}{8(7)} R_\rho^{(0)} \frac{dR_T^{(0)}}{d\zeta} + \frac{15(159)}{32(7)^3} \frac{dR_T^{(0)}}{d\zeta} - \frac{15}{28} \frac{dR_T^{(1)}}{d\zeta} = 0. \quad (\text{III-45})
\end{aligned}$$

Eliminating  $R_T^{(0)}$  and  $R_T^{(1)}$  by means of (III-37) and (III-41),

and taking the difference between (III-44) and (III-45), one finds

$$\frac{dR_\rho^{(1)}}{d\zeta} + \left( 2 R_\rho^{(0)} - 1 \right) R_\rho^{(1)} = \frac{61}{4(7)^2} \left[ R_\rho^{(0)} \right]^2 - \frac{61}{4(7)^2} \left[ R_\rho^{(0)} \right]^3. \quad (\text{III-46})$$

An expression for  $R_T^{(2)}$  is found using (III-46) in the sum

of (III-44) and (III-45). The result is

$$\begin{aligned}
R_T^{(2)} &= R_\rho^{(2)} + \frac{67}{8(7)} \left( 1 - 2 R_\rho^{(0)} \right) R_\rho^{(1)} - \frac{1931}{64(7)^3} R_\rho^{(0)} \\
&- \frac{27037}{64(7)^3} \left[ R_\rho^{(0)} \right]^2 + \frac{28968}{64(7)^3} \left[ R_\rho^{(0)} \right]^3. \quad (\text{III-47})
\end{aligned}$$

Proceeding as before, the fourth-order perturbation calculations give

$$\begin{aligned} \frac{dR_{\rho}^{(2)}}{d\zeta} + \left(2 R_{\rho}^{(0)} - 1\right) R_{\rho}^{(2)} &= 2 \left[ \frac{6}{4(7)^2} \right] R_{\rho}^{(0)} R_{\rho}^{(1)} \\ &- 3 \left[ \frac{61}{4(7)^2} \right] \left[ R_{\rho}^{(0)} \right]^2 R_{\rho}^{(1)} - \left[ R_{\rho}^{(1)} \right]^2 - \frac{20203}{16(7)^4} \left[ R_{\rho}^{(0)} \right]^2 \\ &+ \frac{34794}{16(7)^4} \left[ R_{\rho}^{(0)} \right]^3 - \frac{14591}{16(7)^4} \left[ R_{\rho}^{(0)} \right]^4 \end{aligned} \quad (\text{III-48})$$

and

$$\begin{aligned} R_T^{(3)} &= R_{\rho}^{(3)} + \frac{67}{8(7)} \left(1 - 2 R_{\rho}^{(0)}\right) R_{\rho}^{(2)} \\ &- \frac{1931}{64(7)^3} R_{\rho}^{(1)} - \frac{67}{8(7)} \left[ R_{\rho}^{(1)} \right]^2 - 2 \left[ \frac{27037}{64(7)^3} \right] R_{\rho}^{(0)} R_{\rho}^{(1)} \\ &+ 3 \left[ \frac{28968}{64(7)^3} \right] \left[ R_{\rho}^{(0)} \right]^2 R_{\rho}^{(1)} - \frac{727457}{512(7)^5} R_{\rho}^{(0)} + \frac{2343485}{512(7)^5} \left[ R_{\rho}^{(0)} \right]^2 \\ &+ \frac{10962264}{512(7)^5} \left[ R_{\rho}^{(0)} \right]^3 - \frac{12578292}{512(7)^5} \left[ R_{\rho}^{(0)} \right]^4 \end{aligned} \quad (\text{III-49})$$

In fifth-order, the results are

$$\begin{aligned} \frac{dR_{\rho}^{(3)}}{d\zeta} + \left(2 R_{\rho}^{(0)} - 1\right) R_{\rho}^{(3)} &= \\ &2 \left[ \frac{61}{4(7)^2} \right] R_{\rho}^{(0)} R_{\rho}^{(2)} - 3 \left[ \frac{61}{4(7)^2} \right] \left[ R_{\rho}^{(0)} \right]^2 R_{\rho}^{(2)} + \frac{61}{4(7)^2} \left[ R_{\rho}^{(1)} \right]^2 \\ &- 3 \left[ \frac{61}{4(7)^2} \right] R_{\rho}^{(0)} \left[ R_{\rho}^{(1)} \right]^2 - 2 R_{\rho}^{(1)} R_{\rho}^{(2)} - 2 \left[ \frac{20203}{16(7)^4} \right] R_{\rho}^{(0)} R_{\rho}^{(1)} \\ &+ 3 \left[ \frac{34794}{16(7)^4} \right] \left[ R_{\rho}^{(0)} \right]^2 R_{\rho}^{(1)} - 4 \left[ \frac{14591}{16(7)^4} \right] \left[ R_{\rho}^{(0)} \right]^3 R_{\rho}^{(1)} \end{aligned}$$



$$\begin{aligned}
& + \frac{1971230}{128(7)^6} \left[ R_{\rho}^{(0)} \right]^2 + \frac{3526570}{128(7)^6} \left[ R_{\rho}^{(0)} \right]^3 \\
& - \frac{13336026}{128(7)^6} \left[ R_{\rho}^{(0)} \right]^4 + \frac{7838226}{128(7)^6} \left[ R_{\rho}^{(0)} \right]^5
\end{aligned} \tag{III-50}$$

and

$$\begin{aligned}
R_T^{(4)} = & R_{\rho}^{(4)} + \frac{67}{8(7)} \left( 1 - 2 R_{\rho}^{(0)} \right) R_{\rho}^{(3)} - \frac{1931}{64(7)^3} R_{\rho}^{(2)} \\
& - 2 \left[ \frac{27037}{64(7)^3} \right] R_{\rho}^{(0)} R_{\rho}^{(2)} + 3 \left[ \frac{28968}{64(7)^3} \right] \left[ R_{\rho}^{(0)} \right]^2 R_{\rho}^{(2)} - \frac{727457}{512(7)^5} R_{\rho}^{(1)} \\
& + 2 \left[ \frac{2343485}{512(7)^5} \right] R_{\rho}^{(0)} R_{\rho}^{(1)} + 3 \left[ \frac{10962264}{512(7)^5} \right] \left[ R_{\rho}^{(0)} \right]^2 R_{\rho}^{(1)} \\
& - 4 \left[ \frac{12578292}{512(7)^5} \right] \left[ R_{\rho}^{(0)} \right]^3 R_{\rho}^{(1)} - 2 \left[ \frac{67}{8(7)} \right] R_{\rho}^{(1)} R_{\rho}^{(2)} - \frac{27037}{64(7)^3} \left[ R_{\rho}^{(1)} \right]^2 \\
& + 3 \left[ \frac{28968}{64(7)^3} \right] R_{\rho}^{(0)} \left[ R_{\rho}^{(1)} \right]^2 + \frac{257219941}{4096(7)^7} R_{\rho}^{(0)} + \frac{64012703}{4096(7)^7} \left[ R_{\rho}^{(0)} \right]^2 \\
& - \frac{604826712}{4096(7)^7} \left[ R_{\rho}^{(0)} \right]^3 - \frac{5690706300}{4096(7)^7} \left[ R_{\rho}^{(0)} \right]^4 + \frac{5974300368}{4096(7)^7} \left[ R_{\rho}^{(0)} \right]^5.
\end{aligned} \tag{III-51}$$

There is a pattern in the preceding calculations, although it will probably have escaped the reader's attention. As is pointed out in Appendix C, not all of the numerical coefficients in the differential equations for  $R_{\rho}^{(j)}$  are independent, nor are all the coefficients in the algebraic results for  $R_T^{(j)}$  independent. The pattern involves a limited number of numerical coefficients denoted by  $A_n$ .

Moreover, as also pointed out in Appendix C, there is a conveniently economical way to determine the  $R_{\rho}^{(j)}$  as functionals of  $(1 - R_{\rho}^{(0)})$ . One finds

$$R_{\rho}^{(1)} = R_{\rho}^{(0)} \left[ 1 - R_{\rho}^{(0)} \right] \left\{ -A_1 \ln \left[ 1 - R_{\rho}^{(0)} \right] + Q_1 \right\}, \quad (\text{III-52})$$

$$R_{\rho}^{(2)} = R_{\rho}^{(0)} \left[ 1 - R_{\rho}^{(0)} \right] \left\{ B_1 \left[ 1 - R_{\rho}^{(0)} \right] + B_2 \ln \left[ 1 - R_{\rho}^{(0)} \right] + B_3 \left[ 1 - R_{\rho}^{(0)} \right] \ln \left[ 1 - R_{\rho}^{(0)} \right] + B_4 \ln^2 \left[ 1 - R_{\rho}^{(0)} \right] + B_5 \left[ 1 - R_{\rho}^{(0)} \right] \ln^2 \left[ 1 - R_{\rho}^{(0)} \right] + Q_2 \right\}, \quad (\text{III-53})$$

$$R_{\rho}^{(3)} = R_{\rho}^{(0)} \left[ 1 - R_{\rho}^{(0)} \right] \left\{ C_1 \left[ 1 - R_{\rho}^{(0)} \right] + C_2 \ln \left[ 1 - R_{\rho}^{(0)} \right] + C_3 \left[ 1 - R_{\rho}^{(0)} \right] \ln \left[ 1 - R_{\rho}^{(0)} \right] + C_4 \ln^2 \left[ 1 - R_{\rho}^{(0)} \right] + C_5 \left[ 1 - R_{\rho}^{(0)} \right] \ln^2 \left[ 1 - R_{\rho}^{(0)} \right] + C_6 \ln^3 \left[ 1 - R_{\rho}^{(0)} \right] + C_7 \left[ 1 - R_{\rho}^{(0)} \right]^2 + C_8 \left[ 1 - R_{\rho}^{(0)} \right]^2 \ln \left[ 1 - R_{\rho}^{(0)} \right] + C_9 \left[ 1 - R_{\rho}^{(0)} \right]^2 \ln^2 \left[ 1 - R_{\rho}^{(0)} \right] + C_{10} \left[ 1 - R_{\rho}^{(0)} \right] \ln^3 \left[ 1 - R_{\rho}^{(0)} \right] + C_{11} \left[ 1 - R_{\rho}^{(0)} \right]^2 \ln^3 \left[ 1 - R_{\rho}^{(0)} \right] + Q_3 \right\}. \quad (\text{III-54})$$

In (III-53) and (III-54), the coefficients  $B_n$  and  $C_n$  are functions of the generalized coefficients  $A_n$  and the integration constants  $Q_j$ . The expressions for the  $B_n$  and  $C_n$  in terms of the  $A_n$  are also given in Appendix C. Once  $R_{\rho}^{(0)}$  has been determined for each value of  $\zeta$  via (III-42), the corresponding perturbed quantities  $R_{\rho}^{(j)}$  and  $R_T^{(j)}$  for  $j = 1, 2, 3$  may be evaluated to determine the individual contributions to the normalized density and temperature for each of the above orders of the perturbation

development. The density and temperature profiles depend on the Mach number through the  $R_\rho$ ,  $R_T$ , and  $\kappa$  expansions in terms of the Mach number parameter  $\epsilon$ .

The discussion of the Navier-Stokes perturbation results and comparison with Runge-Kutta numerical integration results is deferred until Chapter V.

## CHAPTER IV

### METHODS TO SOLVE THE HIGHER ORDER GASDYNAMIC EQUATIONS

#### Numerical Integration of the Higher Order Equations

As indicated earlier in this report serious difficulties arise when attempts are made numerically to integrate the Burnett, Super-Burnett, or Super-Super-Burnett equations. The nature of the difficulties may be understood from an analysis of the singular points of the differential equations using the linearized equations, just as in the preceding chapter. Following the Navier-Stokes development, the variations of the normalized flow velocity and normalized temperature from their Rankine-Hugoniot values are assumed to be proportional to  $e^{\kappa_1 z}$  far upstream and far downstream. The coupled pairs of linear differential equations then yield characteristic polynomials for the  $\kappa_1$ .

The (linearized) Burnett equations yield a fourth degree characteristic polynomial,

$$\begin{aligned} &70 L_1^4 - 180 L_1^3 + 291 M_1^2 L_1^2 \\ &+ \left[ 81 - 207 M_1^2 \right] M_1^2 L_1 + 54 M_1^4 \left[ M_1^2 - 1 \right] = 0, \end{aligned} \quad (\text{IV-1})$$

in which

$$L_1 = \frac{\mu_1 M_1}{\rho_1 a_1} \kappa_1. \quad (\text{IV-2})$$

The roots of (IV-1) are presented graphically as a function of  $M_1$  in Appendix B.

The upstream roots indicate that numerical integration is feasible starting downstream, as in the Navier-Stokes case, provided  $M_1 \leq 1.89$ . For  $M_1$  between 1.0 and approximately 1.4, the roots of the upstream characteristic polynomial are real and positive or are complex conjugates with positive real parts. The solutions of the linearized equations are thus damped or oscillatory and damped, and the upstream Rankine-Hugoniot asymptotic values are attained for all solutions as  $z \rightarrow -\infty$ . For values of  $M_1$  between approximately 1.4 and approximately 1.9, all roots are complex with positive real parts. All solutions thus exhibit a somewhat stronger oscillatory behavior far upstream for  $M_1$  between approximately 1.4 and approximately 1.9, but remain damped as  $z \rightarrow -\infty$ . Above  $M_1 = 1.9$ , the real part of one pair of conjugate roots changes sign, and there is a manifold of undamped solutions which precludes numerical integration starting downstream.

The roots of the downstream Burnett characteristic polynomial preclude numerical integration starting upstream for all  $M_1$ . Therefore, numerical integration proceeding in the upstream direction is the only feasible choice. However, the integration may be expected to be successful for only the range of Mach numbers indicated above, and experience confirms this expectation.

The (linearized) Super-Burnett equations yield a sixth degree characteristic polynomial,

$$\begin{aligned}
& 7850 L_i^6 + 29160 L_i^5 = 28980 M_i^2 L_i^4 \\
& + \left[ 20475 M_i^4 - 5427 M_i^2 \right] L_i^3 - 36(291) M_i^4 L_i^2 \\
& + \left[ 36(207) M_i^6 - 36(81) M_i^4 \right] L_i \\
& - 54(36) M_i^6 \left[ M_i^2 - 1 \right] = 0
\end{aligned} \tag{IV-3}$$

with  $L_i$  defined as before.

The results for the upstream and downstream roots as functions of  $M_i$  are given in Appendix B. This graphical presentation shows that some of the real roots and some of the real parts of the complex roots have opposite sign, both upstream and downstream, for all Mach numbers. Under these circumstances there is no reason to expect numerical integration to succeed proceeding in either direction for any Mach number, and experience confirms this expectation.

The results of the linearization of the Super-Super-Burnett equations are qualitatively the same as those found for the Super-Burnett equations. The  $\kappa_i$  are determined from the following characteristic polynomial:

$$\begin{aligned}
& 328399(625) L_i^8 - 200(63)(521) L_i^7 \\
& 6300(3791) M_i^2 L_i^6 - 40(81)(49)(59) M_i^2 L_i^5 \\
& + 350(27)(2287) M_i^4 L_i^4 - 54(49) M_i^4 \left[ 2275 M_i^2 - 603 \right] L_i^3 \\
& + 8(49)(81)(97) M_i^6 L_i^2 - 8(49)(243) M_i^6 \left[ 23 M_i^2 - 9 \right] L_i \\
& + 16(49)(729) M_i^8 \left[ M_i^2 - 1 \right] = 0.
\end{aligned} \tag{IV-4}$$

The graphical representation of the roots of this characteristic polynomial, given in Appendix B, reveals that some of the real roots and some of the real parts of the complex roots again have opposite sign, both upstream and downstream, for every Mach number.

Since the conventional numerical methods fail when applied to the higher order equations, the remainder of this chapter is devoted to the perturbation method developed in the previous chapter.

#### Perturbation Expansion Applied to the Burnett Equations

The Burnett equations containing  $p^{(1)} + p^{(2)}$  and  $q^{(1)} + q^{(2)}$ , may be analyzed in the same way as the Navier-Stokes equations to determine a suitable Mach number dependent length scale. The results of such an analysis are qualitatively the same as for the Navier-Stokes case, and thus suggest a perturbation expansion which incorporates the Burnett result for the physically significant  $\kappa_2$  (negative, tending to zero as  $M_1 \rightarrow \infty$ ). The expansion of  $\frac{\mu_2 M_2}{\rho_2 a_2} \kappa_2$  in powers of  $\epsilon = M_2^2 - 1$  follows from the characteristic polynomial (IV-1).

$$\kappa_2 = \frac{\rho_2 a_2}{\mu_2 M_2} \left[ \frac{3}{7} \epsilon + \frac{102}{2(7)^3} \epsilon^2 - \frac{4194}{4(7)^5} \epsilon^3 + \frac{291234}{8(7)^7} \epsilon^4 + \dots \right]. \quad (\text{IV-5})$$

Since the first term in (IV-5) is the same as the first term in the Navier-Stokes  $\kappa_2$  expansion (III-36), the Burnett calculations do not effect any changes to the Navier-Stokes perturbation

results through second order in  $\epsilon$ , although of course the numerical values of  $\kappa$  are different.

Following the same procedures used for the Navier-Stokes equations, the Burnett calculations in third order yield

$$\frac{dR_{\rho}^{(1)}}{d\zeta} + \left(2 R_{\rho}^{(0)} - 1\right) R_{\rho}^{(1)} = -\frac{87}{4(7)^2} \left[R_{\rho}^{(0)}\right]^2 + \frac{87}{4(7)^2} \left[R_{\rho}^{(0)}\right]^3 \quad (\text{IV-6})$$

and

$$\begin{aligned} R_T^{(2)} = R_{\rho}^{(2)} + \frac{67}{8(7)} \left(1 - 2 R_{\rho}^{(0)}\right) R_{\rho}^{(1)} - \frac{4811}{64(7)^3} R_{\rho}^{(0)} \\ - \frac{18397}{64(7)^3} \left[R_{\rho}^{(0)}\right]^2 + \frac{23208}{64(7)^3} \left[R_{\rho}^{(0)}\right]^3. \end{aligned} \quad (\text{IV-7})$$

Referring to equations (III-46) and (III-47), it can be seen that the third-order perturbation results for the Navier-Stokes equations and the Burnett equations are of the same form; only the values of the corresponding coefficients have changed.

The fourth-order Burnett calculations yield

$$\begin{aligned} \frac{dR_{\rho}^{(2)}}{d\zeta} + \left(2 R_{\rho}^{(0)} - 1\right) R_{\rho}^{(2)} = -2 \left[\frac{87}{4(7)^2}\right] R_{\rho}^{(0)} R_{\rho}^{(1)} \\ + 3 \left[\frac{87}{4(7)^2}\right] \left[R_{\rho}^{(0)}\right]^2 R_{\rho}^{(1)} - \left[R_{\rho}^{(1)}\right]^2 - \frac{56193}{16(7)^4} \left[R_{\rho}^{(0)}\right]^2 \\ + \frac{126828}{16(7)^4} \left[R_{\rho}^{(0)}\right]^3 - \frac{70635}{16(7)^4} \left[R_{\rho}^{(0)}\right]^4 \end{aligned} \quad (\text{IV-8})$$

and



$$\begin{aligned}
R_T^{(3)} = & R_\rho^{(3)} + \frac{67}{8(7)} \left[ 1 - 2 R_\rho^{(0)} \right] R_\rho^{(2)} - \frac{4811}{64(7)^3} R_\rho^{(1)} \\
& - 2 \left[ \frac{18397}{64(7)^3} \right] R_\rho^{(0)} R_\rho^{(1)} + 3 \left[ \frac{23208}{64(7)^3} \right] \left[ R_\rho^{(0)} \right]^2 R_\rho^{(1)} \\
& - \frac{67}{8(7)} \left[ R_\rho^{(1)} \right]^2 - \frac{1878497}{512(7)^5} R_\rho^{(0)} + \frac{21661565}{512(7)^5} \left[ R_\rho^{(0)} \right]^2 \\
& - \frac{28194216}{512(7)^5} \left[ R_\rho^{(0)} \right]^3 + \frac{8411148}{512(7)^5} \left[ R_\rho^{(0)} \right]^4. \quad (IV-9)
\end{aligned}$$

Again, the form of the Burnett results is the same as those found in fourth order for Navier-Stokes, except that the numerical coefficients are different.

The fact that the perturbation equations have the same form for the Burnett equations as the Navier-Stokes equations applies also to the Super-Burnett equations and the Super-Super-Burnett equations. This "pattern" is what gives general utility to the material in Appendix C concerning integration of the perturbation equations.

The fifth-order Burnett results are

$$\begin{aligned}
\frac{dR_\rho^{(3)}}{d\zeta} + \left[ 2R_\rho^{(0)} - 1 \right] R_\rho^{(3)} = & - 2 \left[ \frac{87}{4(7)^2} \right] R_\rho^{(0)} R_\rho^{(2)} \\
& + 3 \left[ \frac{87}{4(7)^2} \right] \left[ R_\rho^{(0)} \right]^2 R_\rho^{(2)} - \frac{87}{4(7)^2} \left[ R_\rho^{(1)} \right]^2 + 3 \left[ \frac{87}{4(7)^2} \right] \left[ R_\rho^{(1)} \right]^2 R_\rho^{(0)} \\
& - 2 R_\rho^{(2)} R_\rho^{(1)} - 2 \left[ \frac{56193}{16(7)^4} \right] R_\rho^{(0)} R_\rho^{(1)}
\end{aligned}$$

$$\begin{aligned}
& + 3 \left[ \frac{126828}{16(7)^4} \right] \left[ R_{\rho}^{(0)} \right]^2 R_{\rho}^{(1)} - 4 \frac{70635}{16(7)^4} \left[ R_{\rho}^{(0)} \right]^3 R_{\rho}^{(1)} \\
& - \frac{39762438}{128(7)^6} \left[ R_{\rho}^{(0)} \right]^2 + \frac{218183394}{128(7)^6} \left[ R_{\rho}^{(0)} \right]^3 \\
& - \frac{324539190}{128(7)^6} \left[ R_{\rho}^{(0)} \right]^4 + \frac{146118234}{128(7)^6} \left[ R_{\rho}^{(0)} \right]^5 \quad (IV-10)
\end{aligned}$$

and

$$\begin{aligned}
R_T^{(4)} = & R_{\rho}^{(4)} + \frac{67}{8(7)} \left( 1 - 2 R_{\rho}^{(0)} \right) R_{\rho}^{(3)} - \frac{4811}{64(7)^3} R_{\rho}^{(2)} \\
& - 2 \left[ \frac{18397}{64(7)^3} \right] R_{\rho}^{(0)} R_{\rho}^{(2)} + 3 \left[ \frac{23208}{64(7)^3} \right] \left[ R_{\rho}^{(0)} \right]^2 R_{\rho}^{(2)} \\
& - \frac{1878497}{512(7)^5} R_{\rho}^{(1)} + 2 \left[ \frac{21661565}{512(7)^5} \right] R_{\rho}^{(0)} R_{\rho}^{(1)} \\
& - 3 \left[ \frac{28194216}{512(7)^5} \right] \left[ R_{\rho}^{(0)} \right]^2 R_{\rho}^{(1)} + 4 \left[ \frac{8411148}{512(7)^5} \right] \left[ R_{\rho}^{(0)} \right]^3 R_{\rho}^{(1)} \\
& - 2 \left[ \frac{67}{8(7)} \right] R_{\rho}^{(1)} R_{\rho}^{(2)} - \frac{18397}{64(7)^3} \left[ R_{\rho}^{(1)} \right]^2 \\
& + 3 \left[ \frac{23208}{64(7)^3} \right] \left[ R_{\rho}^{(1)} \right]^2 R_{\rho}^{(0)} + \frac{277563301}{4096(7)^7} R_{\rho}^{(0)} \\
& + \frac{11550194783}{4096(7)^7} \left[ R_{\rho}^{(0)} \right]^2 - \frac{66307987032}{4096(7)^7} \left[ R_{\rho}^{(0)} \right]^3 \\
& + \frac{94921844100}{4096(7)^7} \left[ R_{\rho}^{(0)} \right]^4 - \frac{40441615152}{4096(7)^7} \left[ R_{\rho}^{(0)} \right]^5 \quad (IV-11)
\end{aligned}$$

Discussion of the solutions to the perturbation equations is deferred until Chapter V.

Perturbation Expansion Applied to the  
Super-Burnett Equations and the  
Super-Super-Burnett Equations

The Super-Burnett equations, containing  $p^{(1)} + p^{(2)} + p^{(3)}$  and  $q^{(1)} + q^{(2)} + q^{(3)}$ , constitute two coupled third-order non-linear differential equations for the velocity (or density) and temperature. The equations provide a rationale for a perturbation expansion which incorporates the Super-Burnett result for the physically significant  $\kappa_2$  (negative, tending to zero as  $M_1 \rightarrow \infty$ ), just as the Navier-Stokes and Burnett equations provide such a rationale. The expansion for  $\frac{\mu_2 M_2}{\rho_2 a_2} \kappa_2$  in powers of  $\epsilon = M_2^2 - 1$  follows from the characteristic polynomial (IV-4),

$$\kappa_2 = \frac{\rho_2 a_2}{\mu_2 M_2} \left[ \frac{3}{7} \epsilon + \frac{102}{2(7)^3} \epsilon^2 - \frac{14190}{4(7)^5} \epsilon^3 - \frac{1123053}{8(7)^7} \epsilon^4 + \dots \right]. \quad (\text{IV-12})$$

Since the first two terms of (IV-12) are the same as the corresponding two terms in the Burnett  $\kappa_2$  expansion, the Super-Burnett calculations do not change the Burnett perturbation results through third order in  $\epsilon$ , except of course through the numerical value of  $\kappa_2$ .

In fourth and fifth orders in  $\epsilon$ , the calculations yield equations for the normalized density and temperature which are of the same form as the perturbation equations derived in the Navier-Stokes and Burnett perturbation work. The generalized equations and the coefficients appropriate to Super-Burnett are given in Appendix C.

The length scale expansion for the Super-Super-Burnett equations is

$$\kappa_2 = \frac{\rho_2 a_2}{\mu_2 M_2} \left[ \frac{3}{7} \epsilon + \frac{102}{2(7)^3} \epsilon^2 - \frac{14190}{4(7)^5} \epsilon^3 + \frac{1058952}{8(7)^7} \epsilon^4 + \dots \right]. \quad (\text{IV-13})$$

It is clear from this form for  $\kappa_2$  that the Super-Super-Burnett calculations do not change the Super-Burnett results through fourth order in  $\epsilon$ . In fifth order, the results are of the same form as the fifth-order results for Navier-Stokes, Burnett, and Super-Burnett. The Super-Super-Burnett coefficients are also given in Appendix C.

The solutions of the perturbation equations derived in this section for the normalized density and temperature profiles will be discussed in the next chapter.

As a concluding remark on the work required in the perturbation development, the determination of the eighty-four coefficients needed through fifth order in  $\epsilon$  was a major effort. The pattern, which ultimately evolved, was not obvious or confirmed until the Super-Burnett development was completed.

The intuitive expectation that the  $R_\rho^{(j)}$  and  $R_T^{(j)}$  ( $j = 1, 2, 3, \dots$ ) should vanish when  $R_\rho^{(0)} = 1$ , in order to satisfy the Rankine-Hugoniot relations, provided a convenient mechanism for checking the coefficients of the powers of  $R_\rho^{(0)}$  in each perturbation equation. That is, the sum of the coefficients of the powers of  $R_\rho^{(0)}$  had to vanish for each perturbation equation in order to satisfy the Rankine-Hugoniot conditions far upstream. Although this was a convenient check on the calculations, the

mechanism was not foolproof. It turns out that within the arithmetic processes of substitution, expansion and collecting terms, it is possible to carry through a mathematical error, undetected; yet, with a result that satisfies the vanishing of this coefficient sum. The calculations are lengthy and require meticulous attention to preclude introducing such casual errors. Errors of this sort may go undetected except by separate and independent checks of the calculations.

In the present work, alternate approaches were employed to determine firm values of the coefficient sets  $A_2$  through  $A_4$ ,  $A_5$  through  $A_8$ ,  $A_{10}$  through  $A_{12}$ ,  $A_{13}$  through  $A_{16}$ , and  $A_{17}$  through  $A_{21}$  as these are the coefficient sets of the powers of  $R_0^{(0)}$  in each of the gasdynamic developments.

The final values for the coefficients in each of the sets are based on the fact that the same results were obtained from at least two independent calculations for each order of  $\epsilon$  of the perturbation expansion in each of the gasdynamic developments.

## CHAPTER V

### SHOCK WAVE PROFILES BASED ON THE METHODS OF NUMERICAL INTEGRATION AND PERTURBATION EXPANSION

#### Results for the Navier-Stokes Equations and the Burnett Equations Based on the Method of Numerical Integration

An increment size of 0.05 upstream Maxwell mean free paths was chosen for the fourth-order Runge-Kutta numerical integration. Smaller increment sizes gave the same results for normalized density and temperature everywhere within the shock wave (through six decimal places). The linearized Navier-Stokes equations and the linearized Burnett equations were used to determine the initial values for the numerical integration, starting from the assigned value downstream

$$\left[ \frac{\rho}{\rho_2} \right] - 1 = -0.001 .$$

Figures 3 through 6 exhibit the normalized density profiles and normalized temperature profiles for  $M_1 = 1.5$  and  $M_1 = 2.0$ . Additional results for the Navier-Stokes normalized density profile at higher Mach numbers are given in the next section. The Navier-Stokes equations were integrated numerically by other authors many

Figure 3 - Gas density profiles in a normal shock wave ( $M_1 = 1.5$ ) based on the numerical integration of the Navier-Stokes and Burnett gasdynamic differential equations.

\_\_\_\_\_ Navier-Stokes normalized density

----- Burnett normalized density

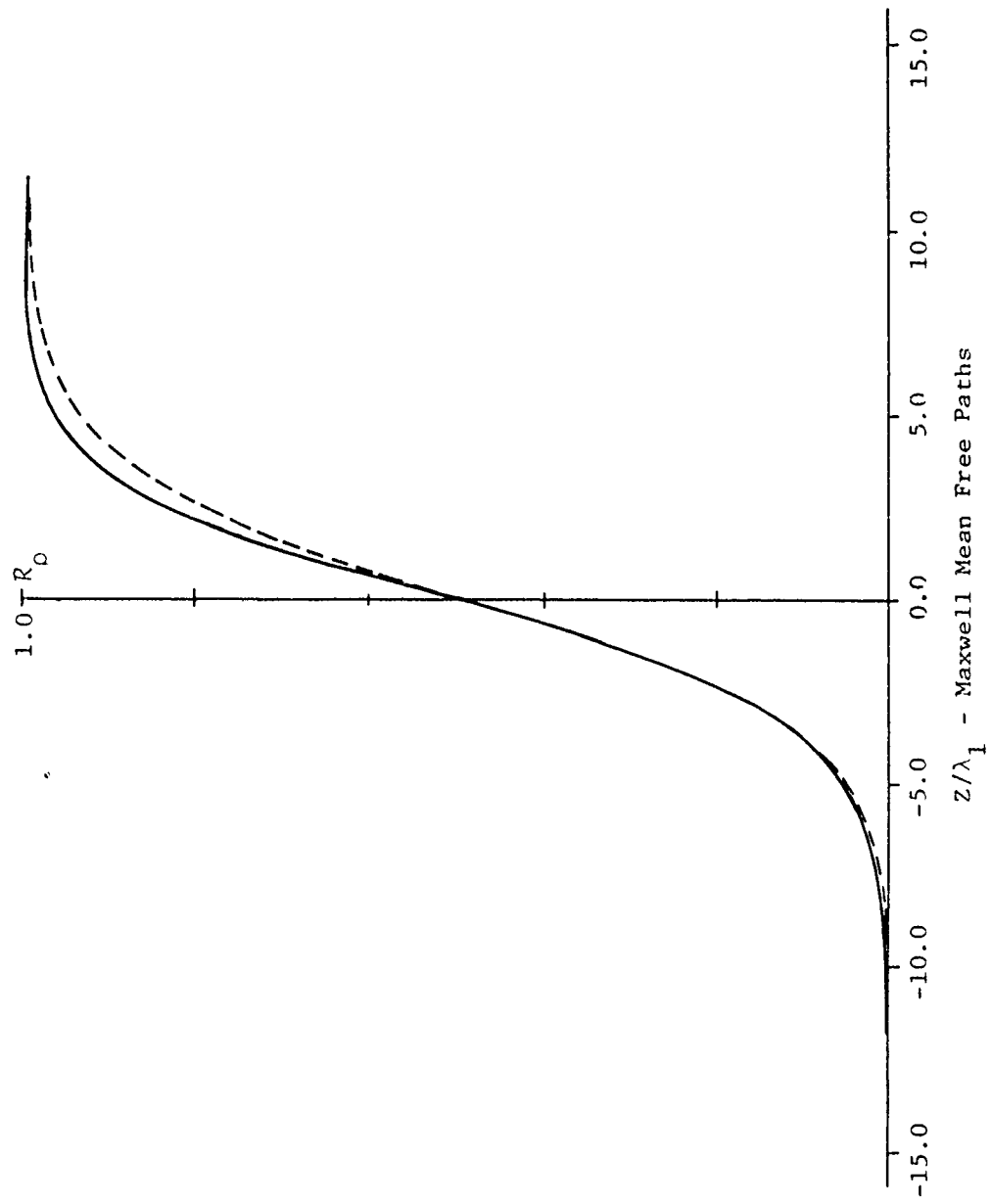




Figure 4 - Gas density profiles in a normal shock wave ( $M_1 = 2.0$ ) based on the numerical integration of the Navier-Stokes and Burnett gasdynamic differential equations.

\_\_\_\_\_ Navier-Stokes normalized density

----- Burnett normalized density

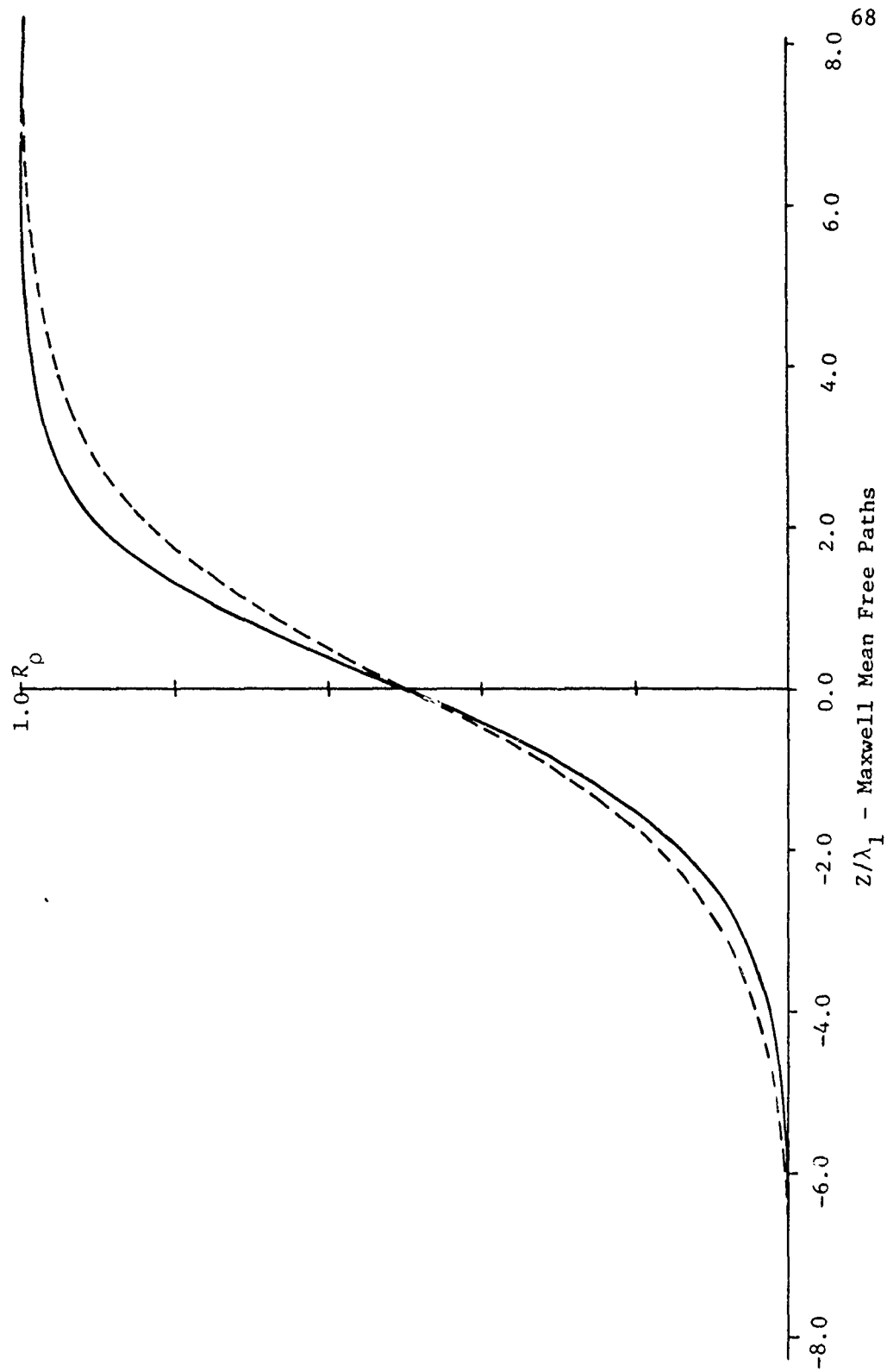


Figure 5 - Gas temperature profiles in a normal shock wave ( $M_1 = 1.5$ ) based on the numerical integration of the Navier-Stokes and Burnett gasdynamic differential equations.

\_\_\_\_\_ Navier-Stokes normalized temperature  
- - - - - Burnett normalized temperature

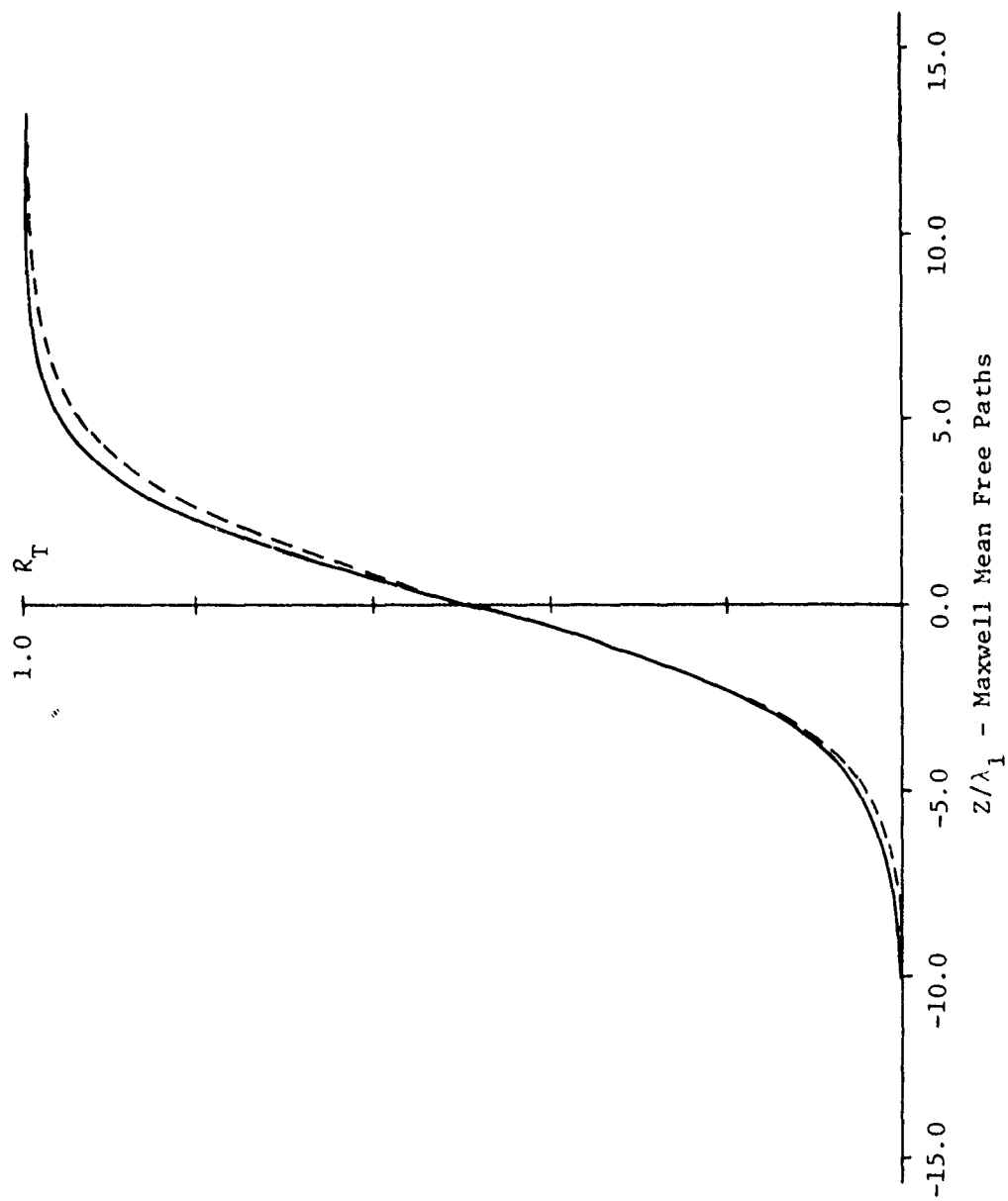
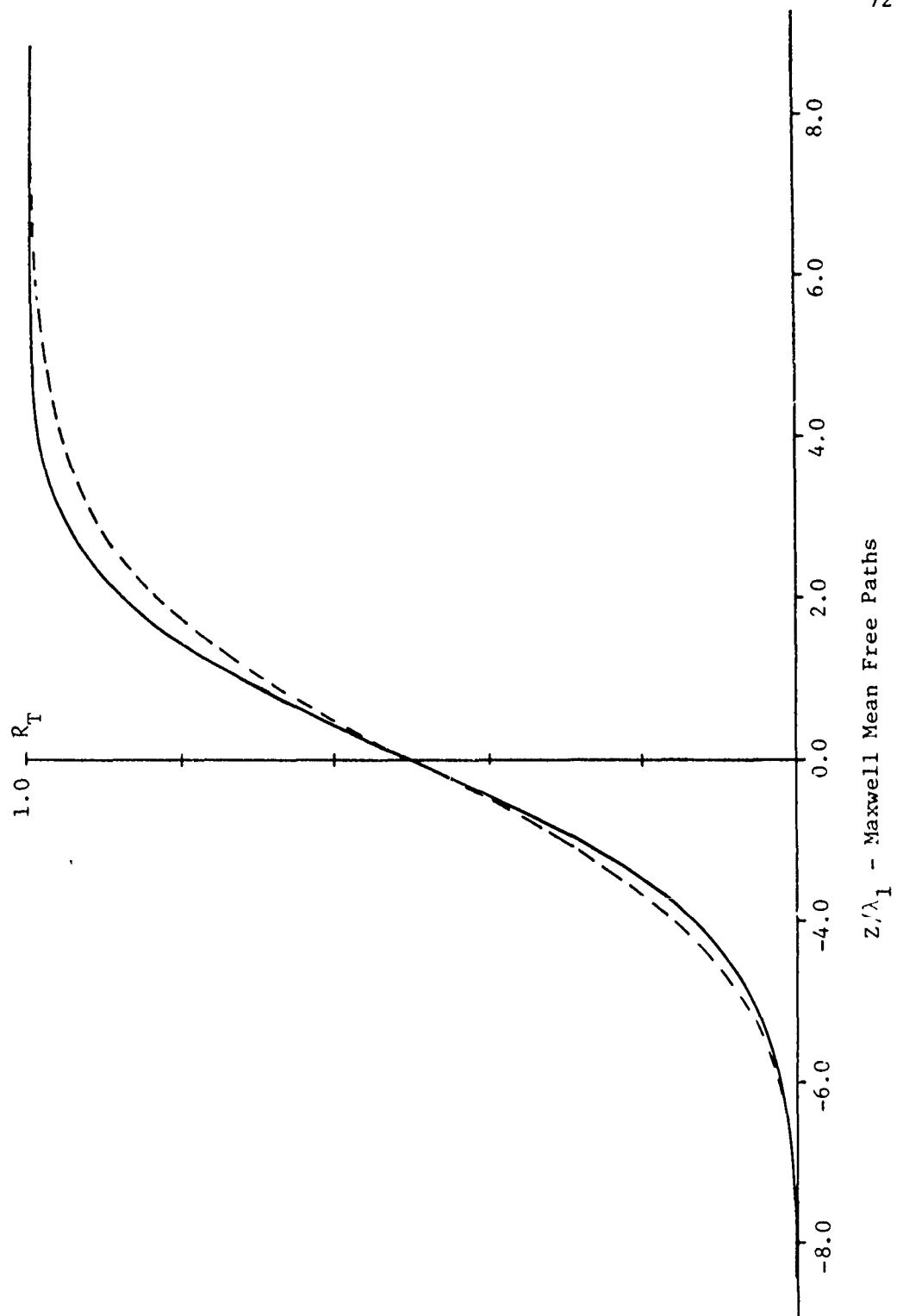


Figure 6 - Gas temperature profiles in a normal shock wave ( $M_1=2.0$ ) based on the numerical integration of the Navier-Stokes and Burnett gasdynamic differential equations.

\_\_\_\_\_ Navier-Stokes normalized temperature

----- Burnett normalized temperature



years ago, but (as mentioned in Chapter I) the Burnett equations have not been integrated numerically before.

Figure 7 shows the Mach number dependence of the distance from the center of the normalized temperature profile to the center of the normalized density profile (the former is always upstream relative to the latter).

As Figures 3 through 7 indicate, there are definite differences between the Navier-Stokes shock structure and the Burnett shock structure, even for  $M_1 \leq 2$ ; the difference in Mach number dependence of the separation of the profiles is particularly conspicuous. The differences in the profiles themselves are accentuated in plots of the asymmetry quotients (introduced in Chapter I) as functions of Mach number, as shown in Figure 8 and Figure 9.

The results of this section suggest that the attention of experimentalists should be directed toward asymmetry quotients for temperature profiles as well as density profiles, and toward the separation of the profiles.

Results for the Navier-Stokes Density Profile  
Based on the Methods of Numerical  
Integration and Perturbation  
Expansion

The success of the perturbation method, as applied to the Navier-Stokes density profile, may be judged from the comparisons in Figures 10 through 13. It is clear from the figures that the

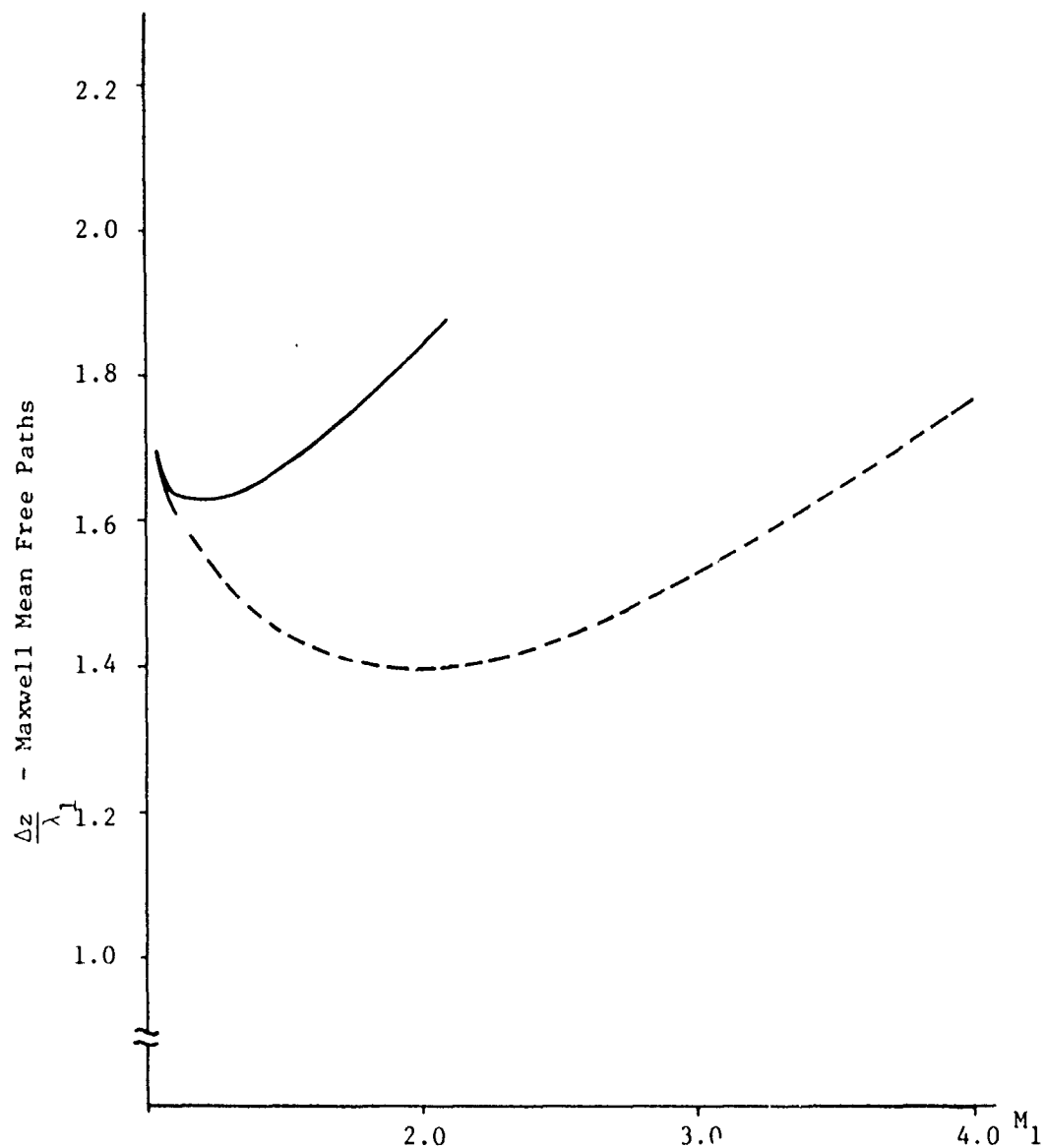


Figure 7 - Mach number ( $M_1$ ) dependence of the temperature-density separation in a normal shock wave based on the numerical integration of the Navier-Stokes and Burnett gasdynamic differential equations.

$$\text{Profile separation } \frac{\Delta z}{\lambda_1} \equiv \left( \frac{z}{\lambda_1} \right)_{R_\rho = 1/2} - \left( \frac{z}{\lambda_1} \right)_{R_T = 1/2}$$

----- Navier-Stokes

————— Burnett



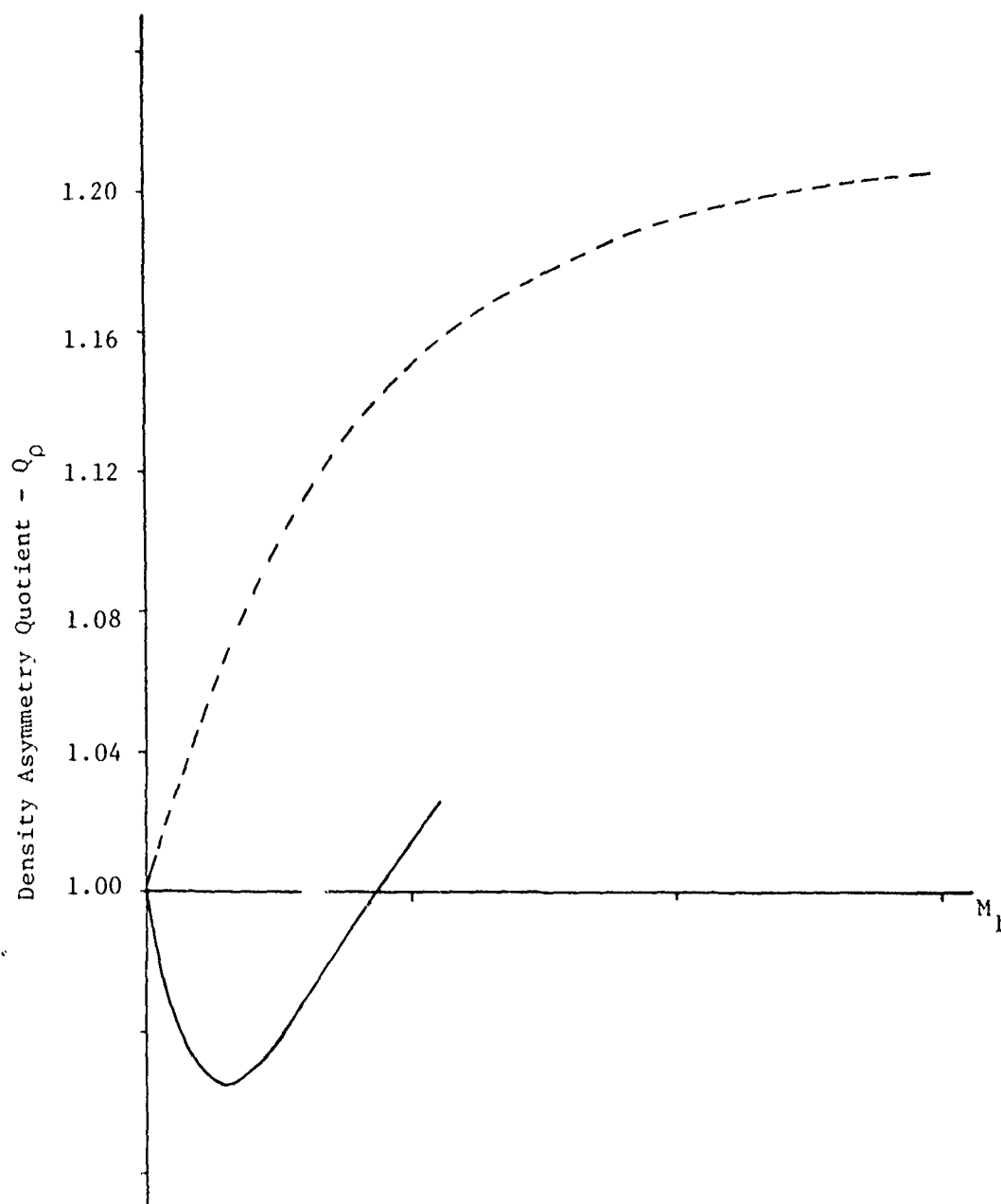


Figure 8 -- Density asymmetry quotient ( $Q_\rho$ ) versus  $M_1$  based on the numerical integration of the Navier-Stokes and Burnett gasdynamic differential equations.

----- Navier-Stokes numerical integration  
 \_\_\_\_\_ Burnett numerical integration

Figure 10 - Navier-Stokes density profiles in a normal shock wave ( $M_1 = 1.5$ ). A comparison of density profiles based on the methods of numerical integration and perturbation expansion.

\_\_\_\_\_ Numerical integration  
 ..... Zeroth order perturbation  
 -.-.-.-.- First order perturbation  
 - - - - - Second order perturbation  
 \_\_\_\_\_ Third order perturbation

The third order perturbation profile is indiscernible from the numerical integration profile within the scale of the figure.

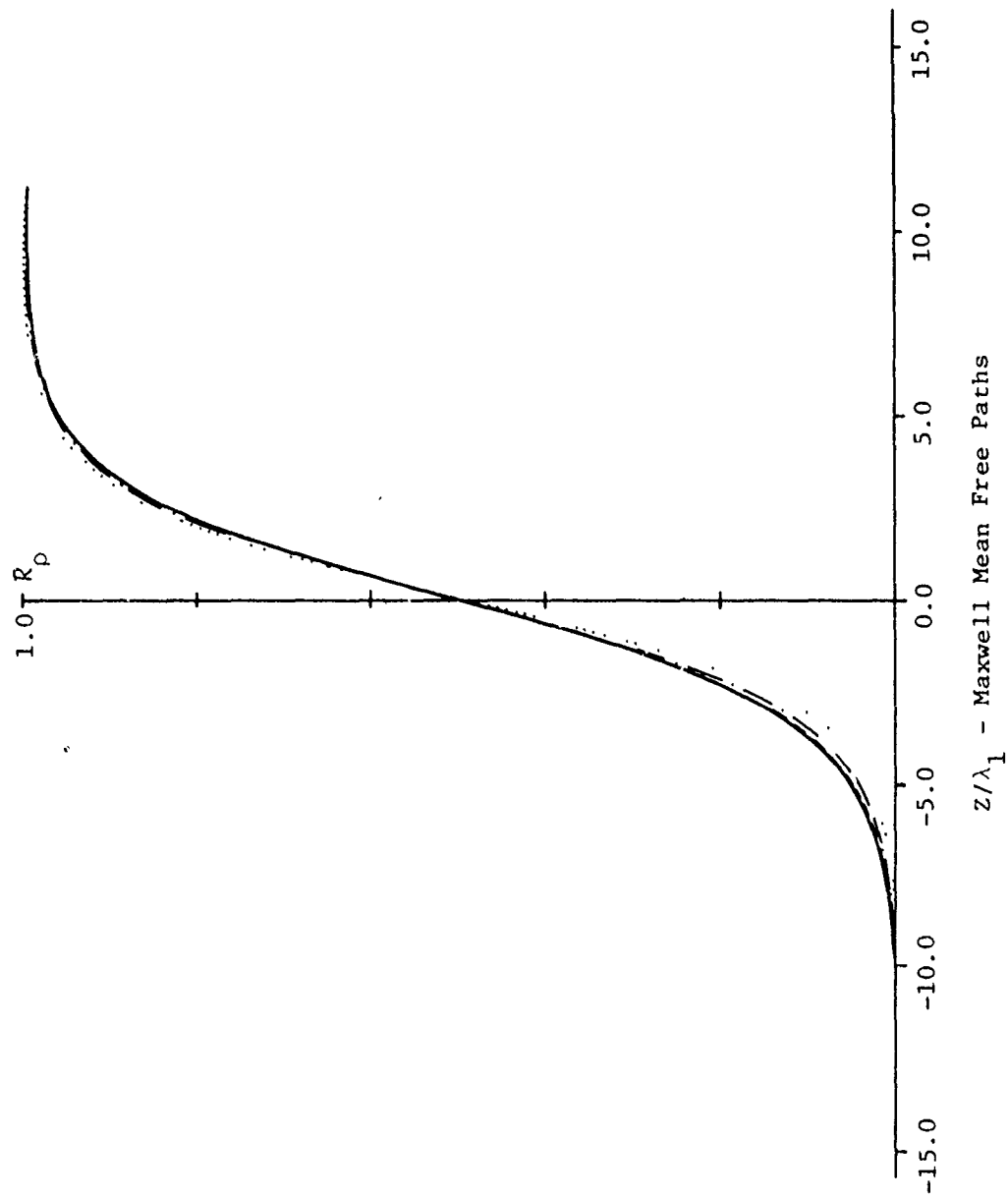


Figure 11 - Navier-Stokes density profiles in a normal shock wave ( $M_1 = 2.0$ ). A comparison of density profiles based on the methods of numerical integration and perturbation expansion.

\_\_\_\_\_ Numerical integration  
..... Zeroth order perturbation  
\_\_\_\_ \_ First order perturbation  
- - - - - Second order perturbation  
\_ \_ \_ \_ \_ Third order perturbation

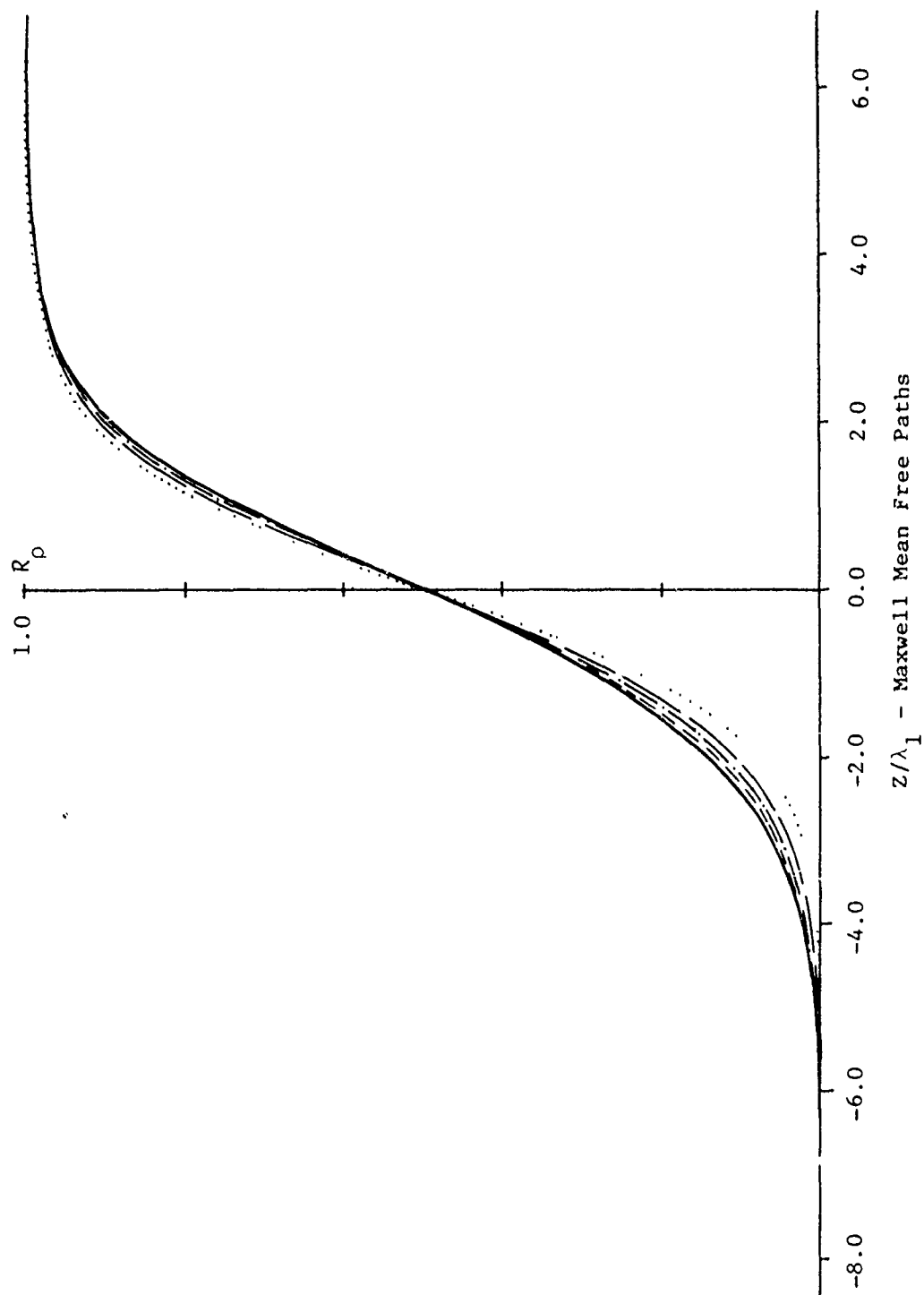


Figure 12 - Navier-Stokes density profiles in a normal shock wave ( $M_1 = 3.0$ ). A comparison of density profiles based on the methods of numerical integration and perturbation expansion.

\_\_\_\_\_ Numerical integration  
..... Zeroth order perturbation  
\_\_\_ \_\_\_ First order perturbation  
..... Second order perturbation  
\_\_\_ \_\_\_ Third order perturbation

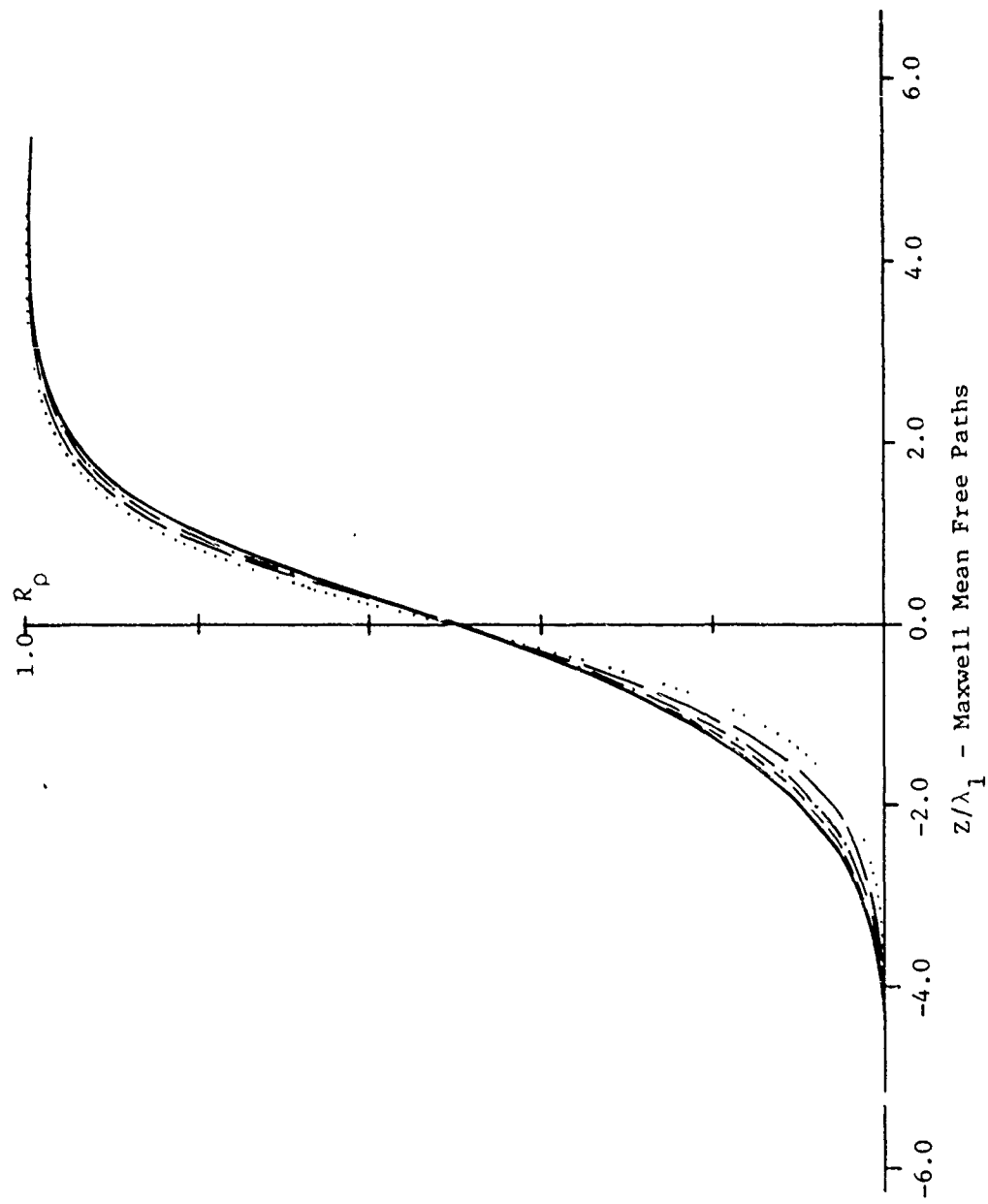
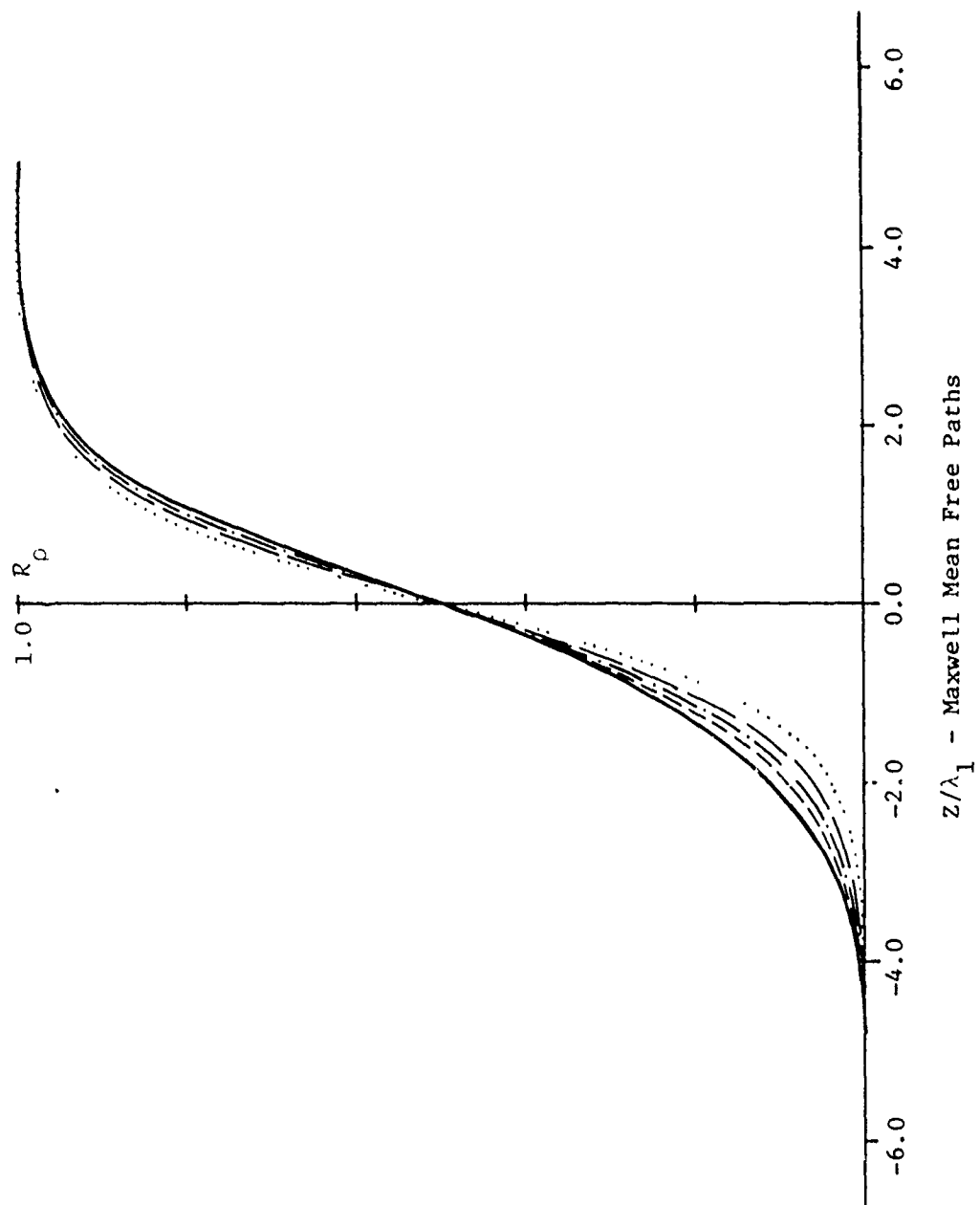


Figure 13 - Navier-Stokes density profiles in a normal shock wave ( $M_1 = 4.0$ ). A comparison of density profiles based on the methods of numerical integration and perturbation expansion.

\_\_\_\_\_ Numerical integration  
..... Zeroth order perturbation  
\_\_\_ \_\_\_ First order perturbation  
- - - - Second order perturbation  
- - - - Third order perturbation





successive approximations of the perturbation method are converging toward the Runge-Kutta result. The agreement between the perturbation results and numerical integration is satisfactory for the lower Mach numbers throughout the profile, but it would be desirable to know the perturbation results to another order or two for the higher Mach numbers to do justice to the upstream portion of the profile.

The convergence of the perturbation results toward the Runge-Kutta result is also manifested in plots of the asymmetry quotient, as shown in Figure 14.

#### Results for the Burnett Density Profile Based on the Methods of Numerical Integration and Perturbation Expansion

The results of the perturbation method, as applied to the Burnett density profile, are compared with the Runge-Kutta results in Figures 15 and 16. Figures 17 and 18 give the perturbation results for Mach numbers beyond the range of applicability of numerical integration. Figure 19 contains a comparison between the asymmetry quotient as determined by numerical integration (up to  $M_1 \doteq 2$ ), and the asymmetry quotient as determined by perturbation expansion.<sup>†</sup>

Figures 15 and 16 show, as in the case of Navier-Stokes equations, that the perturbation results are converging toward the

---

<sup>†</sup> Since  $R_0^{(0)}$  is symmetric yielding  $Q_0 = 1$  for all Mach numbers, these results have been omitted from all plots of the asymmetry quotient.

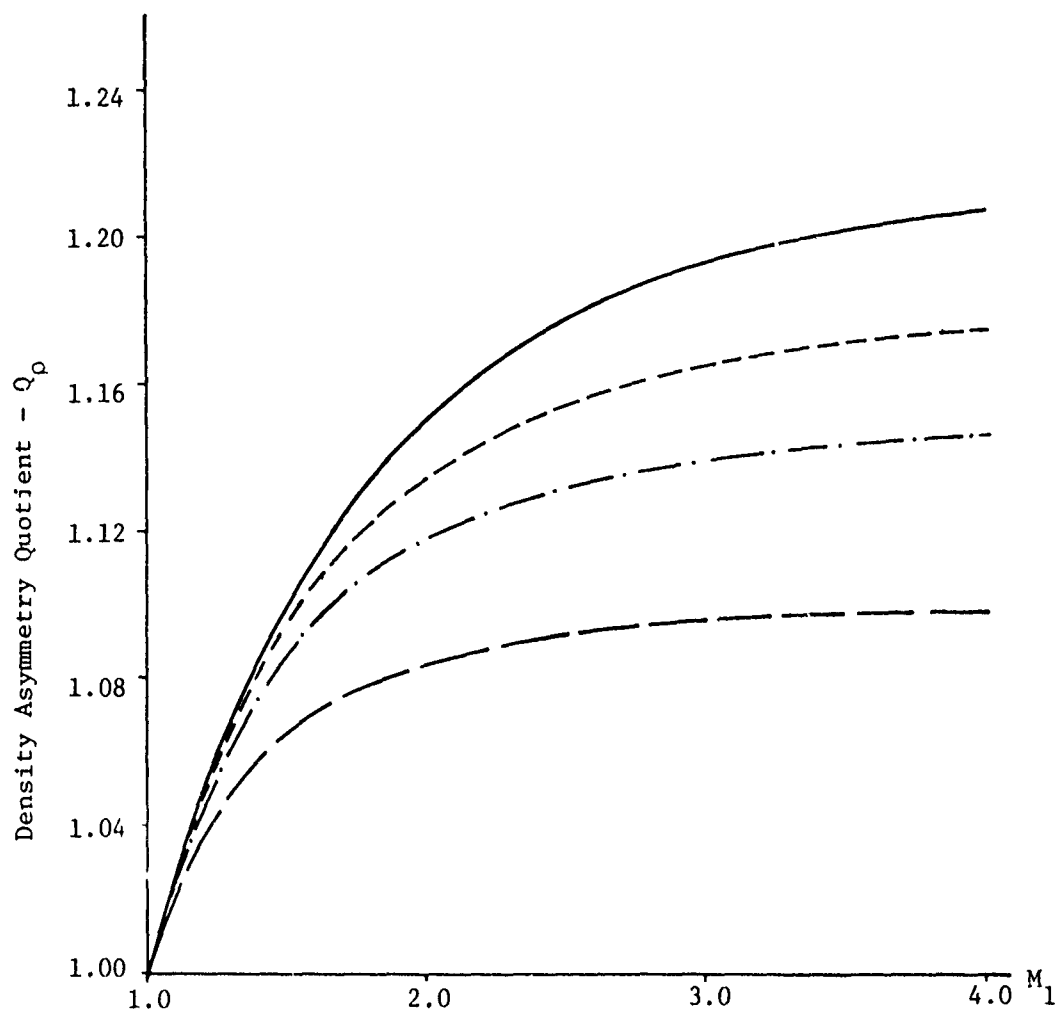


Figure 14 - Density asymmetry quotient ( $Q_p$ ) versus  $M_1$  from the Navier-Stokes perturbation expansion. A comparison of the results for  $Q_p$  based on the methods of perturbation expansion and numerical integration.

- \_\_\_\_\_ Numerical integration
- \_\_\_\_ \_ First order perturbation expansion
- . - . - Second order perturbation expansion
- - - - - Third order perturbation expansion

Figure 15 - Burnett density profiles in a normal shock wave ( $M_1 = 1.5$ ).  
A comparison of density profiles based on the methods of  
numerical integration and perturbation expansion.

\_\_\_\_\_ Numerical integration  
 \_\_\_\_ First order perturbation  
 \_\_\_\_ Second order perturbation  
 \_\_\_\_ Third order perturbation

The third order perturbation profile is indiscernible from  
the numerical integration profile within the scale of the  
figure.

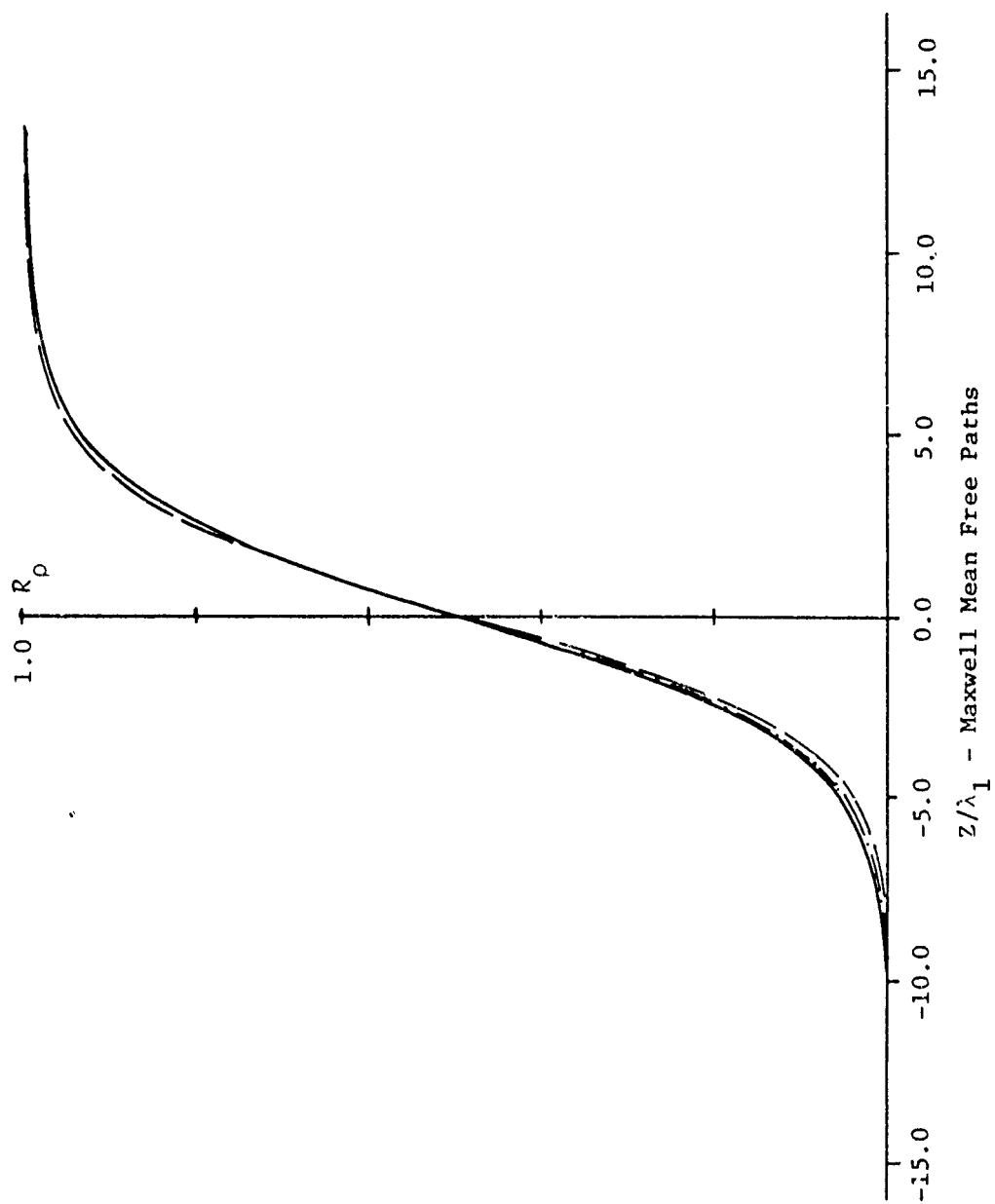


Figure 16 - Burnett density profiles in a normal shock wave ( $M_1 = 2.0$ ).  
A comparison of density profiles based on the methods of  
numerical integration and perturbation expansion.

\_\_\_\_\_ Numerical integration  
\_\_\_\_ \_ First order perturbation  
\_\_\_\_ \_ Second order perturbation  
\_\_\_\_ \_ Third order perturbation

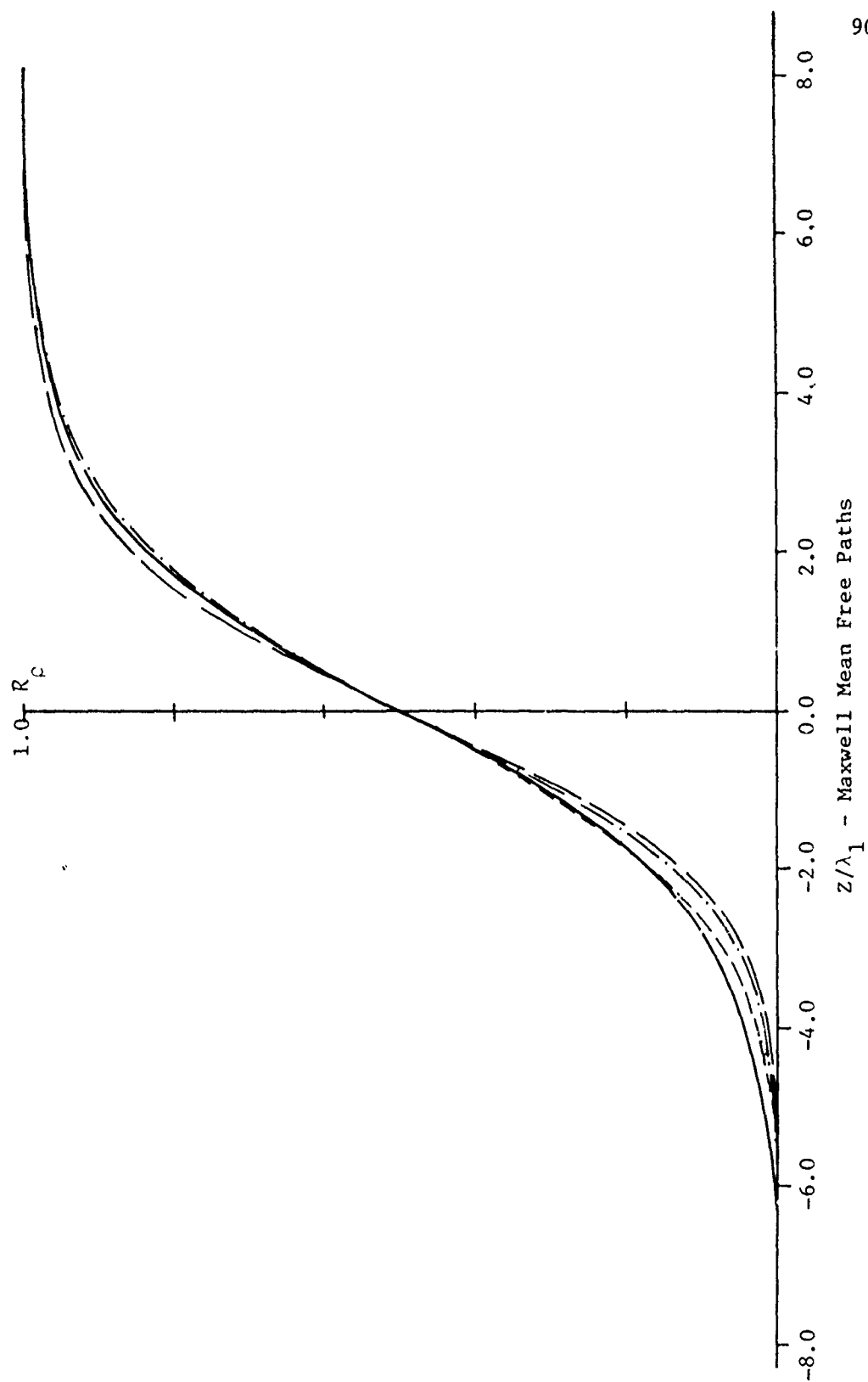


Figure 17 - Burnett density profiles in a normal shock wave ( $M_1 = 3.0$ ).  
A comparison of density profiles determined from the  
perturbation expansion.

— · — · — · — First order perturbation  
— — — — — Second order perturbation  
————— Third order perturbation



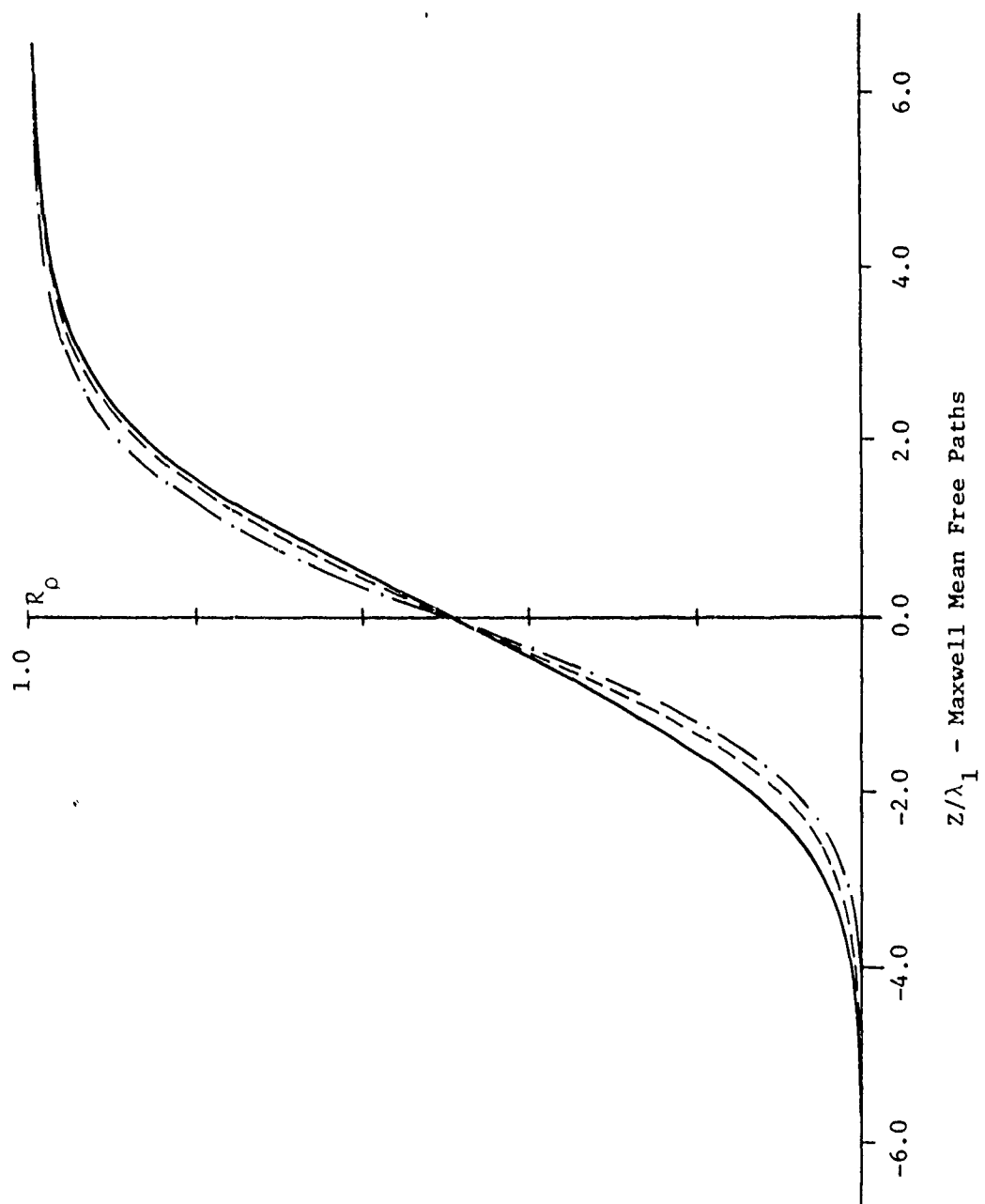
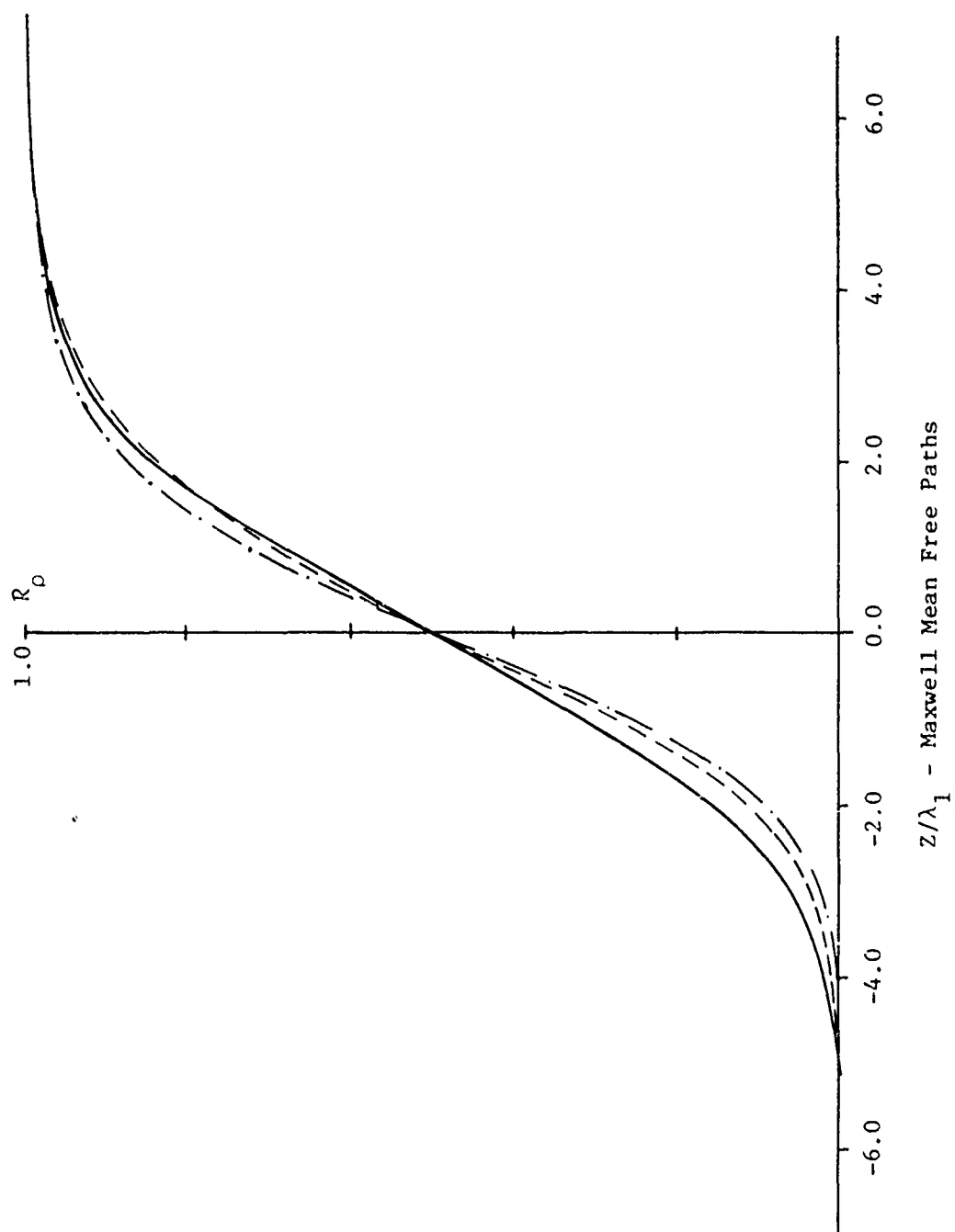


Figure 18 - Burnett density profiles in a normal shock wave ( $M_1 = 4.0$ ).  
A comparison of density profiles determined from the  
perturbation expansion.

— · — · — · — First order perturbation  
- - - - - Second order perturbation  
\_\_\_\_\_ Third order perturbation



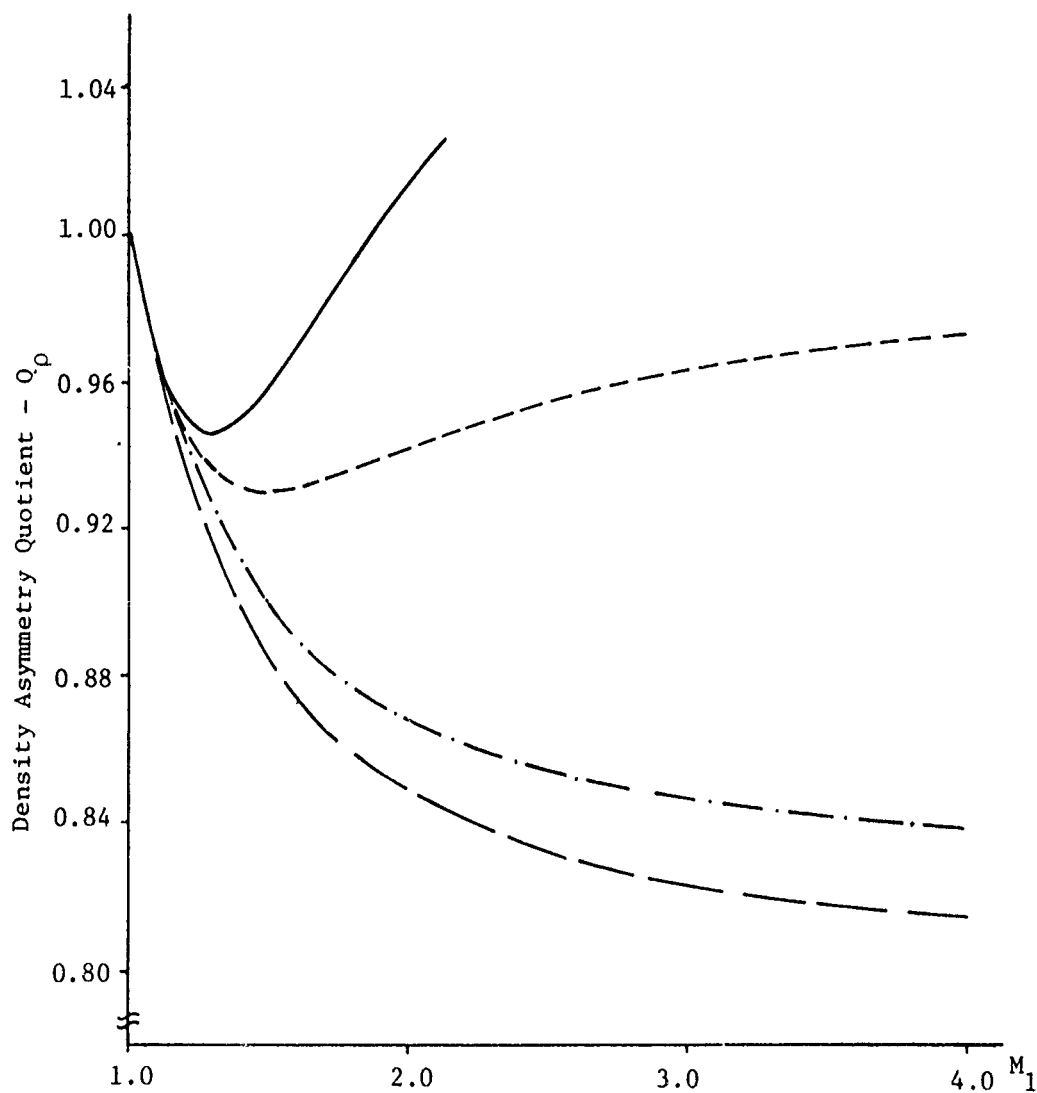


Figure 19 - Density asymmetry quotient ( $Q_0$ ) versus  $M_1$  from the Burnett perturbation expansion. A comparison of the results for  $Q_0$  based on the methods of perturbation expansion and numerical integration.

- \_\_\_\_\_ Numerical integration
- \_\_\_\_\_ First order perturbation expansion
- . - . - . Second order perturbation expansion
- - - - - Third order perturbation expansion

Runge-Kutta result. This conclusion is tempered, but not vitiated, by the comparison of asymmetry quotients in Figure 19, which likewise indicate a tendency toward convergence.

Intuitively Trustworthy Parts of the Results  
for the Density Profile through Super-  
Super-Burnett Order Based on the  
Method of Perturbation Expansion

The Chapman-Enskog development provides a criterion for identifying the trustworthy parts of predictions of the Navier-Stokes or higher order gasdynamic equations. Predictions of the Navier-Stokes equations may be trusted only through first order in the mean free path, because the Burnett contributions to the stress and heat flux are of second order in the mean free path. Similarly, predictions of the Burnett equations may be trusted only through second order in the mean free path, because the Super-Burnett contributions to the stress and heat flux are of third order in the mean free path, etc.

In the previous chapter it was pointed out that the perturbation expansion may be applied with equal justification to all the higher order gasdynamic equations through Super-Super-Burnett order, and presumably this feature persists to all orders of the Chapman-Enskog development. Accordingly, the results of a particular order of the perturbation expansion may be regarded as trustworthy only if they are unaffected by additional Chapman-Enskog contributions to the stress and heat flux. Thus, the Navier-Stokes result for  $R_{\rho}^{(0)}$  is trustworthy, but  $R_{\rho}^{(1)}$ ,  $R_{\rho}^{(2)}$ , and  $R_{\rho}^{(3)}$  are not trustworthy

because they are modified by the inclusion of Burnett (and higher Chapman-Enskog order) contributions to the stress and heat flux. Likewise, the Burnett results for  $R_{\rho}^{(0)}$  and  $R_{\rho}^{(1)}$  are trustworthy, but  $R_{\rho}^{(2)}$  and  $R_{\rho}^{(3)}$  are not trustworthy, etc.

According to the viewpoint explained in the preceding two paragraphs, the trustworthy part of the Super-Burnett result for the density profile is

$$R_{\rho}^{(0)} + \epsilon R_{\rho}^{(1)} + \epsilon^2 R_{\rho}^{(2)}$$

and the trustworthy part of the Super-Super-Burnett result is

$$R_{\rho}^{(0)} + \epsilon R_{\rho}^{(1)} + \epsilon^2 R_{\rho}^{(2)} + \epsilon^3 R_{\rho}^{(3)} .$$

These trustworthy parts of the predictions of the density profile are exhibited in Figures 20 through 23, and the corresponding results for the asymmetry quotient are exhibited in Figure 24. The trustworthy parts of the Navier-Stokes and Burnett calculations have been omitted from Figures 20 through 24 to avoid undue cluttering of the figures, but the Navier-Stokes numerical integration results have been included to provide an indication of the magnitude of higher order Chapman-Enskog effects. These figures may be said to provide a hint that extremely high orders of the Chapman-Enskog development will not be required for a satisfactory theory of shock structure.

Figure 20 - Super-Burnett and Super-Super-Burnett density profiles in a normal shock wave ( $M_1 = 1.5$ ). A comparison of the trustworthy parts of the perturbation results for Super-Burnett and Super-Super-Burnett with the Navier-Stokes numerical integration results.

----- Navier-Stokes numerical integration  
- . - . - . Second order Super-Burnett perturbation  
\_\_\_\_\_ Third order Super-Super-Burnett perturbation

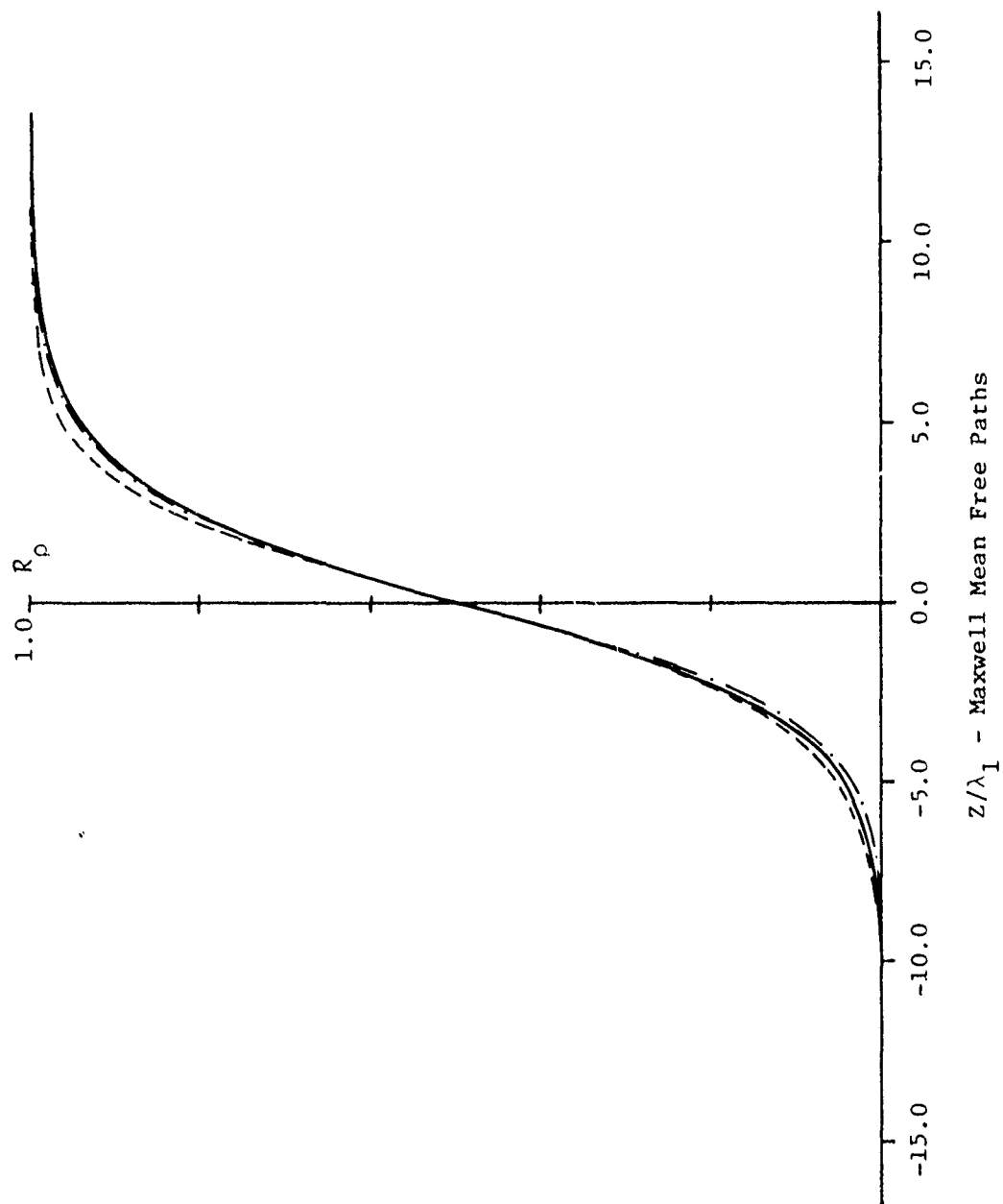




Figure 21 - Super-Burnett and Super-Super-Burnett density profiles in a normal shock wave ( $M_1 = 2.0$ ). A comparison of the trustworthy parts of the perturbation results for Super-Burnett and Super-Super-Burnett with the Navier-Stokes numerical integration results.

----- Navier-Stokes numerical integration  
- . - . - . Second order Super-Burnett perturbation  
\_\_\_\_\_ Third order Super-Super-Burnett perturbation

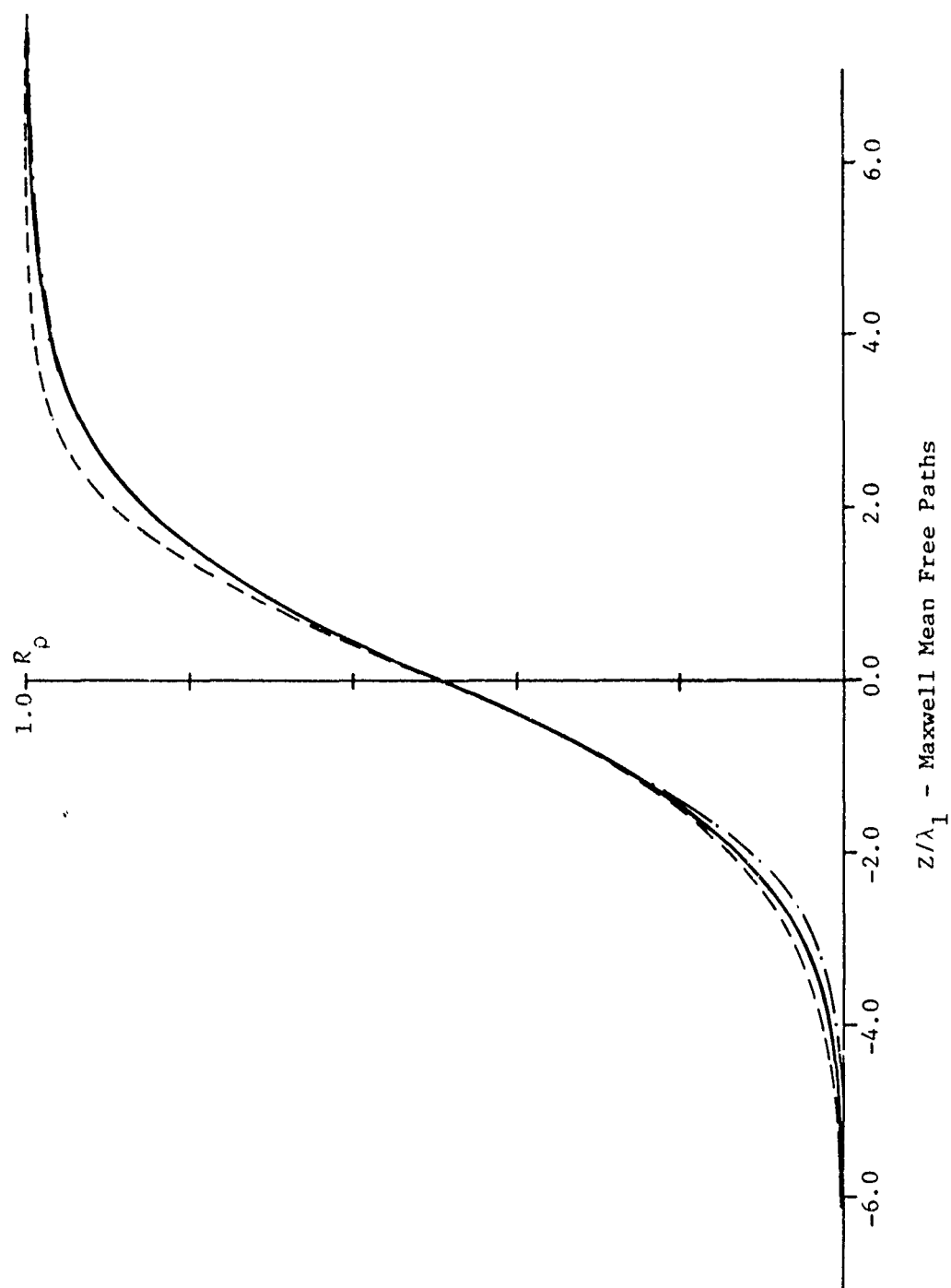


Figure 22 - Super-Burnett and Super-Super-Burnett density profiles in a normal shock wave ( $M_1 = 3.0$ ). A comparison of the trustworthy parts of the perturbation results for Super-Burnett and Super-Super-Burnett with the Navier-Stokes numerical integration results.

----- Navier-Stokes numerical integration  
- . - . - . Second order Super-Burnett  
\_\_\_\_\_ Third order Super-Super-Burnett

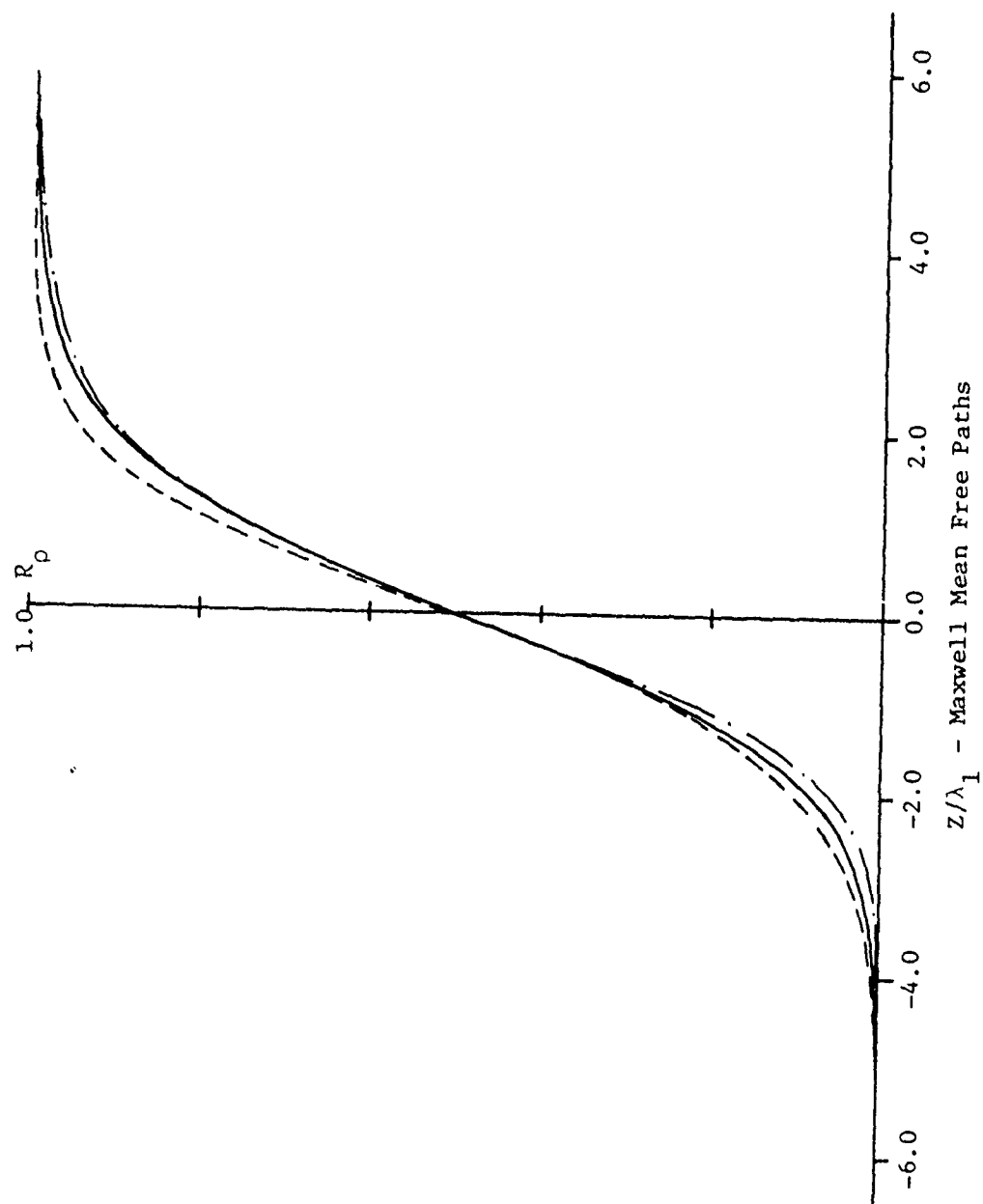
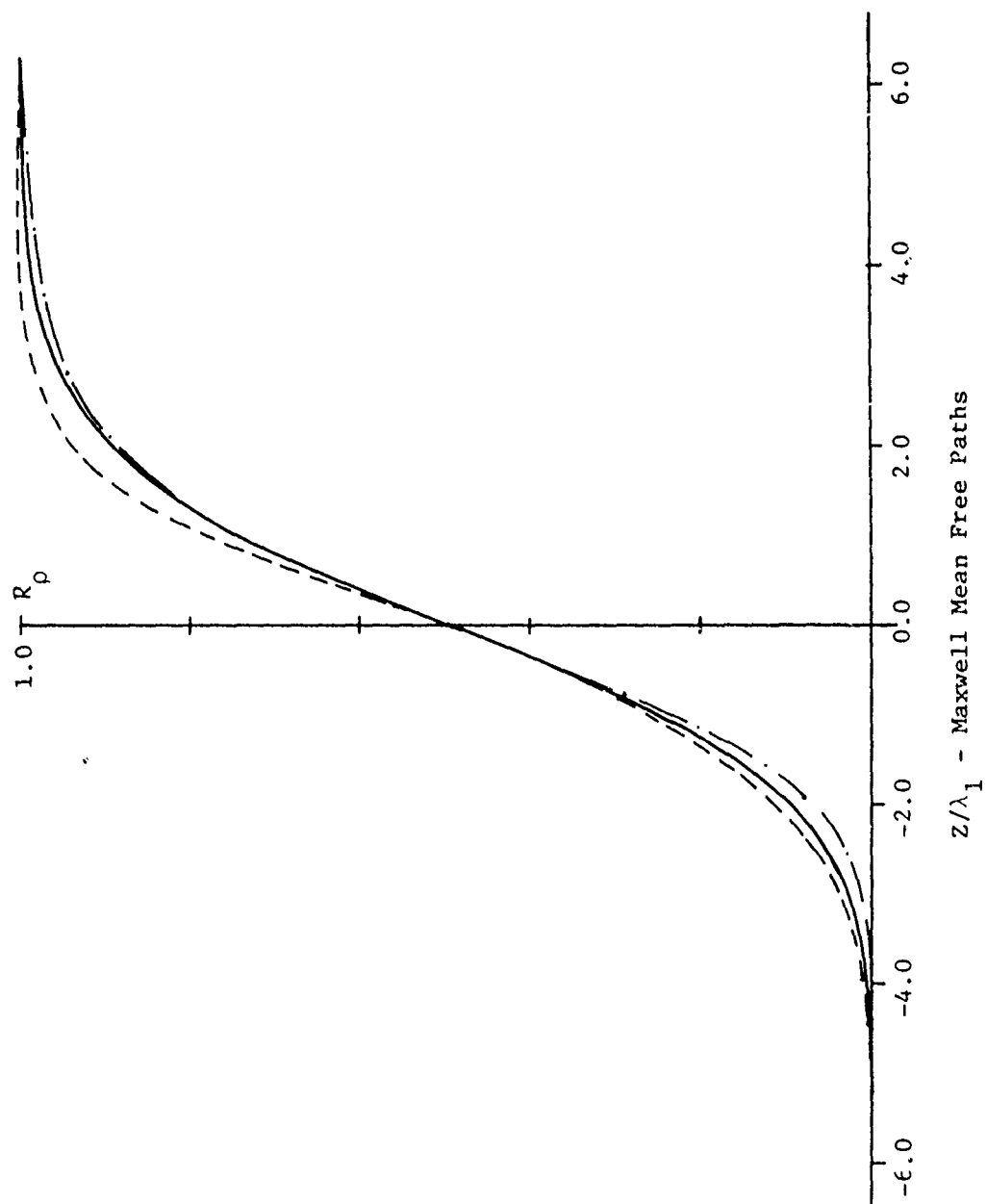


Figure 23 - Super-Burnett and Super-Super-Burnett density profiles in a normal shock wave ( $M_1 = 4.0$ ). A comparison of the trustworthy parts of the perturbation results for Super-Burnett and Super-Super-Burnett with the Navier-Stokes numerical integration results.

\_\_\_\_\_ Navier-Stokes numerical integration  
\_\_\_\_.\_\_\_\_.\_\_\_\_.Second order Super-Burnett  
\_\_\_\_\_ Third order Super-Super-Burnett



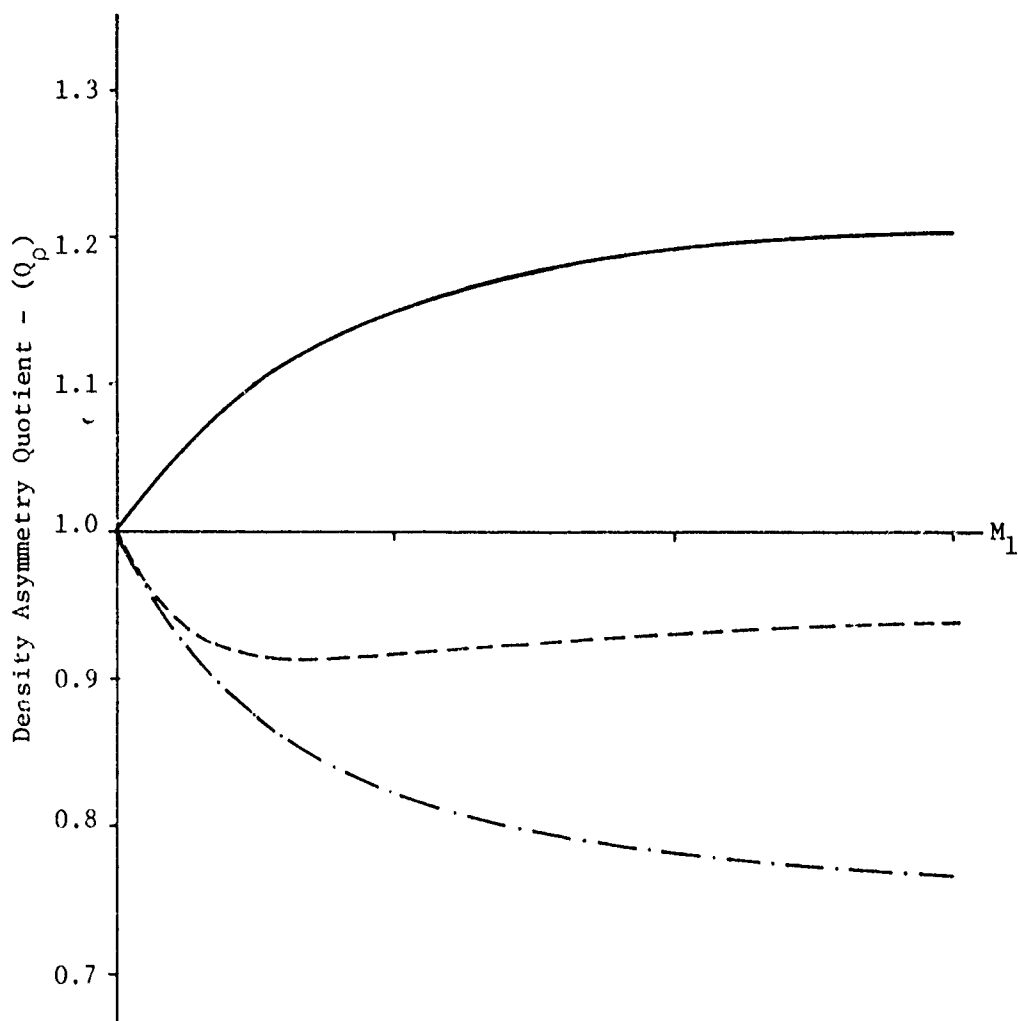


Figure 24 - Density asymmetry quotient ( $Q_\rho$ ) versus  $M_1$  from the Super-Burnett and Super-Super-Burnett perturbation expansions. A comparison of the trustworthy parts of the perturbation results for Super-Burnett and Super-Super-Burnett expansions with Navier-Stokes numerical integration results.

\_\_\_\_\_ Navier-Stokes numerical integration  
 - . - . - . Second order Super-Burnett perturbation  
 - - - - - Third order Super-Super-Burnett perturbation

## CHAPTER VI

### COMMENTS AND OUTLOOK

The general pattern among the numerical coefficients in the perturbation results derived in the preceding chapters may be obtained from the differential equation

$$\begin{aligned} \frac{dR_\rho}{d\zeta} = & R_\rho - [R_\rho]^2 + \left\{ A_1 [R_\rho]^2 - A_1 [R_\rho]^3 \right\} \epsilon \\ & + \left\{ A_2 [R_\rho]^2 + A_3 [R_\rho]^3 + A_4 [R_\rho]^4 \right\} \epsilon^2 \\ & + \left\{ A_5 [R_\rho]^2 + A_6 [R_\rho]^3 + A_7 [R_\rho]^4 + A_8 [R_\rho]^5 \right\} \epsilon^3 + \dots \quad (VI-1) \end{aligned}$$

and the algebraic relation

$$\begin{aligned} R_T = & R_\rho + \left\{ A_9 [1-R_\rho] R_\rho \right\} \epsilon \\ & + \left\{ A_{10} R_\rho + A_{11} [R_\rho]^2 + A_{12} [R_\rho]^3 \right\} \epsilon^2 \\ & + \left\{ A_{13} R_\rho + A_{14} [R_\rho]^2 + A_{15} [R_\rho]^3 + A_{16} [R_\rho]^4 \right\} \epsilon^3 \\ & + \left\{ A_{17} R_\rho + A_{18} [R_\rho]^2 + A_{19} [R_\rho]^3 + A_{20} [R_\rho]^4 + A_{21} [R_\rho]^5 \right\} \epsilon^4 + \dots \quad (VI-2) \end{aligned}$$

by expanding  $R_\rho$  and  $R_T$  in powers of  $\epsilon$ . This observation constitutes an explanation or interpretation of the general pattern. The first-order differential equation (VI-1) is in terms of the unexpanded normalized density  $R_\rho$  and may be integrated using standard Runge-Kutta numerical integration methods. The normalized



temperature profile may then be determined from the algebraic equation (VI-2) relating  $R_T$  and  $R_\rho$ .

In carrying out the algebraic determination of the  $R_T^{(j)}$  for an expansion of  $\kappa_2$  in which the numerical values of the coefficients were unspecified

$$\kappa_2 = \frac{\rho_2 a_2}{\mu_2 M_2} \left\{ \alpha_1 \epsilon + \alpha_2 \epsilon^2 + \alpha_3 \epsilon^3 + \alpha_4 \epsilon^4 + \dots \right\} \quad (\text{VI-3})$$

it was found that all of the terms containing the expansion coefficients ( $\alpha_i$ ) cancel during the calculation. Thus, the final relationship (VI-2) between  $R_T$  and  $R_\rho$  is independent of the choice for  $\kappa_2$ . This is a satisfying result because  $R_T$  should be uniquely determined by  $R_\rho$ , assuming each is a monotonic function of  $z$ , quite independent of any reciprocal length scale  $\kappa_2$ . Also, in the analytic expression for the  $R_\rho^{(j)}$ , it turns out that the  $\alpha_i$  are uniquely determined for each set of the gasdynamic equations from the requirement that the ratio  $R_\rho^{(j)}/R_\rho^{(0)}$  be bounded throughout the shock wave for each  $(j)$ . In order for this ratio to be finite, the  $\alpha_i$  must have the values as specified in Table I for each of the gasdynamic developments.

The upstream-downstream symmetry observed in the basic gasdynamic differential equations leads to interrelationships among the perturbation coefficients  $A_n$  in (VI-1). Since formally equivalent expansions for  $dR_\rho/dz$  may be obtained based on  $(M_2^2-1)$  and  $\kappa_2$  or  $(M_1^2-1)$  and  $\kappa_1$ , and since the expansions must represent one and the same differential equation for  $R_\rho$ , roughly half the

TABLE I  
COEFFICIENTS  $\alpha_1$  FOR  $\kappa_2$

$\alpha_1$	Navier-Stokes	Burnett	Super-Burnett	Super-Super-Burnett
$\alpha_1$	$\frac{3}{7}$	$\frac{3}{7}$	$\frac{3}{7}$	$\frac{3}{7}$
$\alpha_2$	$-\frac{9}{2(7)^3}$	$\frac{102}{2(7)^3}$	$\frac{102}{2(7)^3}$	$\frac{102}{2(7)^3}$
$\alpha_3$	$\frac{369}{4(7)^5}$	$-\frac{4194}{4(7)^5}$	$-\frac{14190}{4(7)^5}$	$-\frac{14190}{4(7)^5}$
$\alpha_4$	$-\frac{13509}{8(7)^7}$	$\frac{291234}{8(7)^7}$	$-\frac{1123053}{8(7)^7}$	$\frac{1058952}{8(7)^7}$

coefficients in each order of  $\epsilon$  are determined by the other half (and coefficients from lower orders of  $\epsilon$ ).

The consequences of upstream-downstream symmetry indicate that it may be possible to extend the perturbation results to higher order in  $\epsilon$  with somewhat less labor than was expended in this report.

All profile and asymmetry data calculated in this report. have been for Maxwell molecules, for which the viscosity-temperature relation is  $\mu \propto T$ . Numerical integration results for the Navier-Stokes gasdynamic equations may also be obtained for more realistic intermolecular potentials by using the viscosity-temperature relation  $\mu \propto T^\omega$ , where  $\omega$  is fractional. For purposes of these final remarks, the Navier-Stokes results for a realistic potential ( $\mu \propto T^{0.68}$ ) have been calculated and are compared with recent experimental data and perturbation results for Maxwell molecules in Figure 25.

The perturbation results for the asymmetry in the density profile in a Maxwell gas, although based on an idealized molecular model, resemble the trend of discrepancy between current experimental results and the quantitatively incorrect Navier-Stokes results.

It seems reasonable to hope that use of a more realistic potential model, together with an extension of the perturbation method to one or perhaps two additional orders, might lead to definitive checks on the nonlinear features of the Boltzmann collision operator, especially in view of the inadequacy of the Navier-Stokes equations even for low Mach numbers.

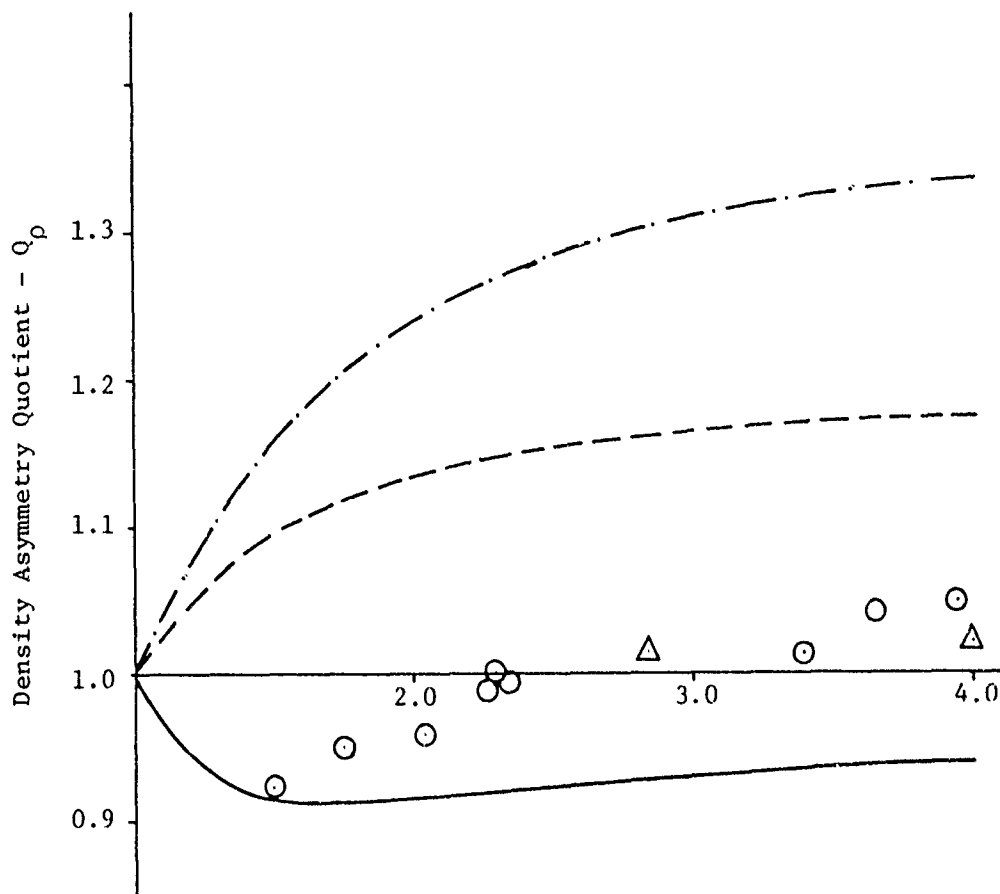


Figure 25 - Density asymmetry quotient ( $Q_p$ ) in a normal shock wave as a function of upstream Mach number ( $M_1$ ). A comparison of Navier-Stokes numerical integration (realistic potential) and third order perturbation (Maxwell molecules) results with experiment.

— · — · — Navier-Stokes numerical integration

— — — Navier-Stokes third order perturbation

— — — Super-Super-Burnett third order perturbation

⊙ Experiment - Alsmeyer (1975)

△ Experiment - Schmidt (1969)

## BIBLIOGRAPHY

- Alsmeyer, H. To be published in Journal of Fluid Mechanics.
- Bhatnagar, P. L., E. P. Gross, and M. Krook. Physical Review 94, 511 (1954).
- Bird, G. A. Journal of Fluid Mechanics 30, 479 (1967).
- Bird, G. A. Physics of Fluids 6, 1518 (1963).
- Bird, G. A. Physics of Fluids 13, 1172 (1970).
- Bird, G. A. Physics of Fluids 13, 2676 (1970).
- Bird, G. A. In Proceedings of the Fourth International Symposium on Rarefied Gas Dynamics, edited by J. H. de Leeuw (Academic Press, 1965) 1, 216.
- Bird, G. A. In Proceedings of the Sixth International Symposium on Rarefied Gas Dynamics, edited by L. Trilling and H. Y. Wachman (Academic Press, 1969) 1, 301.
- Chang, C. S. Wang and G. E. Uhlenbeck. In Studies in Statistical Mechanics, edited by J. de Boer and G. E. Uhlenbeck (North Holland, Amsterdam, 1970), Vol. V.
- Chapman S. and T. G. Cowling. The Mathematical Theory of Non-Uniform Gases (Third edition, Cambridge University Press, 1970).
- Fiszdon, W. In Proceedings of the Ninth International Symposium on Rarefied Gas Dynamics, edited by E. Becker (Academic Press, 1974) 2, B. 23.
- Foch, J. P., Jr. and G. W. Ford. In Studies in Statistical Mechanics, edited by J. de Boer and G. E. Uhlenbeck (North Holland, Amsterdam, 1970), Vol. 5.
- Gilbarg, D. and D. Paolucci. Journal of Rational Mechanics and Analysis 2, 617 (1953).
- Hicks, B. L. and S. M. Yen. Physics of Fluids 10, 458 (1967).
- Hicks, B. L., S. M. Yen, and J. Reilly. Journal of Fluid Mechanics 53, 85 (1972).

- Holtz, T., E. P. Muntz, and S. M. Yen. Physics of Fluids 14, 545 (1971).
- Montgomery, J. T. Physics of Fluids 18, 148 (1975).
- Mott-Smith, H. M. Physical Review 82, 885 (1951).
- Muckenfuss, C. Physics of Fluids 5, 1325 (1962).
- Nordsieck, A. and B. L. Hicks. In Proceedings of the Fifth International Symposium on Rarefied Gas Dynamics, edited by C. L. Brundin (Academic Press, 1967) 1, 695.
- Schmidt, B. Journal of Fluid Mechanics 39, 361 (1969).
- Schwartz, L. M. and D. F. Hornig. Physics of Fluids 12, 1669 (1963).
- Sherman, F. S. and L. Talbott. In Proceedings of the First International Symposium on Rarefied Gas Dynamics, edited by F. M. Devienne (Pergamon, New York, 1960), 161.
- Sturtevant, B. and E. A. Steinhilper. In Proceedings of the Eighth International Symposium on Rarefied Gas Dynamics, edited by K. Karamcheti (Academic Press, 1974) 1, 159.
- Talbot, L. and F. S. Sherman, NASA Memorandum 12-14-58W (1959).
- Vincenti, W. G. and C. H. Kruger, Jr. Introduction to Physical Gas Dynamics (John Wiley & Sons, 1965).
- Yen, S. M. International Journal of Heat and Mass Transfer 14, 1865 (1971).
- Yen, S. M. Physics of Fluids 9, 1417 (1966).
- Yen, S. M., and W. Ng. Journal of Fluid Mechanics 65, 127 (1974).
- Yen, S. M., W. Ng, R. M. Osten, and W. P. Walters. Coordinated Science Laboratory Progress Report- July 1971 through June 1972, August 1972.
- Yen, S. M., W. P. Walters, W. Ng, and J. R. Flood. In Proceedings of the Eighth International Symposium on Rarefied Gas Dynamics, edited by K. Karamcheti (Academic Press, 1974) 1, 137.

APPENDIX A

THE MAXWELL EIGENFUNCTIONS

The eigenfunctions  $\Psi_{r,\ell}(\vec{c})$  used in the moment calculations of Chapter II are formed from associated Laguerre polynomials  $L_r^{\ell+1/2}(c^2)$  and zonal harmonics  $c^\ell P_\ell(\hat{c}_z)$ ,<sup>†</sup>

$$\Psi_{r,\ell}(\vec{c}) = L_r^{\ell+1/2}(c^2) c^\ell P_\ell(\hat{c}_z). \quad (\text{A-1})$$

The associated Laguerre polynomials may be determined from the generating function

$$\frac{e^{-c^2 \frac{t}{1-t}}}{(1-t)^{\ell+3/2}} = \sum_{r=0}^{\infty} L_r^{\ell+1/2}(c^2) t^r \quad (\text{A-2})$$

and the Legendre polynomials  $P_n(x)$  may be determined from Rodrigues' formula

$$P_n(x) = \frac{1}{2^n n!} \frac{d^n}{dx^n} \left[ x^2 - 1 \right]^n. \quad (\text{A-3})$$

The Maxwell eigenfunctions needed in this effort together with their associated eigenvalues,  $c_{r,\ell}$ , are given in Table II.

In Table II,  $\tilde{A}_2$  is a pure number which has been defined in Chapter II.

Useful relations among the  $\Psi_{r,\ell}(\vec{c})$  are listed below:

$$c_z \Psi_{0,0}(\vec{c}) = \Psi_{0,1}(\vec{c}); \quad (\text{A-4})$$

$$c_z \Psi_{r,0}(\vec{c}) = \Psi_{r,1}(\vec{c}) - \Psi_{r-1,1}(\vec{c}), \quad r \geq 1; \quad (\text{A-5})$$

---

<sup>†</sup>We adopt the convention that  $\hat{A}$  denotes a unit vector parallel to  $\vec{A}$  for any  $\vec{A}$ .



TABLE II  
MAXWELL EIGENFUNCTIONS AND ASSOCIATED EIGENVALUES

r	l	$\Psi_{r,l}(c)$	$\epsilon_{r,l}$
0	0	1	--
1	0	$\frac{3}{2} - c^2$	--
2	0	$\frac{15}{8} - \frac{5}{2} c^2 + \frac{1}{2} c^4$	$-\pi \tilde{A}_2$
0	1	$c_z$	--
1	1	$\left(\frac{5}{2} - c^2\right) c_z$	$-\pi \tilde{A}_2$
2	1	$\left(\frac{35}{8} - \frac{7}{2} c^2 + \frac{1}{2} c^4\right) c_z$	$-\frac{3}{2} \pi \tilde{A}_2$
0	2	$\left(\frac{3}{2} c_z^2 - \frac{1}{2} c^2\right)$	$-\frac{3}{2} \pi \tilde{A}_2$
1	2	$\left(\frac{7}{2} - c^2\right) \left(\frac{3}{2} c_z^2 - \frac{1}{2} c^2\right)$	$-\frac{7}{4} \pi \tilde{A}_2$
0	3	$\left(\frac{5}{2} c_z^3 - \frac{3}{2} c_z c^2\right)$	$-\frac{9}{4} \pi \tilde{A}_2$

$$c_z \Psi_{0,\ell}(\vec{c}) = \frac{\ell}{2\ell+1} \left\{ \left( \ell + \frac{1}{2} \right) \Psi_{0,\ell-1}(\vec{c}) - \Psi_{1,\ell-1}(\vec{c}) \right\} \\ + \frac{\ell+1}{2\ell+1} \Psi_{0,\ell+1}(\vec{c}), \quad \ell \geq 1; \quad (\text{A-6})$$

$$c_z \Psi_{r,\ell}(\vec{c}) = \frac{\ell}{2\ell+1} \left\{ \left( r + \ell + \frac{1}{2} \right) \Psi_{r,\ell-1}(\vec{c}) - (r+1) \Psi_{r+1,\ell-1}(\vec{c}) \right\} \\ + \frac{\ell+1}{2\ell+1} \left\{ \Psi_{r,\ell+1}(\vec{c}) - \Psi_{r-1,\ell+1}(\vec{c}) \right\}; \quad (\text{A-7})$$

$$\frac{\partial}{\partial c_z} \Psi_{0,\ell}(\vec{c}) = \ell \Psi_{0,\ell-1}(\vec{c}). \quad (\text{A-8})$$

## APPENDIX B

### ROOTS OF THE CHARACTERISTIC POLYNOMIALS

The Mach number dependent length scales alluded to in Chapters III and IV (in conjunction with the linearization of the gasdynamic differential equations) may be determined by solving for the roots of the characteristic polynomials which are obtained as a result of the linearization process. The characteristic polynomials in  $L_i \equiv \frac{\mu_i M_i}{\rho_i a_i} \kappa_i$  given below, containing the Mach number  $M_i$  as a parameter, were so obtained.

NAVIER-STOKES:

$$20 L_i^2 + (9 - 23M_i^2) L_i + 6 M_i^2 (M_i^2 - 1) = 0 \quad (B-1)$$

BURNETT:

$$70 L_i^4 - 180 L_i^3 + 291 M_i^2 L_i^2 + \left[ 81 - 207 M_i^2 \right] M_i^2 L_i + 54 M_i^4 (M_i^2 - 1) = 0 \quad (B-2)$$

SUPER-BURNETT:

$$7850 L_i^6 + 29160 L_i^5 - 28980 M_i^2 L_i^4 + \left[ 20475 M_i^4 - 5427 M_i^2 \right] L_i^3 - 36(291) M_i^4 L_i^2 + \left[ 36(207) M_i^6 - 36(81) M_i^4 \right] L_i - 54(36) M_i^6 \left[ M_i^2 - 1 \right] = 0 \quad (B-3)$$

## SUPER-SUPER-BURNETT :

$$\begin{aligned}
& 328399(625)L_1^8 - 200(63)(521)L_1^7 \\
& + 6300(3791)M_1^2 L_1^4 - 40(81)(49)(59)M_1^2 L_1^5 \\
& + 350(27)(2287)M_1^4 L_1^4 - 54(49)M_1^4 \left[ 2275M_1^2 - 603 \right] L_1^3 \\
& + 8(49)(81)(97)M_1^6 L_1^2 - 8(49)(243)M_1^6 \left[ 23M_1^2 - 9 \right] L_1 \\
& + 16(49)(729)M_1^8 \left[ M_1^2 - 1 \right] = 0 . \quad (B-4)
\end{aligned}$$

The roots of each characteristic polynomial far upstream ( $L_1$ ) or far downstream ( $L_2$ ) may be determined for any selected upstream Mach number ( $M_1$ ) or its corresponding Rankine-Hugoniot downstream Mach number ( $M_2$ ) using standard computer library routines. The results given in the tables and figures which follow were computed to twelve decimal accuracy.

Figures 26, 27, 28, and 29 present plots of the results for  $L_1$  versus  $M_1$  and  $L_2$  versus  $M_1$  as determined from computer solutions of equations (B-1), (B-2), (B-3), and (B-4), respectively. The real  $L_1$  and the real parts of the complex  $L_1$  are plotted as solid lines and the imaginary parts of the complex  $L_1$  are plotted as broken lines in the figures. The corresponding real and imaginary parts of the conjugate pairs are appropriately identified in each figure.

The physically significant roots  $\kappa_2$ , which provide appropriate length scales for each of the gasdynamic developments, are presented for a range of upstream Mach numbers in Table III

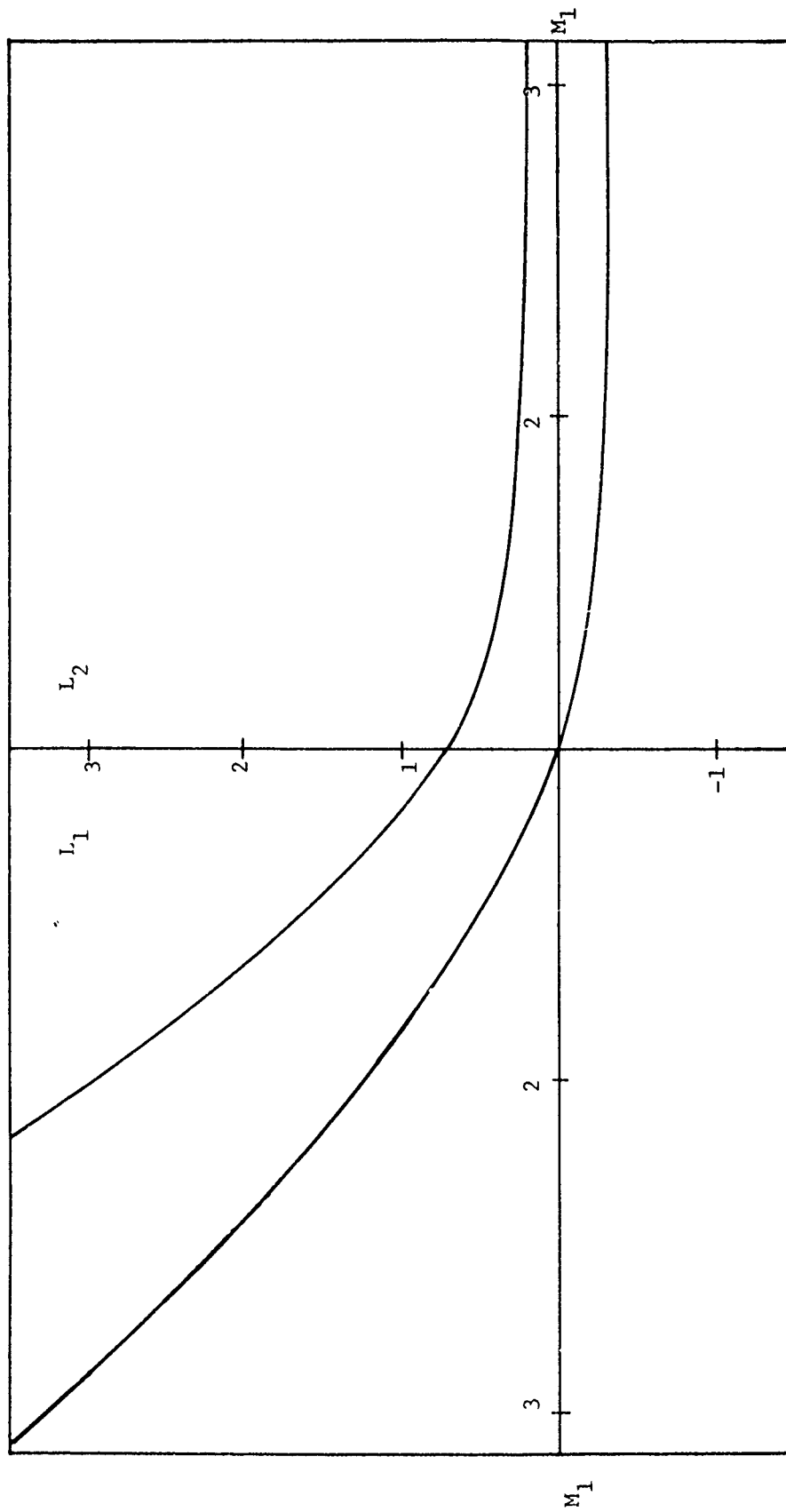


Figure 26 - Roots of the Navier-Stokes characteristic polynomial.  
Upstream roots ( $L_1$ ) and downstream roots ( $L_2$ ) versus  $M_1$ .

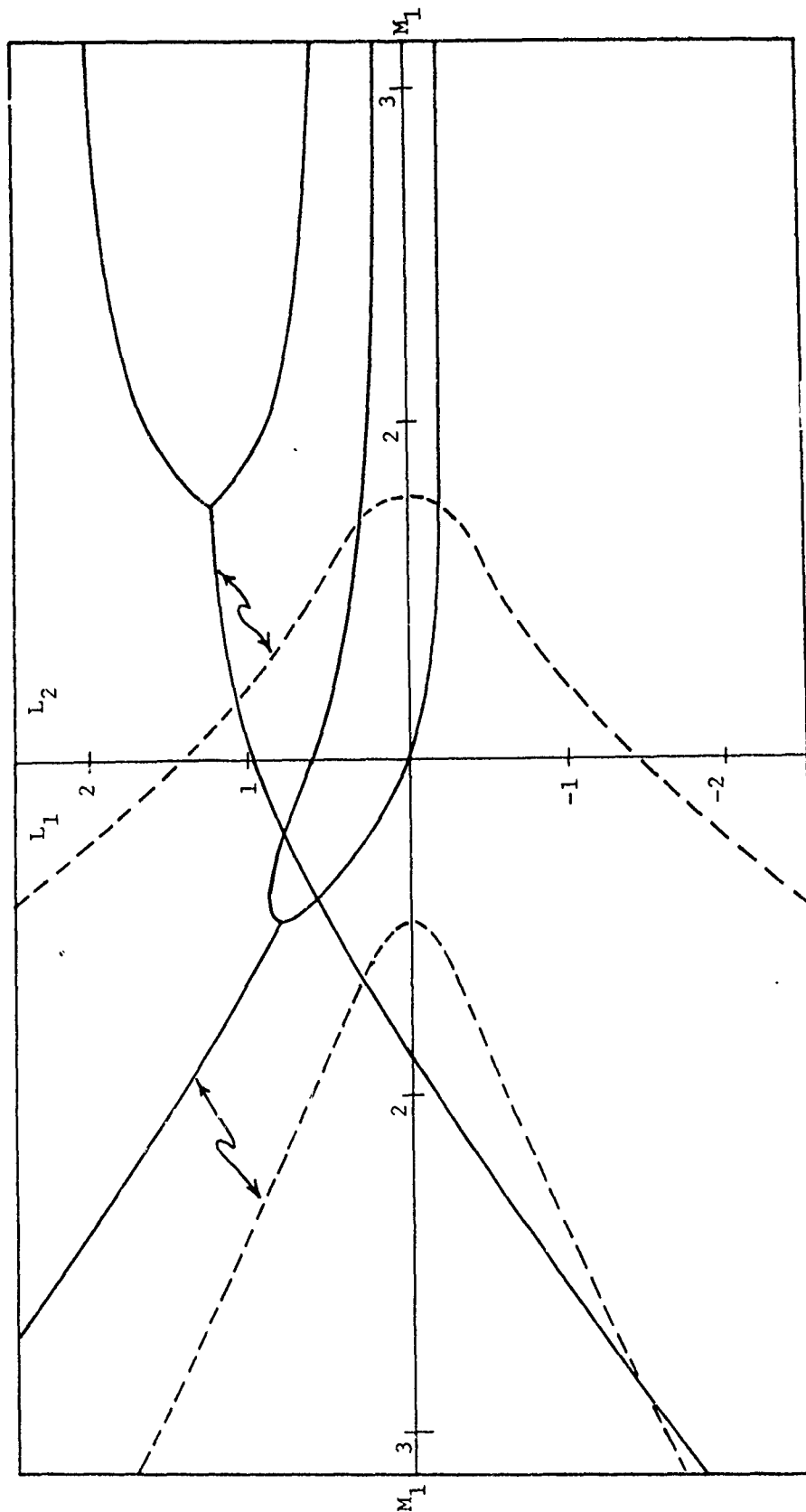


Figure 27 - Roots of the Burnett Characteristic polynomial.  
Upstream roots ( $L_1$ ) and downstream roots ( $L_2$ ) versus  $M_1$ .





TABLE III  
PHYSICALLY SIGNIFICANT  $\kappa_2$

$M_1$	Naiver-Stokes	Burnett	Super-Burnett	Super-Super-Burnett
1.1	-0.07167703	-0.06685100	-0.06633523	-0.06612403
1.2	-0.12285635	-0.10793995	-0.10594205	-0.10475777
1.3	-0.16089605	-0.13425755	-0.13066329	-0.12708902
1.4	-0.19005288	-0.15164829	-0.14673941	-0.14077175
1.5	-0.21295431	-0.16341863	-0.15753600	-0.14923111
1.6	-0.23130542	-0.17153184	-0.16496566	-0.15452634
1.7	-0.24625774	-0.17720053	-0.17017150	-0.15784456
1.8	-0.25861475	-0.18119856	-0.17386660	-0.15989620
1.9	-0.26895253	-0.18403361	-0.17651194	-0.16112073
2.0	-0.27769376	-0.18604662	-0.17841433	-0.16179769
2.1	-0.28515479	-0.18747177	-0.17978304	-0.16210907
2.2	-0.29157651	-0.18847010	-0.18076370	-0.16217567
2.3	-0.29714518	-0.18915860	-0.18145944	-0.16207889
2.4	-0.30200677	-0.18961924	-0.18194438	-0.16187431
2.5	-0.30627706	-0.18991189	-0.18227243	-0.16160018
2.6	-0.31004889	-0.19008036	-0.18248322	-0.16128305
2.7	-0.31339746	-0.19015700	-0.18260620	-0.16094136
2.8	-0.31638419	-0.19016584	-0.18266339	-0.16058798
2.9	-0.31905971	-0.19012490	-0.18267137	-0.16023179
3.0	-0.32146603	-0.19004769	-0.18264270	-0.15987893

TABLE III (continued)

$M_1$	Naiver-Stokes	Burnett	Super-Burnett	Super-Super-Burnett
3.1	-0.32363828	-0.18994443	-0.18258696	-0.15953354
3.2	-0.32560601	-0.18982285	-0.18251144	-0.15919835
3.3	-0.32739421	-0.18968880	-0.18242175	-0.15887508
3.4	-0.32902418	-0.18954675	-0.18232219	-0.15856475
3.5	-0.33051413	-0.18940005	-0.18221604	-0.15826785
3.6	-0.33187970	-0.18925125	-0.18210585	-0.15798450
3.7	-0.33313441	-0.18910227	-0.18199355	-0.15771459
3.8	-0.33428998	-0.18895455	-0.18188062	-0.15745783
3.9	-0.33535662	-0.18880913	-0.18176819	-0.15721379
4.0	-0.33634327	-0.18866679	-0.18165710	-0.15698200

## APPENDIX C

GENERAL FORM OF THE EQUATIONS FROM THE PERTURBATION DEVELOPMENT  
AND GENERAL FORM OF THE SOLUTIONS TO THE DIFFERENTIAL EQUATIONS  
FOR THE NORMALIZED DENSITY

The perturbation methods applied in each of the gasdynamic developments of Chapter II produce a set of first order linear differential equations for the perturbed density contributions  $R_{\rho}^{(0)}$ ,  $R_{\rho}^{(1)}$ ,  $R_{\rho}^{(2)}$ ,  $R_{\rho}^{(3)}$ , etc., and a set of algebraic relationships for the perturbed temperature contributions  $R_T^{(0)}$ ,  $R_T^{(1)}$ ,  $R_T^{(2)}$ ,  $R_T^{(3)}$ , etc., in terms of the perturbed densities. In the course of the perturbation calculations, a pattern in the analytical results recurred in each of the gasdynamic developments.

Thus, the perturbation equations for the normalized density and temperature, applicable to any of the gasdynamic developments, are of the following general form:

$$\frac{dR_{\rho}^{(0)}}{d\zeta} = R_{\rho}^{(0)} - \left[ R_{\rho}^{(0)} \right]^2 ; \quad (C-1)$$

$$\frac{dR_{\rho}^{(1)}}{d\zeta} = \left[ 1 - 2R_{\rho}^{(0)} \right] R_{\rho}^{(1)} + A_1 \left[ R_{\rho}^{(0)} \right]^2 - A_1 \left[ R_{\rho}^{(0)} \right]^3 ; \quad (C-2)$$

$$\begin{aligned} \frac{dR_{\rho}^{(2)}}{d\zeta} = & \left[ 1 - 2R_{\rho}^{(0)} \right] R_{\rho}^{(2)} + 2A_1 R_{\rho}^{(0)} R_{\rho}^{(1)} - 3A_1 \left[ R_{\rho}^{(0)} \right]^2 R_{\rho}^{(1)} - \left[ R_{\rho}^{(1)} \right]^2 \\ & + A_2 \left[ R_{\rho}^{(0)} \right]^2 + A_3 \left[ R_{\rho}^{(0)} \right]^3 + A_4 \left[ R_{\rho}^{(0)} \right]^4 ; \end{aligned} \quad (C-3)$$

$$\begin{aligned} \frac{dR_{\rho}^{(3)}}{d\zeta} = & \left[ 1 - 2R_{\rho}^{(0)} \right] R_{\rho}^{(3)} + 2A_1 R_{\rho}^{(0)} R_{\rho}^{(2)} - 3A_1 \left[ R_{\rho}^{(0)} \right]^2 R_{\rho}^{(2)} - 2R_{\rho}^{(1)} R_{\rho}^{(2)} \\ & + A_1 \left[ R_{\rho}^{(1)} \right]^2 - 3A_1 R_{\rho}^{(0)} \left[ R_{\rho}^{(1)} \right]^2 + 2A_2 R_{\rho}^{(0)} R_{\rho}^{(1)} + 3A_3 \left[ R_{\rho}^{(0)} \right]^2 R_{\rho}^{(1)} \\ & + 4A_4 \left[ R_{\rho}^{(0)} \right]^3 R_{\rho}^{(1)} + A_5 \left[ R_{\rho}^{(0)} \right]^2 + A_6 \left[ R_{\rho}^{(0)} \right]^3 + A_7 \left[ R_{\rho}^{(0)} \right]^4 + A_8 \left[ R_{\rho}^{(0)} \right]^5 ; \end{aligned} \quad (C-4)$$

$$R_T^{(0)} = R_\rho^{(0)} ; \quad (C-5)$$

$$R_T^{(1)} = R_\rho^{(1)} + A_9 \left( 1 - R_\rho^{(0)} \right) R_\rho^{(0)} ; \quad (C-6)$$

$$R_T^{(2)} = R_\rho^{(2)} + A_9 \left( 1 - 2R_\rho^{(0)} \right) R_\rho^{(1)} + A_{10} R_\rho^{(0)} + A_{11} \left[ R_\rho^{(0)} \right]^2 + A_{12} \left[ R_\rho^{(0)} \right]^3 ; \quad (C-7)$$

$$R_T^{(3)} = R_\rho^{(3)} + A_9 \left( 1 - 2R_\rho^{(0)} \right) R_\rho^{(2)} + A_{10} R_\rho^{(1)} + 2A_{11} R_\rho^{(0)} R_\rho^{(1)} + 3A_{12} \left[ R_\rho^{(0)} \right]^2 R_\rho^{(1)} - A_9 \left[ R_\rho^{(1)} \right]^2 + A_{13} R_\rho^{(0)} + A_{14} \left[ R_\rho^{(0)} \right]^2 + A_{15} \left[ R_\rho^{(0)} \right]^3 + A_{16} \left[ R_\rho^{(0)} \right]^4 ; \quad (C-8)$$

$$R_T^{(4)} = R_\rho^{(4)} + A_9 \left( 1 - 2R_\rho^{(0)} \right) R_\rho^{(3)} + A_{10} R_\rho^{(2)} + 2A_{11} R_\rho^{(0)} R_\rho^{(2)} + 3A_{12} \left[ R_\rho^{(0)} \right]^2 R_\rho^{(2)} + A_{13} R_\rho^{(1)} + 2A_{14} R_\rho^{(0)} R_\rho^{(1)} + 3A_{15} \left[ R_\rho^{(0)} \right]^2 R_\rho^{(1)} + 4A_{16} \left[ R_\rho^{(0)} \right]^3 R_\rho^{(1)} - 2A_9 R_\rho^{(1)} R_\rho^{(2)} + A_{11} \left[ R_\rho^{(1)} \right]^2 + 3A_{12} R_\rho^{(0)} \left[ R_\rho^{(1)} \right]^2 + A_{17} R_\rho^{(0)} + A_{18} \left[ R_\rho^{(0)} \right]^2 + A_{19} \left[ R_\rho^{(0)} \right]^3 + A_{20} \left[ R_\rho^{(0)} \right]^4 + A_{21} \left[ R_\rho^{(0)} \right]^5 . \quad (C-9)$$

The coefficients  $A_n$  determined in each of the gasdynamic developments are listed in Table IV.

The solution of the differential equations for  $R_\rho^{(1)}$ ,  $R_\rho^{(2)}$ ,  $R_\rho^{(3)}$ , etc., may be expressed as functionals of the quantity  $(1 - R_\rho^{(0)})$ . In each instance, the differential equations can be arranged in the form

$$\frac{dR_\rho^{(n)}}{d\zeta} + \left[ 2R_\rho^{(0)} - 1 \right] R_\rho^{(n)} = I^{(n)} . \quad (C-10)$$

TABLE IV  
COEFFICIENTS  $A_n$  FOR THE PERTURBATION EQUATIONS

$A_n$	Navier-Stokes	Burnett	Super-Burnett	Super-Super-Burnett
$A_1 \cdot 4(7)^2$	61	-87	-87	-87
$A_2 \cdot 16(7)^4$	-20203	-56193	23775	23775
$A_3 \cdot 16(7)^4$	34794	126828	-33108	-33108
$A_4 \cdot 16(7)^4$	-14591	-70635	9333	9333
$A_5 \cdot 128(7)^6$	1971230	-39762438	100208610	-62714430
$A_6 \cdot 128(7)^6$	3526570	218183394	-360418014	221449986
$A_7 \cdot 128(7)^6$	-13336026	-324539190	437272434	-260969166
$A_8 \cdot 128(7)^6$	7838226	146118234	-177063030	102233610
$A_9 \cdot 8(7)$	67	67	67	67
$A_{10} \cdot 64(7)^3$	-1931	-4811	-4811	-4811

TABLE IV (continued)

$A_n$	Navier-Stokes	Burnett	Super-Burnett	Super-Super-Burnett
$A_{11} \cdot 64(7)^3$	-27037	-18397	-18397	-18397
$A_{12} \cdot 64(7)^3$	28968	23208	23208	23208
$A_{13} \cdot 512(7)^5$	-727457	-1878497	3013663	3013663
$A_{14} \cdot 512(7)^5$	2343485	21661565	-12583555	-12583555
$A_{15} \cdot 512(7)^5$	10962264	-28194216	30511704	30511704
$A_{16} \cdot 512(7)^5$	-12578292	84111148	-20941812	-20941812
$A_{17} \cdot 4096(7)^7$	257219941	277563301	1985679781	-3062921819
$A_{18} \cdot 4096(7)^7$	64012703	11550194783	-37292378017	38436645983
$A_{19} \cdot 4096(7)^7$	-604826712	-66307987032	133555564968	-118874515032
$A_{20} \cdot 4096(7)^7$	-5690706300	94921844100	-174009599100	128906496900
$A_{21} \cdot 4096(7)^7$	5974300368	-40441615152	75760732368	-45405706032

An equivalent expression for (C-10) is

$$\frac{d}{d\zeta} \left\{ \frac{R_{\rho}^{(n)}}{R_{\rho}^{(0)} [1-R_{\rho}^{(0)}]} \right\} = \frac{I^{(n)}}{R_{\rho}^{(0)} [1-R_{\rho}^{(0)}]} , \quad (C-11)$$

or

$$\frac{d}{d\zeta} \left\{ \frac{R_{\rho}^{(n)}}{R_{\rho}^{(0)} [1-R_{\rho}^{(0)}]} \right\} = \frac{d}{d\zeta} F^{(n)} [1-R_{\rho}^{(0)}] . \quad (C-12)$$

Using the chain rule to obtain the functional  $F^{(n)} [1-R_{\rho}^{(0)}]$

$$\frac{d}{d[1-R_{\rho}^{(0)}]} \left\{ F^{(n)} [1-R_{\rho}^{(0)}] \right\} = - \frac{I^{(n)}}{[1-R_{\rho}^{(0)}]^2 [R_{\rho}^{(0)}]^2} \quad (C-13)$$

yields

$$F^{(n)} [1-R_{\rho}^{(0)}] = - \int d[1-R_{\rho}^{(0)}] \frac{I^{(n)}}{[1-R_{\rho}^{(0)}]^2 [R_{\rho}^{(0)}]^2} . \quad (C-14)$$

With  $F^{(n)} [1-R_{\rho}^{(0)}]$  known, both sides of equation (C-12) are exact differentials and may be integrated to yield  $R_{\rho}^{(n)}$  with the integration constant determined from the conditions that at  $\zeta = 0$ ,  $R_{\rho}^{(n)} = \frac{1}{2} \delta_{n0}$  where  $\delta_{n0}$  is the Kronecker delta.

For example, the differential equation for  $R_{\rho}^{(1)}$  is

$$\frac{dR_{\rho}^{(1)}}{d\zeta} + 2 \left[ R_{\rho}^{(0)} - 1 \right] R_{\rho}^{(1)} = A_1 \left[ 1-R_{\rho}^{(0)} \right] \left[ R_{\rho}^{(0)} \right]^2 . \quad (C-15)$$

The results for  $I^{(1)}$  and  $F^{(1)} [1-R_{\rho}^{(0)}]$  are

$$I^{(1)} = A_1 \left\{ 1 - \left[ 1-R_{\rho}^{(0)} \right]^2 \right\} \left[ 1-R_{\rho}^{(0)} \right] \quad (C-16)$$

and

$$F^{(1)} [1-R_{\rho}^{(0)}] = - A_1 \int \frac{d[1-R_{\rho}^{(0)}]}{[1-R_{\rho}^{(0)}]} . \quad (C-17)$$



Thus, using (C-17) in (C-12) and integrating, the result is

$$R_{\rho}^{(1)} = R_{\rho}^{(0)} \left[ 1 - R_{\rho}^{(0)} \right] \left\{ - A_1 \ln \left[ 1 - R_{\rho}^{(0)} \right] + Q_1 \right\}, \quad (C-18)$$

where  $Q_1$  is an integration constant. Evaluating  $Q_1$  from the boundary conditions on  $R_{\rho}^{(0)}$  and  $R_{\rho}^{(1)}$  at  $\zeta = 0$  yields

$$Q_1 = \frac{1}{2} A_1 \ln 2. \quad (C-19)$$

The differential equations for  $R_{\rho}^{(2)}$  and  $R_{\rho}^{(3)}$  may be solved using the same procedures described above. The solutions are given in equations (III-53) and (III-54). The differential equation for  $R_{\rho}^{(0)}$  can be integrated without using this method. The result for  $R_{\rho}^{(0)}$  is given in equation (III-42).

Since the differential equations for the  $R_{\rho}^{(j)}$  have the same general form for each gasdynamic development, the solutions for the  $R_{\rho}^{(n)}$  may also be expressed in a general form. The coefficients of the integrated results are functions of the original  $A_n$ . The results for  $R_{\rho}^{(0)}$  and  $R_{\rho}^{(1)}$  are relatively simple. However, the coefficients in  $R_{\rho}^{(2)}$  and  $R_{\rho}^{(3)}$  are much more involved, namely

$$\begin{aligned} R_{\rho}^{(2)} = R_{\rho}^{(0)} \left[ 1 - R_{\rho}^{(0)} \right] \left\{ B_1 \left[ 1 - R_{\rho}^{(0)} \right] + B_2 \ln \left[ 1 - R_{\rho}^{(0)} \right] \right. \\ \left. + B_3 \left[ 1 - R_{\rho}^{(0)} \right] \ln \left[ 1 - R_{\rho}^{(0)} \right] + B_4 \ln^2 \left[ 1 - R_{\rho}^{(0)} \right] \right. \\ \left. + B_5 \left[ 1 - R_{\rho}^{(0)} \right] \ln^2 \left[ 1 - R_{\rho}^{(0)} \right] + Q_2 \right\} \end{aligned} \quad (C-20)$$

and

$$\begin{aligned}
R_{\rho}^{(3)} = R_{\rho}^{(0)} \left[ 1 - R_{\rho}^{(0)} \right] & \left\{ C_1 \left[ 1 - R_{\rho}^{(0)} \right] + C_2 \ln \left[ 1 - R_{\rho}^{(0)} \right] \right. \\
& + C_3 \left[ 1 - R_{\rho}^{(0)} \right] \ln \left[ 1 - R_{\rho}^{(0)} \right] + C_4 \ln^2 \left[ 1 - R_{\rho}^{(0)} \right] \\
& + C_5 \left[ 1 - R_{\rho}^{(0)} \right] \ln^2 \left[ 1 - R_{\rho}^{(0)} \right] + C_6 \ln^3 \left[ 1 - R_{\rho}^{(0)} \right] \\
& + C_7 \left[ 1 - R_{\rho}^{(0)} \right]^2 + C_8 \left[ 1 - R_{\rho}^{(0)} \right]^2 \ln \left[ 1 - R_{\rho}^{(0)} \right] \\
& + C_9 \left[ 1 - R_{\rho}^{(0)} \right]^2 \ln^2 \left[ 1 - R_{\rho}^{(0)} \right] + C_{10} \left[ 1 - R_{\rho}^{(0)} \right] \ln^3 \left[ 1 - R_{\rho}^{(0)} \right] \\
& \left. + C_{11} \left[ 1 - R_{\rho}^{(0)} \right]^2 \ln^3 \left[ 1 - R_{\rho}^{(0)} \right] + Q_3 \right\} . \quad (C-21)
\end{aligned}$$

The results for the coefficients  $B_n$  and  $C_n$  are presented in Tables V and VI respectively.

TABLE V  
COEFFICIENTS  $B_n$  FOR  $R_\rho^{(2)}$

$n$	$B_n$
1	$-A_4 - A_1^2 - A_1 Q_1 + Q_1^2$
2	$A_3 + 2A_4 + A_1 Q_1$
3	$A_1^2 - 2A_1 Q_1$
4	$-1/2 A_1^2$
5	$A_1^2$

TABLE VI  
COEFFICIENTS  $C_n$  FOR  $R_\rho^{(3)}$

$n$	$C_n$
1	$5A_1A_4 + A_1^3 + 2A_1A_3 - A_7 - 3A_8 + (2A_1^2 + A_3 + 4A_4)Q_1$ $+ A_1Q_1^2 - A_1Q_2 + 2Q_1Q_2$
2	$A_6 + 2A_7 + 3A_8 + (-A_3 - 2A_4)Q_1 + A_1Q_2$
3	$-2A_1^3 - 2A_1A_3 - 6A_1A_4 + (-3A_1^2 + 2A_3 + 4A_4)Q_1 + 2A_1Q_1^2 - 2A_1Q_2$
4	$A_1A_3 + 2A_1A_4 + 1/2A_1^2Q_1$
5	$3/2A_1^3 - 2A_1A_3 - 4A_1A_4 - 3A_1^2Q_1$
6	$1/2A_1^3 + 1/2A_8 + (-2A_1^2 - 3A_4)Q_1 - 5/2A_1Q_1^2 + Q_1^3$
7	$2A_1^3 + 3A_1A_4 + 5A_1^2Q_1 - 3A_1Q_1^2$
8	$-5/2A_1^3 + 3A_1^2Q_1$
9	$-1/6A_1^3$
10	$A_1^3$
11	$-A_1^3$